EURISOL User Group

Report on the third EURISOL User Group Topical Meeting [1]

Physics of Light Exotic Nuclei

Instituto Superior Técnico (IST), Lisbon, Portugal, 15-19 October 2012

The research leading to these results has received funding from the European Union Seventh Framework Programme FP7/2007- 2013 under Grant Agreement n. 262010 - ENSAR.
The EC is not liable for any use that can be made on the information contained herein.

[1] Coordinated by Angela Bonaccorso, INFN, Sez. di Pisa, Italy, Lidia Ferreira, IST, Lisbon, Portugal and Björn Jonson, Chalmers University of Technology, Göteborg, Sweden.

.

THIRD EURISOL TOPICAL MEETING

Physics of Light Exotic Nuclei

Foreword

This report contains the highlights of the third EURISOL Topical Meeting, which was held in Lisbon, from October 15th to 17th 2012. It followed the EURISOL Topical Meetings in Catania (2009) on "The formation and structure of r-process nuclei, between N=50 and 82 (including ^{78}Ni and ^{132}Sn areas)" and in Valencia (2011) on "Neutron-deficient nuclei and the physics of the proton-rich side of the nuclear chart". It was organized by the EURISOL Users Group and supported by ENSAR and CFIF.

The workshop lasted two and a half days. There were about forty participants including almost all members of the previous and present EURISOL User Group Executive Committee. The twenty-six presentations were all followed by lively discussions. The programme and the presentations are available at the workshop web site http://cfif.ist.utl.pt/~eurisol/.

Light exotic nuclei were at the core of the early discovery of phenomena like the "nuclear halo", which boosted the experimental and theoretical activities related to Physics with Radioactive beams. They still hold a special place in the panorama of recent activities, as we shall see in the following. They provide in fact the testing grounds of all basic structure models, from shell model to cluster models towards the most recent "ab-initio" theories. The large intensity values of light radioactive beams allow for the most precise measurements of quantities such as absolute cross sections, angular distribution, momentum distributions, and nuclear decay observables, which are of key importance for modern reaction theories.

In the following we give a short account of the topics discussed at the workshop.

Elastic scattering and fusion (M. Borge, P. Figuera, P.Gomes, G. Baiocco, R. de Diego, H. Arellano, G. Cardella)

The first session of the Lisbon topical meeting was devoted to the discussion of elastic scattering experiments with the talks of Maria Borge,

Pierpaolo Figuera and Paulo Gomes, which clarified how breakup and transfer reactions influence elastic angular distributions by comparing results from halo nuclei and their closest neighbors. Elastic scattering is typically depleted by the strong effect of the breakup. The same seems to be the case also for fusion at or above barrier energies. Below the barrier the situation is still unclear. Thus, a low energy branch of a facility like EURISOL would be necessary for further studies. The elastic scattering technique and its interpretation are now well established and it has been argued during the workshop that such experiments constitute a new and interesting case for EURISOL. In this respect there was yet another interesting method presented the last day by Giuseppe Cardella. He showed how one could use a 4π charged particle detector to get accurate elastic scattering- angular distributions from fragmentation of beams by using event-by-event identification techniques. When a large variety of beams with high intensity will become available the study of elastic scattering will be among the first experiments to be performed for any new exotic nucleus.

Ab-initio structure models (A. Schwenk, C. Barbieri, C. Forssen)

Carlo Barbieri presented a new method to calculate binding energies, which is applicable to open shell isotopes such as ^{44}Ca. It is based on the Gorkov's approach, which handles intrinsic degeneracies of open shell systems by allowing the breaking of particle number symmetry. Preliminary inclusion of three-body forces was also presented. There are at present several versions of ab-initio methods, originating in subtle differences.

C. Forssen clarified that "ab initio" many-body methods are those that solve the relevant quantum mechanical many-body equations with controlled approximations (e.g. number of channels), which are allowed as they can be increasingly improved to the point that convergence is reached for the observable. Converged results are considered precise "ab initio" results. His contribution contains a review of such methods. An important conclusion, which consistently emerges from these theoretical analyses, is that three-nucleon forces are crucial for both global nuclear properties and detailed nuclear structure, and that many-body correlations due to the coupling to the particle continuum are essential as one approaches particle drip lines. The ongoing efforts to extend the range of

applicability of "ab initio" methods were discussed by Achim Schwenk. He presented examples from the new generation of many-body methods in particular those that can use realistic nuclear interactions from chiral EFT and three-nucleon interactions. Chiral 3N forces lead to repulsive contributions to the interactions among excess neutrons that change the location of the neutron dripline from ^{28}O (with NN forces only) to the experimentally observed ^{24}O. This is the first explanation of the oxygen anomaly based on nuclear forces (cf. C. Barbieri contribution). Also in first studies for calcium isotopes, it was shown that 3N forces are key to explain the N=28 magic number, leading to a high 2^+ excitation energy. Moreover, chiral 3N forces improve the agreement with experimental masses predicting a flat behavior of the two-neutron separation energy from ^{50}Ca to ^{52}Ca (cf. TITAN data). Finally the calculations of neutron matter energy provides tight constraints for the symmetry energy and chiral EFT interactions constrain the properties of neutron-rich matter below nuclear densities to a much higher degree than is reflected in current neutron star modeling.

Direct reactions and breakup (P. Descouvemont, A. Obertelli, M. Assiè, R. Crespo, T. Nakamura, D. Galaviz)

A review talk on reaction theory was given by Pierre Descouvemont, who discussed microscopic Continuum Discretized Coupled Channel calculations for energies around the Coulomb barrier, with two-body and three-body projectile wave functions. He also showed preliminary results with cluster wave functions. The eikonal model, which is appropriate at high energies, was also revised. Theory talks by Raul Diego and Raquel Crespo discussed details of the reaction dynamics via core excitation. The three-body Faddeev/AGS multiple scattering expansion was discussed by Daniel Galaviz as a method to analyze data for breakup on a proton target. Ugo Arellano introduced microscopic calculations of the optical potential for light nuclei, in which volume and surface effects are distinguished. Alexandre Obertelli, also presented mechanisms of direct reactions, like knock out and transfer, in order to obtain spectroscopic information on single particle state occupancies. The case of nuclei with large asymmetries in the proton/neutron separation energies was analized in detail. T. Nakamura gave an overview of the present RIKEN facility and he reviewed Coulomb breakup data. Such data are a well established high

energy method to obtain spectroscopic factors as the reaction calculations are basically exact.

Clustering phenomena (M. Ploszajczak, H. Feldmeier, M. Assiè)

Clustering was discussed from the structure theory point of view by Marek Ploszajczak and Hans Feldmeier. Both of them showed evidences for clustering as a "threshold" effect. Marek Ploszajczak discussed the occurrence of clustering within the Continuum Shell model. Here the coupling to positive energy states and the use of energy dependent Hamiltonians give rise above particle-emission threshold to non-Hermitian components of the effective Hamiltonian. Such components concentrate the continuum coupling on a single state thus giving rise to clustering via the appearence of collective near-threshold phenomena in the ensemble of Shell Model states. H. Feldmeier and collaborators use the Fermioni Molecular Dynamics method, which starts with Gaussian wave packets, builds up Slater determinants are many-body states and then diagonalize the Hamiltonian. Then the derivation of a low-momentum effective interaction is the clue to getting an accurate description of the lightest *s-p* shell nuclei. Recent results are the description of the large extension of the Hoyle state (O_2^+)+ in ^{12}C, the radii of ^{17}Ne, ^{18}Ne and ^{19}Ne described in terms of cluster structures due to ^{16}O - ^{3}He and ^{15}O – ^{4}He configurations, the rates of the important astrophysical reactions $^{3}He(\alpha, \gamma)\ ^{7}Be$ and $^{3}He(\alpha,\gamma)^{7}Li$.
From the experimental side Marlene Assiè presented clustering evidence and paring effects in breakup reactions. Giorgio Baiocco presented a quite original research program in progress at the Legnaro laboratory aiming an understanding of the statistical properties of light nuclei at excitation energies above particle emission threshold by measurement of observables linked to the presence of cluster structures of nuclear excited levels and the development of a Monte-Carlo Hauser-Feshbach code for the evaporation of the compound nucleus, which explicitly includes all the experimentally measured particle unstable levels from the online archive NUDAT2.

Shell model (A. Signoracci)

Angelo Signoracci covered the present status and future perspectives of the modern shell model. He stressed an interesting aspect, namely that

shell structure is accessed via effective single-particle energies (ESPEs), as described by the standard shell model. However it has recently been shown that ESPEs are basis-independent but not observable, depending significantly on the resolution scale characterizing the Hamiltonian. The practical reconstruction of ESPEs is contaminated by theoretical uncertainties, due in part to incomplete spectroscopic data. Thus the continuous application of direct reaction experimental techniques is strongly recommended. The shell model success relay heavily on the accuracy of the effective interaction used. This is at presently been pursued via the introduction of higher order terms, three-body forces and possibly inclusion of positive energy states.

Resonance phenomena (N. Lo Iudice)

Nicola Lo Iudice discussed multiphonon excitations used to describe the pygmy resonance effects. The dipole response in the neutron-rich nucleus ^{20}O has been studied via a new method based on an equation-of-motion phonon method (EMPM). The results show that this mode is excited with a relatively small strength. Indeed, the main role is played by the quasi-particle neutron configurations with large weight, while the many-proton states contribute with small amplitudes. Moreover, the coupling and the coexistence with multiphonon excitations damp the dipole mode. Thus the two-phonon components play a crucial role in fragmenting and shaping the Giant Dipole Resonance and are determinant in pushing a residual strength down in the low-energy sector, in agreement with experiments. Only one of the peaks shown by the calculations may be associated to the Pigmy Dipole Resonance. The EMPM represents an important advance with respect to the other approaches that extend the Random Phase Approximation.

Nuclear Astrophysics (A. Laird, C. Spitaleri, E. Maglione)

Nucleo-synthesis reactions can be studied accurately at ISOL facilities and this subject was covered by Alison Laird with special interest at the proton-rich side of the nuclear chart where a number of flagship experiments e.g. with ^{21}Na, ^{26}Al, ^{17}F and ^{18}F, have already been performed to study both (p,a) and (a,p) reactions taking advantage of the forward focusing of the reaction products. Alison stressed the necessity to have in the future low energy, proton-rich beams (less than 2 MeV/u) with intensities in excess of 10^7 pps, and high purity. Claudio Spitaleri reviewed

indirect techniques, which use "surrogate reactions" by the Trojan horse method, to estimate rates of very low energy reactions like ^{6}Li+n and ^{17}O + n. In particular the reaction ^{18}F(d,α^{15}O)n, which is the first application of the method using a radioactive beam at RIKEN, was illustrated. An important reaction of astrophysical interest is the two-proton decay from excited states in ^{18}Ne, for which Enrico Maglione presented a microscopic shell-model calculation of the sequential process, showing the possibility to assign the angular momentum and parity of specific high energy excited states in ^{18}Ne. These states are very narrow, and prefer to decay by one proton emission to the excited states of the daughter ^{17}F, rather than to the ground state. Since at these energies proton decay is faster than γ-decay, the nucleus prefers to emit sequentially the second proton to reach ^{16}O, instead of a photon that would lead to bound states of ^{17}F.

Beta-decay (K. Riisager)

Karsten Riisager reviewed the present status of beta decay studies for light dripline nuclei. Beta-delayed multi-particle emission is energetically allowed only close to the driplines. It is of course also of interest in other nuclei since it proceeds via highly excited states in the daughter nucleus and can give unique physics information: particle emission can populate many more states than the ones allowed by beta-decay spin-parity selection rules. Thus several types of experiments will with our present experimental techniques require long beam times and/or significantly increased intensities of the radioactive beams. This can be due to very small branching ratios of the interesting physics or due to inherent low detection efficiency, e.g. neutron detection with accurate time-of-flight (this applies even more if one attempts to do neutron coincidences) or gamma-detection with crystal spectrometers. Thus facilities like EURISOL will be necessary for progressing in the field.

Unbound nuclei (H. Simon)

Nuclei at and beyond the dripline are one of the more interesting aspects of physics of light exotic nuclei. They live as resonance states in a similar way as elementary particles. They can be obtained by different reaction mechanisms such as neutron transfer to the continuum from a deuteron target or projectile fragmentation of an exotic bound nucleus. The goal is

to establish the ordering of the levels, their resonance energies and angular momenta. This field still needs detailed studies to establish a correct understanding of the reaction mechanisms; the best observables to be measured and a method to extract unambiguously structure information from the data. In particular the interplay between initial and final state, which is well understood in transfer reactions, still need to be clarified in projectile fragmentation reactions. Haik Simon reviewed these topics.

Conclusions

Structure investigations of exotic nuclei started almost thirty years ago with the study of very light nuclei. They still constitute a very interesting field, in which challenging "ab initio" methods have been developing and will lead to the unification of structure and reaction models. This path will clarify also the clustering phenomena appearing as threshold effects. Besides the bound exotic nuclei we are now able to study unbound nuclei just across the drip-line. They represent another open field of research, in which experimental techniques and theoretical models have to be developed further. Some unbound nuclei are sub-constituents of borromean nuclei. Here the three-body description of the system asks for a very accurate knowledge of the neutron-core and neutron-neutron interactions. Direct peripheral reactions and their influence on elastic scattering and fusion plus particle decay studies together with the shell model will help obtaining such knowledge. Nuclear astrophysics, the kingdom of "free and ever lasting exotic nuclei" will benefit from all such progress. Last but not least beta-decay experiments and related models, from which and for which radioactive beams were first developed will continue to be of fundamental importance and often the only mean to study high lying excited states.

Local Organizing Committee

Ricardo Augusto (IST, Lisbon, Portugal)
Lidia Ferreira (IST, Lisbon, Portugal - Chair)
Isabel Lopes (LIP, Coimbra, Portugal)
Yuriy Romanets (ITN/IST, Lisbon, Portugal)
Pedro Vaz (ITN/IST, Lisbon, Portugal)

Advisory Committee

Dieter Ackermann (GSI, Darmstadt, Germany)
Vítor Amaral (Uni. Aveiro, Portugal)
Bertram Blank (CEN, Bordeaux, France)
Yorick Blumenfeld (CERN, Geneve, Switzerland)
Angela Bonaccorso (INFN, Pisa, Italy)
Raquel Crespo (CFNUL and IST, Lisbon, Portugal)
Lidia Ferreira (IST, Lisbon, Portugal)
Hans Fynbo (Uni. Aarhus, Denmark)
João Guilherme Correia (ITN/IST, Lisbon and CERN)
Ari Jokinen (Uni. Jyvaskyla, Finland)
Marek Lewitowicz (Ganil, Caen, France)
Adam Maj (Inst. Nucl. Phys., Kraków, Poland)
Paddy Regan (Uni. Surrey, Great Britain)

Programme Topical Meeting

Monday, 15th October 2012

(Amphitheatre "Complexo Interdisciplinar")

13:00 - **Registration**

14:15 - **Opening**

Chairperson: Lídia Ferreira (IST)

14:30 - **Maria J.G. Borge** (ISOLDE, CERN) *"Influence of the halo structure in the scattering with heavy targets at energies below and around the Coulomb barrier"*

15:00 - **Pierpaolo Figuera** (INFN, LNS, Catania) *"Collisions induced by halo nuclei: what did we learn from elastic scattering experiments?"*

15:30 - **Paulo Gomes** (Univ. Fed. Fluminense, Niteroi) *"Fusion, transfer and breakup of light weakly bound and halo nuclei at near barrier energies"*

16:00 - **Coffee Break**

Chairperson: Maria Borge (ISOLDE,CERN)

16:30 - **Giorgio Baiocco** (Univ. and INFN, Bologna, and LPC Caen) *"Towards a Reconstruction of Thermal Properties of Light Nuclei from Fusion-Evaporation Reactions"*

16:50 - **Alison Laird** (York Univ.) *"Explosive nucleosynthesis with ISOL beams"*

17:20 - **Achim Schwenk** (TU Darmstadt and EMMI) *"Three-nucleon forces and exotic nuclei"*

17:50 - **Raul de Diego** (CFNUL, Lisbon) *"Dynamic core excitation effects in the scattering of halo nuclei"*

18:10 - **Hugo F. Arellano** (U. of Chile, Santiago) *"Discontinuity of the BBG self-consistent solutions and its role in low energy elastic scattering"*

18:30 - **End of session and Welcome drink**

Tuesday, 16th October 2012

(Amphitheatre "Complexo Interdisciplinar")

Chairperson: Hans Fynbo (Univ. Aarhus)

9:00 - **Marek Ploszajczak** (CEA, Caen) *"On the origin of nuclear clustering"*

9:30 - **Hans Feldmeier** (GSI, Darmstadt) *"Clusters, Halos and S-Factors in Fermionic Molecular Dynamics"*

10:00 - **Marlene Assie** (IPN Orsay, France) *"Study of pairing in light nuclei and clusterization through nuclear break-up"*

10:20 - **Coffee Break**

10:40 - **Alexandre Obertelli** (CEA, Saclay) *"Direct reactions with exotic nuclei"*

11:10 - **Claudio Spitaleri** (INFN, Catania) *"Reaction induced by neutron on RIB via Trojan Horse Method"*

11:40 - **Raquel Crespo** (IST, Lisbon) *"Breakup of Halo nuclei on a proton target"*

12:10 - **Lunch**

Chairperson: Adam Maj (IFJ PAN)

14:00 - **Pierre Descouvemont** (Univ. Libre Brussels) *"Theoretical models for reactions involving exotic nuclei"*

14:30 - **Carlo Barbieri** (Univ. Surrey, UK) *"Toward an Ab-Initio Description of Exotic Open-Shell Isotopes"*

15:00 - **Christian Forssen** (Univ. Chalmers, Gothenburg, Sweden) *"Ab initio approach to the structure of light nuclei"*

15:30 - **Coffee Break**

16:00 - **Angelo Signoracci** (CEA/SACLAY-IRFU) *"The future of shell model techniques"*

16:30 - **Nicola Lo Iudice** (Universita' di Napoli, Italy) *"Study of the Pygmy Resonance within a New Microscopic Multiphonon Approach"*

17:00 - **End of session**

Wednesday, 17th October 2012

(Amphitheatre "Complexo Interdisciplinar")

Chairperson: Angela Bonaccorso (INFN, Pisa)

9:00 - **Takashi Nakamura** (TITEC, Tokyo) *"Spectroscopy of nuclei near and beyond the neutron drip line by direct reactions at new-generation RI beam facilities"*

9:30 - **Karsten Riisager** (Aarhus Univ., Denmark) *"Beta-decay in light dripline nuclei"*

10:00 - **Haik Simon** (GSI, Darmstadt) *"Stepping stones across the dripline"*

10:30 - **Coffee Break**

11:00 - **Giuseppe Cardella** (INFN, Catania) *"Study of light exotic nuclei with CHIMERA detector at LNS"*

11:20 - **Enrico Maglione (**Padova, Italy) *"The resonances of 18Ne"*

11:40 - **Daniel Galaviz** (CFNUL, Lisbon, Portugal) *"Neutron breakup reactions on light nuclei around the Quasi-Free Scattering limit"*

12:00 - **Bjorn Jonson** (Chalmers, Gothenburg) *"Summary talk"*

12:30 - **Closing**

Influence of the halo structure in the scattering with heavy targets at energies around the Coulomb barrier

M. J. G. Borge[a,b]

[a]*Instituto de Estructura de la Materia, CSIC, Serrano 113bis, 28006-Madrid, Spain.*
[b]*PH-ISOLDE, CERN, 1211-Geneva 23, Switzerland*

INTRODUCTION

Twenty five years ago, Hansen and Jonson [1], interpreted the large interaction cross section with light targets observed in some neutron rich light nuclei [2] as due to the high probability of the outermost nucleons to be at large distances from the central core. They referred to thus system as a halo structure. The halo structure is a threshold phenomenon due to the low binding energy of the last nucleons. Halo nuclei have several features in common, such as a rather compact core, an extended nucleon distribution and very few excited states, if any. The discovery of halo nuclei brought renewed interest in the modelling of nuclear reactions. This peculiar structure should affect the reaction properties at near Coulomb barrier energies. Due to the low blinding energy of the last nucleons, it is expected that the description of the reactions involving the halo nuclei should incorporate the coupling to the continuum.

Due to the loosely bound structure, the neutron halo is easily polarizable in the strong electric field of a heavy target such as ^{208}Pb, in contrast to normal nuclei, where the E1 response is dominated by the giant dipole resonance. The paradigm of the two-neutron halo nuclei is ^{11}Li with S_{2n}=369.15(65) keV [3]. The ground state density distribution of ^{11}Li extends well beyond its core, i.e., the rms matter radius for ^{11}Li is 41% larger than for the closest bound isotope, ^{9}Li. In fact strong E1 transition was observed at low excitation energy in an exclusive measurement of the Coulomb dissociation of ^{11}Li at 770 MeV at RIKEN [4]. Very large B(E1) values where also measured for the archetype of the one-neutron halo ^{11}Be where both the ground state and the only bound excited state have halo structure with S_n=501.19(58) keV and S_n=181.19(58) keV, respectively.

When the halo nucleus scatters with a heavy target, it will be strongly polarized due to its large E1 strength, giving rise to long-range Coulomb couplings. According to [5] this effect should manifest itself at Coulomb barrier energies as a departure from the elastic Rutherford scattering. This deviation can shed light on the structure as well as how the scattering process depends on the coupling to the continuum. The interplay of two effects will occur. First, the Coulomb break-up reduces the elastic cross section. Second, the distortion of the wave function generated by the displacement of the charged core with respect to the centre of mass of the nucleus reduces the Coulomb

repulsion, and thus the elastic cross sections. This phenomenon has been previously observed in the scattering of ^{6}He on ^{208}Pb [6,7] and it is even stronger for ^{11}Li + ^{208}Pb due to the larger E1 of ^{11}Li [8]. Furthermore, at small angles the amount of the deviation is proportional to the B(E1) strength at low excitation energies. Since the B(E1) is very sensitive to the model used to describe the halo nucleus structure, a precise analysis of the elastic scattering can shed light on the structure of the halo nucleus. Consequently, the study of the scattering of the halo nucleus at low energies on the intense electric field created by a high Z target can reveal new features of halo nuclei, and provide complementary information to that obtained at higher energies. Figure 1 illustrates the scattering process of the 2n-halo ^{11}Li and 1n-halo ^{11}Be.

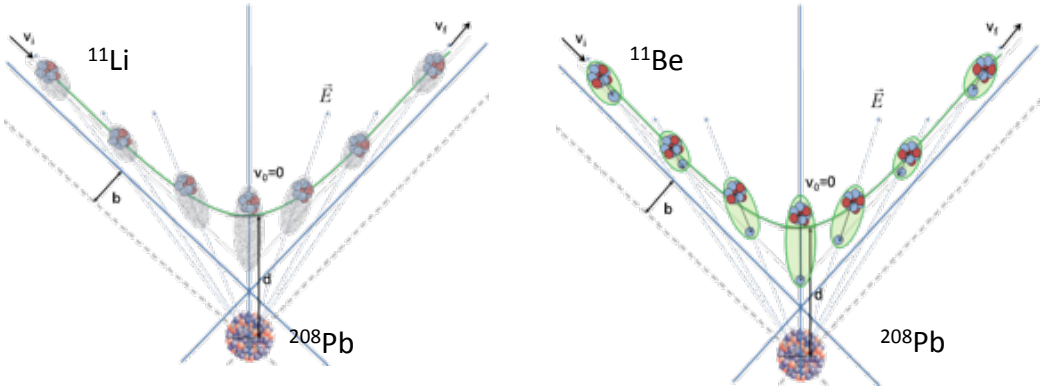

FIGURE 1. Illustration of the scattering process of a 2n-halo and 1n-halo nuclei on a heavy target at energies close to the Coulomb barrier. The intense electric field is mainly sensed by the core producing a shift of the charge away from the center of mass. This creates a dipole moment of the nucleus in the direction of the field. Courtesy of Mario Cubero.

RESULTS

A series of experiments has been done at different facilities (CRC, ISOLDE and TRIUMF) to study the behaviour of the scattering of the halo nuclei ^{6}He, ^{11}Li and ^{11}Be on a double magic high Z nucleus such as ^{208}Pb. To understand the influence of the neutron skin on the scattering process ^{8}He + ^{208}Pb was also investigated in this case at GANIL. Figure 2 shows the setups used in the different experiments. The intensity of the different beams determined the complexity and granularity of the setup used. Even with intensities as low as a few thousand per second, as it was the case for the ^{11}Li beam, the angular distribution of the scattering process was studied down to 140º with angular resolution better than 5º degrees. In all cases the study allowed to separate the elastic from the breakup channels in a certain angular range. The simplest case from the theoretical point of view, ^{11}Be + ^{208}Pb, was at the same time the most difficult one experimentally, since ^{11}Be had an excited state at 320 keV and the difference in masses of the elastic and breakup ejectiles was the smallest. The experimental results for the ^{11}Li + ^{208}Pb case have been interpreted using the 4-body Continuum-Discretized Coupled-Channel calculations.

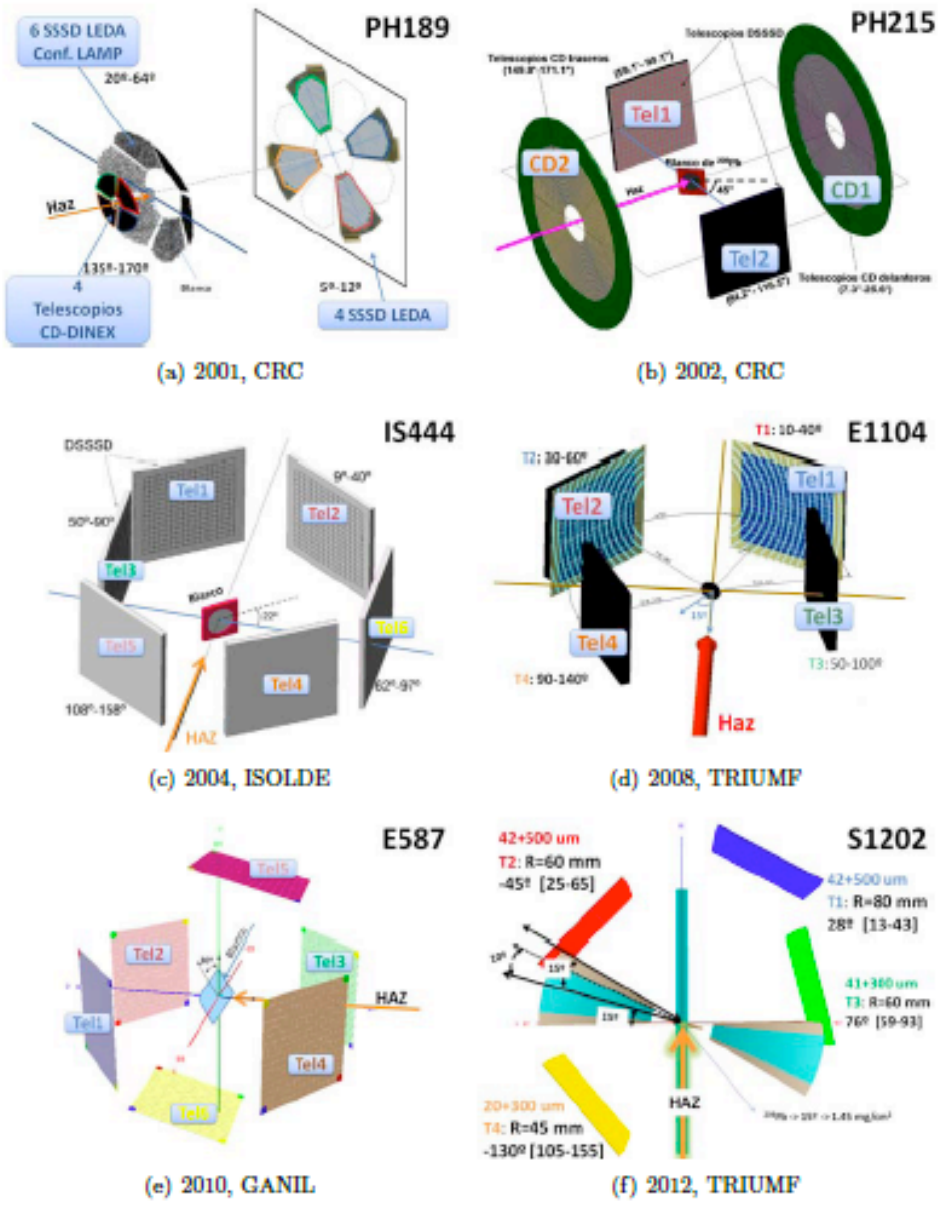

FIGURE 2. Illustration of the different experiments and setups used by our collaboration to study the scattering process of the nuclei ^{6}He + ^{208}Pb (CRC 2001 [6,9] and 2002 [10]), ^{11}Be + (^{64}Zn & ^{120}Sn) (ISOLDE 2004 [11 & 12], ^{11}Li (TRIUMF 2008 [8,13]), ^{8}He + ^{208}Pb (GANIL 2010 [14]), and ^{11}Be + ^{208}Pb at energies close to the Coulomb barrier. Telescopes were used in these inclusive studies to mass separate the elastic from the breakup channels. The angular coverage was mainly determined by the low intensity of the incoming beam and available beam time.

The departure from Rutherford scattering at energies below the barrier is well beyond the expected behaviour. The B(E1) probability is defined as the ratio of the breakup events divided by the sum of the elastic plus breakup ones. Theoretical calculations suggest that these are the dominant channels, with negligible contribution from the rest, at least for the cases of ^{6}He and ^{11}Li reactions on lead. For the case of ^{11}Li +

^{208}Pb, it is found that the breakup channel is significant at angles as small as 14º degrees even at energies well below the barrier (24.3 MeV) being the breakup branch comparable to the elastic channel for angles beyond 90º, see figure 3. The energy distribution of the breakup ejectile indicates that for ^{6}He on lead the dominant process at intermediate angles is 2n-tranfer while for ^{11}Li on lead the breakup is mainly direct. Certainly a measurement at forward angles for the ^{6}He + ^{208}Pb reaction near the Coulomb barrier is desirable to confirm or reject this difference in breakup process. This difference can be due to the fact that the B(E1) is more reduced in ^{6}He and that threshold of B(E1) occurs at low energy in ^{11}Li.

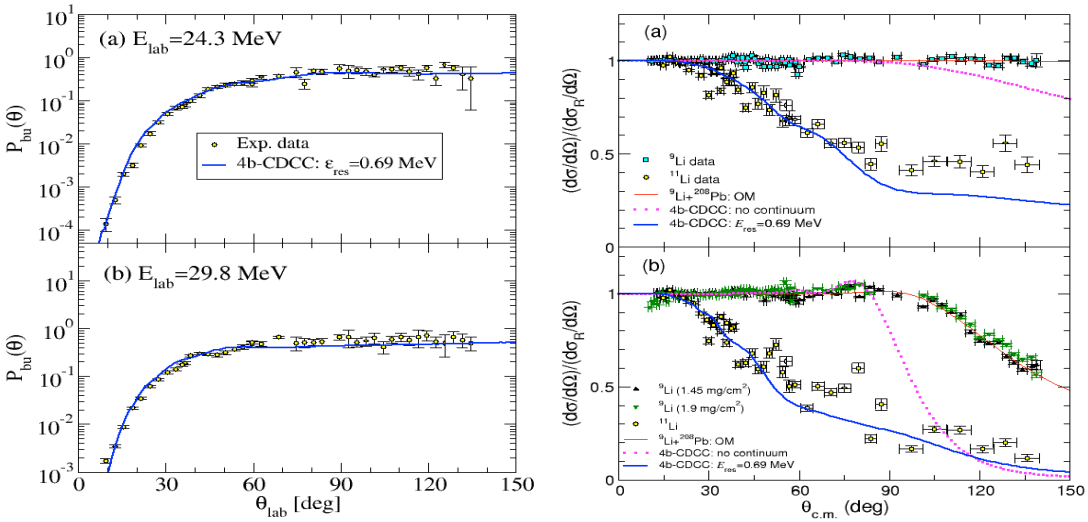

FIGURE 3. On the left hand side it is shown the breakup probability distribution of ^{11}Li + ^{208}Pb at energies below (24.3 MeV)(a) and above (29.8 MeV)(b) the Coulomb barrier. Figure taken from [13]. Form the same incoming beam energies the differential elastic cross section divided by Rutherford is shown both for ^{11}Li + ^{208}Pb and its core ^{9}Li + ^{208}Pb measured in the same experiment. Notice the spectacular difference in elastic cross section for ^{11}Li and ^{9}Li. Taken from [8].

The breakup probability data shed light on the effective breakup energy as well as on the slope of the B(E1) distribution close to the breakup threshold. The differential elastic cross section and the breakup probabilities are reasonable well described by the four-body version of continuum discretized coupled channel method (CDCC) [15], in which the projectile is described as a three-body system and the continuum states of the projectile are included up to a certain angular momentum and excitation energy. The breakup probability data shed light on the effective breakup energy as well as on the low-lying behaviour of the B(E1) distribution. The break-up at small angles is due to Coulomb couplings. This allowed for a description of the breakup probability by the semi-classical Coulomb excitation theory. In this case, one can get a reduced breakup probability that is independent of the collision parameters and that allows to extract the B(E1) distribution near the energy threshold. This indicates that one can use the breakup probability from inclusive reactions to determine the nucleon separation energy for nuclei were it is not possible to determine it otherwise. This result obtained for the ^{11}Li case should be confirmed in the new data of ^{11}Be + ^{208}Pb currently under analysis.

SUMMARY AND OUTLOOK

The structure of exotic nuclei has many surprises. The low binding of the last nucleons typical of systems near the drip line profoundly affect their scattering properties at energies near the coulomb barrier where the interaction is slow enough to probe the structure of the projectile. In these studies a double magic nucleus of high Z was chosen as target to facilitate the interpretation of the results since is this particular case the structure of the target can be disregarded.

The elastic scattering behaviour deviates strongly from the Rutherford scattering formula. Very high breakup probability is found even at energies well below the Coulomb barrier. The scattering process can be described in the framework of 4-body CDCC. The study of ^{11}Be will challenge the theory as elastic, inelastic and breakup channels should be simultaneously described. Further the scattering of neutron skin nuclei such as ^{8}He + ^{208}Pb is very challenging as some of the approaches done here are not valid.

With the advent of more intense beams it would be possible to do a systematic study of the scattering of halo nuclei in the full angular range with detailed determination of the energy distribution of the breakup products. It is important to understand the dominant breakup process and be able to explain why in the ^{6}He + ^{208}Pb dispersion dominates the two-neutron transfer while in the ^{11}Li + ^{208}Pb case the direct breakup is the main process. Higher intensities will allow for an extension of the studies to nuclei of higher masses. The dipolarizability effect could be affected if the nucleus besides the loosely bound nucleons has a cluster structure in the core. Extensive elastic scattering studies of light nuclei with extreme structures near the Coulomb barrier is of great importance for the future.

REFERENCES

1. P. G. Hansen and B. Jonson, *Euro. Phys. Lett.* **4**, 409- (1987).
2. I. Tanihata et al., *Phys. Rev. Lett.* **55**, 2676- (1985).
3. M. Smith et al., *Phys. Rev. Lett*. **101**, 202501 (2008).
4. T. Nakamura et al., *Phys. Rev. Lett*. **96**, 252502 (2006).
5. M. V. Andrés and J. Gómez-Camacho, *Phys. Rev. Lett*. **82**, 1387 (1999).
6. A. M. Sánchez-Benítez et al., *Nuc. Phys*. **A803**, 30-45 (2008).
7. O.R. Kakuee et al., *Nuc. Phys*. **A765**, 294 (2006).
8. M. Cubero et al., *Phys. Rev. Lett* **A109**, 262701 (2012).
9. D. Escrig et al., *Nuc. Phys*. **A792**, 2-17 (2007).
10. L. Acosta et al., *Phys*. Rev. **C84**, 044604 (2011).
11. A. Di Pietro et al., *Phys. Rev. Lett* **A105**, 022701 (2010).
12. L. Acosta et al., *Eur. Phys. J.* **A42**, 461 (2009), erratum *Eur. Phys. J.* **A42**, 623 (2009).
13. J. P. Fernández-García et al., *Phys. Rev. Lett* **,** *accepted* (2013).
14. G. Marquinez-Duran et al., *Acta Phys. Pol.* **B43**, 239 (2012) & **B44**, 467 (2013).
15. M. Rodríguez Gallardo et al., *Phys*. Rev. **C80**, 051601(R) (2009).

Collisions Induced By Halo And Light Exotic Nuclei: What Did We Learn From Elastic Scattering ?

Pierpaolo Figuera[a]

[a]*INFN Laboratori Nazionali del Sud, Catania, Italy .*

INTRODUCTION

The study of collisions induced by halo or, more in general, weakly bound exotic nuclei has been object of many publications in the last years. In fact, it has been shown that the peculiar structure of such nuclei, which have very low break-up thresholds and an extended matter distribution in the case of halo nuclei, can strongly affect the dynamics of the collision (e.g. [1] and references therein). For such projectiles, one expects a large contribution of direct processes like breakup or transfer, moreover coupling to continuum effects are also expected to be important. As a consequence, elastic scattering angular distributions for halo and weakly bound nuclei are strongly affected by the structure of the projectiles (e.g. [2] and references therein). Most of the available experimental data have been analyzed within the Optical Model (OM) or within the Continuum Discretized Coupled Channel (CDCC) approach. In the OM framework a Dynamic Polarization Potential (DPP) has often been added to include coupling effects. Since coupling to continuum originates a repulsive DPP (e.g. [3]) the usual Threshold Anomaly (TA) in the Optical Potential (OP) may disappear. Such an absence of the usual TA in the OP has been observed for collisions induced by several stable and radioactive weakly bound projectiles (see e.g. [1,4,5]) and was named 'breakup threshold anomaly' in the literature.
In the next section an overview of results for elastic scattering of halo nuclei will be presented.

SCATTERING OF HALO NUCLEI

Elastic scattering with halo nuclei has been measured on a wide range of energies and target masses. Most of the data are relative to ^{6}He scattering, since this beam has been available for long time, at different RIB facilities, with reasonable currents.

Scattering of halo nuclei on heavy targets has been measured for different systems at energies around the Coulomb barrier, showing a very strong suppression of the elastic angular distribution in the region of the Coulomb nuclear interference peak. ^{6}He+^{208}Pb scattering was measured at different energies around the barrier [6,7], and

showed a suppression in the region of the Coulomb nuclear interference peak when compared with alpha scattering [8] at the same energy, indicating the presence of long range absorption for ^{6}He. OM analysis of the data failed to reproduce them when using a Woods-Saxon potential having the same geometry as the one given by global parameters for ^{6}Li scattering, allowing to reproduce the data only using very large imaginary diffuseness. The inclusion of a DPP, taking into account coupling to inelastic and breakup via the Coulomb dipole interaction, shows that this effect is important but is not the only one suppressing the elastic yield. Somehow similar results were observed for ^{6}He scattering on other heavy targets such as for instance ^{197}Au [9]. The ^{6}He scattering data on ^{208}Pb and ^{197}Au were also reproduced within the CDCC approach in [6,10]. ^{11}Li+^{208}Pb elastic scattering around the Coulomb barrier was reported in [11] and compared with the scattering of ^{9}Li on the same target. A huge suppression of the ^{11}Li elastic angular distribution with respect to the ^{9}Li one, much larger than the one observed for ^{6}He, was found. CDCC calculations confirm that, also for this system, coupling to continuum via the Coulomb dipole interaction gives an important contribution to the disappearance of the Coulomb nuclear interference peak.

Very few experiments have been performed concerning elastic scattering of halo nuclei on medium mass targets. In [12] the elastic scattering for ^{6,4}He+^{64}Zn was measured at energies around the Coulomb barrier. Two main features were observed: a) the total reaction cross section for ^{6}He is much larger (about a factor two) than the one for ^{4}He; b) the Coulomb nuclear interference pattern is reduced although not as much as it was observed for heavy targets. In subsequent papers [e.g. 10] these ^{6}He scattering data were reproduced within the CDCC approach confirming the importance of coupling to continuum effects. In [13] the ^{11,10}Be+^{64}Zn elastic scattering was measured at E_{cm} = 24.5 MeV. A suppression of the elastic angular distribution in the region of the Coulomb nuclear interference peak, much stronger than the one observed in the ^{6}He case on the same target, was observed for ^{11}Be.

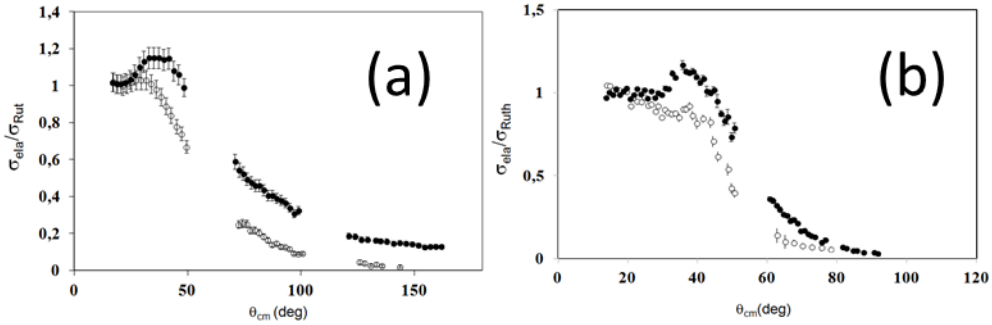

FIGURE 1. (a) Elastic scattering angular distributions for the collisions ^{6}He+^{64}Zn (open symbol) and ^{4}He+^{64}Zn (closed symbols) at the same Ecm. (b) As (a) but for the collisions ^{11}Be+^{64}Zn (open symbols) and ^{10}Be+^{64}Zn (closed symbols). In both figures one observes, for the halo nucleus case, a suppression of the elastic cross section which has been explained as due to coupling effects to the continuum.

Data have been reproduced within the OM using as bare potential the one that reproduces ^{10}Be scattering, and adding a phenomenological DPP having the shape of a

Woods-Saxon derivative. A good fit was obtained with a DPP having a large diffuseness of the order of 3.5 fm in agreement with [14]. On the contrary, the use of a theoretical DPP taking into account coupling to inelastic and breakup via the Coulomb dipole interaction failed to reproduce the data. Indeed the ^{11}Be data were also reproduced within the CDCC frame, showing that the suppression of the Coulomb nuclear interference peak is due to the combined effect of Coulomb and nuclear couplings to continuum.

The collision dynamics for p-halo nuclei is expected to be different than the one for the n-halo case, since the proton in the halo feels the Coulomb interaction; unfortunately only very limited information is available for p-halo scattering at near barrier energies [15,19]. Scattering of the p-halo nucleus ^{8}B on ^{58}Ni has been measured at energies close to Coulomb barrier in [15]. The data have been reproduced within the OM, using phenomenological Woods-Saxon potentials, finding an enhancement in total reaction cross section similar to the one observed for neutron halo nuclei.

Contrary to what happens on heavier targets, with light targets the effect of Coulomb breakup is expected to be smaller, therefore continuum coupling effects are mainly due to nuclear couplings. Elastic scattering angular distributions for ^{6}He on ^{6,7}Li and ^{12}C can be found in [16,17]. Scattering data on ^{6,7}Li were reproduced using global OM potential parameters obtained for reactions induced by ^{6}Li on the same targets, while for scattering on ^{12}C the OP parameters used were the ones for ^{6}Li+^{12}C at similar energies. Such result is very different from what observed in ^{6}He+^{208}Pb scattering [7], where attempts to reproduce the data, using an OP having the same shape as the one predicted by a ^{6}Li scattering systematics, failed to reproduce the experimental results. Scattering of ^{6}He on ^{27}Al was measured in [18] around the Coulomb barrier. The authors extracted total reaction cross sections performing OM fits and concluded that they had similar values as the ones for collisions induced by stable weakly bound nuclei on the same target. Elastic scattering of the p-halo ^{8}B on ^{12}C was measured in [19]. CDCC calculations showed that the effect of coupling to continuum for this systems is very weak. Reduced total reaction excitation functions for ^{8}B,^{6}He and other light weakly bound nuclei such as ^{6,7,8}Li, ^{7}Be on ^{12}C are rather similar, a result which is different from what observed for halo nuclei on heavier targets.

Elastic scattering at intermediate energies has been measured for halo nuclei on light targets. As an example, elastic scattering data for ^{6}He+^{12}C at 38 MeV/nucleon and for ^{11}Be+^{12}C at 49 MeV/nucleon and associated OM and CDCC calculations, are reported and discussed in [e.g. 20,21,22,14]. Both these data sets showed effects due to coupling to continuum and were reproduced within the CDCC frame and within the OM using different polarization potentials taking into account coupling to continuum effects.

SUMMARY AND CONCLUSIONS

Elastic scattering with halo nuclei has been measured in different energy and target mass ranges, and some common features can be found. In low energy scattering, a

partial or total suppression of typical Frenel-like oscillations is observed with a strong increase of total reaction cross section. Such features appear to be less pronounced for the scattering on very light targets. Experimental data have been reproduced taking into account coupling to continuum including DPPs in the OM approach or with CDCC calculations. Coupling to continuum effects are also evident in intermediate energy scattering.

Although presently available results start to show some common features, most of available data are with ^{6}He beams and, in some cases, the results are limited by poor beam quality. Therefore, additional data with different good quality beams, including p-halo ones, are needed to build a wider systematics and allow a deeper understanding of the discussed topic.

Before closing our discussion on elastic scattering with light exotic nuclei, we would also like to mention that several resonant elastic scattering experiments with the thick target technique in inverse kinematics allowed to measure with low beam currents, typical of RIBs, high quality elastic excitation functions, whose analysis allowed to extract spectroscopic information on unbound states[see e.g. 23-25].

In summary, hundred years after Rutherford experiment, elastic scattering is still a useful promising 'tool' to provide us valuable information on nuclear structure and reaction dynamics.

REFERENCES

1. L.F.Canto et al., Phys. Rep. 424, 1, (2006)
2. N.Keeley et al., Prog. Part. And Nucl. Phys. 63, 396, (2009)
3. Y. Sakuragi, Phys. Rev. C35, 2161, (1987)
4. A.R. Garcia et al., Phys. Rev. C76, 067603, (2007)
5. A.Gomez Camacho et al., Nucl. Phys. A833, 156, (2010)
6. L. Acosta et al.: Phys. Rev. C 84, 044604 (2011)
7. A. M. Sanchez Benitez et al., Nucl. Phys. A803, 30, (2008)
8. A. R. Barnett et al., Phys. Rev. C9, 2010, (1974)
9. O.R. Kakuee et al., Nucl. Phys. A765, 294, (2006)
10. A.M. Moro et al., Phys. Rev. C75, 064607, (2007)
11. M. Cubrero et al., Phys. Rev. Lett. 109, 262701, (2012)
12. A. Di Pietro et al.: Phys.Rev.C 69,044613,2004
13. A. Di Pietro et al., Phys. Rev. C 85, 054607 (2012)
14. A.Bonaccorso et al., Nucl. Phys. A706,322,(2002)
15. E.Aguilera et al., Phys. Rev. C79, 021601, (2009)
16. M.Milin et al., Nucl. Phys. A 746,183,(2004)
17. M.Milin et al., Nucl. Phys. A 730,285,(2004)
18. E.A. Benjamin et al.: Phys. Lett. B 647, 30, (2007)
19. A. Barioni et al., Phys. Rev. C84, 014603, (2011)
20. V.Lapoux et al., Phys. Rev. C66, 034608, (2002)
21. M.Takashima et al., Phys. Rev. C67, 037601, (2003)
22. T. Matsumoto et al., Phys. Rev., C70, 061601(R), (2004)
23. M. Freer et al., Phys. Rev. Lett. 96, 042501, (2006)
24. C.Angulo et al., Nucl. Phys. A716, 211,(2003)
25. D.W. Lee et al., Phys Rev C76,024314, (2007)

Fusion, Transfer and Breakup of Light Weakly Bound and Halo Nuclei at Near Barrier Energies

P. R. S. Gome and J. Lubian

Instituto de Física, Universidade Federal Fluminense, Av. Litoranea s/n, Niteroi, R.J., 24210-340, Brazil

The effect of the breakup of weakly bound nuclei, both stable and radioactive, on the fusion cross section has been a subject of great interest in the last years [1, 2, 3]. Several systems have been studied, both theoretically and experimentally, including stable weakly bound (^{6,7}Li, ^{9}Be) and radioactive projectiles, like ^{6,8}He, ^{7,11}Be, ^{8}B and ^{17}F, on different targets. The basic question is whether the breakup process enhances or hinders the fusion cross section. The first point to make on this subject is to be clear about enhancement or suppression in relation to which reference. Also, different breakup effects may occur, like static and dynamic effects. The first is caused by the longer tail of the optical potential, owing to the low binding energies of the weakly bound and specially halo nuclei. This effect gives rise to lower and thicker barriers when compared with tightly bound systems, and enhances fusion cross section at near-barrier energies (not too much below the barrier) [4, 5]. This effect, we believe, is no longer a matter of discussion. The second kind of effect is the dynamic, which is due to the strong coupling between the elastic channel and the continuum states representing the breakup channel. This is a much more complex effect to be predicted. In any situation, if one compares data with theoretical predictions, the choice of the bare interacting potential plays a major role, and contradictory conclusions can be drawn with the same data set depending on the potential used. If one uses double folding potentials with realistic densities of the colliding nuclei as the bare potential, the possible static effects of the weakly bound nuclei, specially halo nuclei, are already taken into account, and so the differences between data and calculations show only the dynamic effects of the channels not included in the calculations. Recently Canto et al. [4] proposed the use of dimensionless quantities, which appropriately eliminates static effects, as a procedure to investigate dynamic effects on the fusion cross sections due to the breakup couplings. Furthermore, the proposed method allows reaching a systematic understanding of this subject, since it allows the comparison of any kind of system in the same graphic. This method uses a benchmark curve, called the Universal Fusion Function (UFF), given by $F_0(x) = \ln [1 + \exp(2\pi x)]$, where $x = (E\text{-}V_B) / \hbar\omega$ and $F(x) = (2 E_{c.m.} / \pi R^2_B \hbar\omega) \sigma_{fus}$. $\hbar\omega$ is related to the barrier curvature, σ_{fus} is the fusion cross section and $F(x)$ is called fusion function. The differences between the experimental fusion functions and UFF curve are dynamic effects due to the channels

left out of the coupled channel calculations, in this case, breakup and transfer reactions.

With this method, preliminary systematic behaviors of fusion cross sections were obtained [4, 6], by considering the available data for a large number of weakly bound systems. Complete fusion of stable weakly bound nuclei show suppression at energies above the barrier and enhancement below the barrier. Total fusion for those systems coincides with the benchmark UFF curve at energies above the barrier. For neutron halo systems, the measured total fusion cross sections show suppression above the barrier and enhancement at sub-barrier energies. For the "proton halo" $^{17}F + ^{208}Pb$ system (^{17}F is halo only in its first excited state) [7], the fusion cross section coincides with UFF at energies above the barrier. One may ask whether all systems involving exotic nuclei follow these systematic. The answer is no, since a few of them do not follow the behaviors mentioned above. The total fusion of $^{6}He + ^{197}Au$, for which the systematic says that it should be suppressed at energies above the barrier, does not show any effect [8] and the sub-barrier fusion of $^{6}He + ^{206}Pb$ [8] has a completely anomalous behavior. For proton-halo fusion, ^{8}B on ^{58}Ni [9], there is only one reported set of data, which is also the only one showing fusion enhancement at energies above the barrier. For $^{6}He + ^{206}Pb$, other measurements were performed [10] and the systematic behavior was found.

Figure 1 shows the comparison of fusion cross sections for radioactive projectiles in comparison with UFF. The linear scale is more appropriate to observe the effects above the barrier, whereas the usual logarithmic scale is better to investigate the sub-barrier energy regime. Data are from Ref. [7, 9, 10, 11, 12, 13, 14, 15]. It is very important to have more high precision data for fusion of radioactive nuclei, especially the exotic halo nuclei, to have a better understanding of the effect of couplings to continuum states produced by breakup and also couplings to transfer channels, which were shown to be very important for neutron-halo nuclei. So far, it seems that the behaviors of fusion of proton-halo and neutron-halo nuclei are very different.

Apart from the fusion of the ^{8}B nucleus, we understand the systematic behavior of the other weakly bound nuclei as the following, using the approach of energy dependent optical model and dynamic polarization potentials (DPP). Recent calculations [16, 17, 18] show that the direct breakup produces repulsive DPP, owing to the couplings among continuum breakup states (continuum-continuum couplings), which increases the barrier height and suppress fusion. On the other hand, there are recent experimental evidences [19, 20, 21] which show that breakup of stable weakly bound nuclei triggered by nucleon transfer may predominate over the direct breakup, at sub-barrier energies. So, the polarization potentials for each one should then be evaluated separately and the results summed. Thus, the suppression of complete fusion above the Coulomb barrier should result from the predominance of the DPP associated with direct breakup, whereas transfer and transfer followed by breakup, both producing attractive DPP, predominates at sub-barrier energies, especially for neutron-halo nuclei. The suppression above the barrier can also be explained by the so-called Breakup Threshold Anomaly (BTA) proposed by Hussein et al. [22]. Only very recently [23], the first calculation of DPP for the transfer followed by breakup, for the ^{7}Li weakly bound nucleus, showed that indeed, the corresponding DPP is attractive.

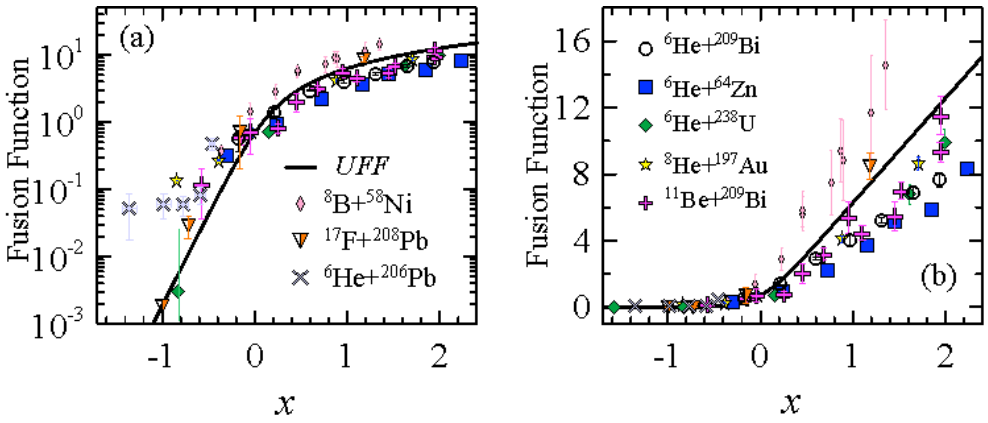

FIGURE 1. Experimental fusion functions for several neutron-halo, for the ^{17}F + ^{208}Pb and ^{8}B + ^{58}Ni systems. The curve is the UFF. X is a reduced energy parameter. See text for details.

REFERENCES

1. L. F. Canto, P.R. S. Gomes, R. Donangelo, M. S. Hussein, *Phys. Rep*. **424**, 1 (2006).
2. J. F. Liang, C. Signorini, *Int. J. Mod. Phys. E* **14**, 1121 (2005).
3. N. Keeley, R. Raabe, N. Alamanos, J.L. Sida, *Prog. Part. Nucl. Sci* **59**, 579 (2007).
4. L.F. Canto et al., J. Phys. G 36, 015109 (2009); *Nucl. Phys A* **821**, 51 (2009).
5. P.R. S. Gomes et al., *Phys. Lett. B* **695**, 320 (2011)
6. P.R.S. Gomes, J. Lubian, L.F. Canto, *Phys. Rev. C* **79**, 027606 (2009)
7. K.E. Rehm et al., *Phys. Rev. Lett*. **81**, 3341 (1998).
8. Y. E. Penionzhkevich et al., *Europ. Phys. J. A* **31**, 185 (2007)
9. E. F. Aguilera et al., *Phys. Rev. Lett*. **107**, 092701 (2011)
10. R. Wolski et al., *Europ. Phys. J A* **47**, 111 (2011)
11. A. Di Pietro et al., *Phys. Rev. C* **69**, 044613 (2004)
12. A. Lemasson et al., *Phys. Rev. Lett*. **103**, 232701 (2009)
13. R. Raabe et al., *Nature* **431**, 823 (2004)
14. J.J. Kolata et al., *Phys. Rev. Lett*. **81**, 4580 (1998)
15. C. Signorini et al., *Europ. Phys. J A* **5**, 7 (1999).
16. S. Santra et al., *Phys. Rev. C* **83**, 034616 (2011)
17. L. F. Canto et al., *Phys. Rev. C* **80**, 047601 (2009)
18. J. Lubian et al., *Nucl. Phys. A* **791**, 24 (2007).
19. D. H. Luong et al., *Phys. Lett. B* **695**, 105 (2011)
20. A. Shrivastava et al., *Phys. Lett. B* **633**, 463 (2006)
21. R. Rafiei et al., *Phys. Rev. C* **81**, 024601 (2010).
22. M.S. Hussein et al., *Phys. Rev. C* **73**, 044610 (2006).
23. P. R. S. Gomes et al., *J. Phys. G* **39**, 115103 (2012)

Towards a Reconstruction of Thermal Properties of Light Nuclei from Fusion-Evaporation Reactions

G. Baiocco[a,b], L. Morelli[a], F. Gulminelli[b], M. D'Agostino[a], M. Bruno[a], U. Abbondanno[c], S. Barlini[d,e], M. Bini[d,e], S. Carboni[d,e], G. Casini[e], M. Cinausero[f], M. Degerlier[g], F. Gramegna[f] , V. L. Kravchuk[f,h], T. Marchi[f,i] , A. Olmi[e] , G. Pasquali[d,e], S. Piantelli[e] and Ad. R. Raduta[l]

[a]*Dipartimento di Fisica ed Astronomia dell'Università and INFN, Bologna, Italy*
[b]*LPC (IN2P3-CNRS/Ensicaen et Université), F-14076 Caen cédex, France*
[c]*INFN Trieste, Italy*
[d]*Dipartimento di Fisica ed Astronomia dell'Università, Firenze, Italy*
[e]*INFN Firenze, Italy*
[f]*INFN, Laboratori Nazionali di Legnaro, Italy*
[g]*University of Nevsehir, Science and Art Faculty, Physics Department, Nevsehir, Turkey*
[h]*National Research Center "Kurchatov Institute", Moscow, Russia*
[i]*Dipartimento di Fisica ed Astronomia dell'Universit`a, Padova, Italy and*
[l]*NIPNE, Bucharest-Magurele, POB-MG6, Romania*

Introduction

This work addresses the topic of highly excited states for light α - clustered nuclei ($N = Z$ even - even nuclei). Dissipative nuclear reactions are chosen as a tool to investigate finite temperature properties for such nuclei. Through this kind of study we are interested in understanding to what extent the picture of an equilibrated compound nucleus holds in case of collisions between light nuclei, either when reaction partners are particle - stable nuclei, but with a subjacent cluster structure, or, in perspective, when dealing with exotic beams.

A great attention is paid to the exclusive nature of the proposed experimental study, which means aiming at the achievement of a (quasi)complete event reconstruction. A set of events corresponding to the fusion - evaporation process is selected out of the entire reaction cross-section, in order to extract information on the nuclear Level Density (*LD*). In order to put in evidence deviations from a statistical behavior we compare the outcome of the reaction to the predictions of a dedicated Monte Carlo Hauser-Feshbach (HF) decay code [1], highly constrained to existing data.

Few data coming from exclusive measurements exist altogether for $\rho(A, E^*, N/Z)$ in the chosen mass-excitation energy region: $A \sim 10$ - 20 and $E^* \sim 1$ - 3 A.MeV, already for stable systems. In this same region, inclusive measurements for fusion reactions involving loosely bound nuclei have put in evidence an entrance channel dependence in the outcome of the decay, but data could always be satisfactorily reproduced by statistical model calculations, if taking into account the renormalization of the *LD* parameter $a(A, E^*)$ and deformation at high angular momentum [2].

Available energies and intensities for radioactive beams in existing facilities make fusion - evaporation studies a difficult experimental challenge. When extending to more exotic nuclei, the dependence of the *LD* on the *N/Z* also comes strongly into play, which is currently a matter of debate. Finally, studying how cluster correlations (if persistent) are modified varying not only the temperature but also the isotopic content of (n * α) nuclei is for sure a perspective of great interest.

In this context the NUCL-EX collaboration has undertaken a series of reference studies on light stable nuclei at Laboratori Nazionali di Legnaro (LNL-INFN), in Italy, with the GARFIELD + Ring-Counter (RCo) experimental setup. Results for the first measurement: ^{12}C (at 95 MeV beam energy) + ^{12}C have been presented at the Eurisol Topical Meeting in Lisbon, 15th-19th October 2012, and are briefly reported hereafter.

The ^{12}C+ ^{12}C Experiment

The ^{12}C + ^{12}C reaction has been a widely studied case in the seek for nuclear molecular states, whose existence and decay are not subject to a statistical model description. Several interesting resonances have been observed for this reaction in the inelastic and α - transfer channel, suggesting that resonant structures persist in the ^{24}Mg system up to around 50 MeV excitation energy. At such a high excitation energy, a pure statistical behavior might be indeed expected due to the extremely high number of available states. This reaction is therefore the ideal case to understand whether α correlations may affect even more dissipative channels, typically associated to the compound nucleus formation and decay [3].

The reaction has been measured at a beam energy of 95 MeV at LNL, with the RCo + GARFIELD setup. More details on the apparatuses and experimental techniques can be found in [3,4]. In particular, for this measurement, the coincidence between a light charged particle (LCP) detected at GARFIELD angles ($30° \leq \theta \leq 150°$) (identified in charge and mass) and a residue detected in the RCo at forward angles ($5° \leq \theta \leq 18°$) (identified in charge) has been chosen as the experimental fusion - evaporation trigger, together with the request of the detection of the total charge available in the entrance channel ($Z_{tot} = 12$). HF code calculations have been performed for the complete fusion source, a ^{24}Mg compound nucleus excited at $E^*_{fus} = 61.4$ MeV, with even J values coming from a triangular distribution with a maximum of 12 $h/2\pi$.

Without selecting any specific residue a good model reproduction for global observables (charge distribution of reaction products, multiplicities) is achieved, but it is found that no unique choice on the *LD* model parameters can be done in order to reproduce at the same time protons and α particles energy spectra. In particular, the largest discrepancy is found for α's in coincidence with oxygen fragments.

In order to check if this discrepancy is linked to the dominance of α decay chains leaving a $Z = 8$ residue, we have performed a very exclusive study on triple (α - α - oxygen) coincidences. Having detected the total charge available in the entrance channel of the reaction, we can build for such events a Q-value spectrum, where the quantity Q_{kin} is given by the difference between the sum of all kinetic energies in the

outgoing channel and the beam energy. If, besides the charge, also the total mass of the entrance channel is collected (i.e. residue is $N = Z$), then Q_{kin} is the real reaction Q-value. This is the case of events of the type (α, α, $^{16}O_{gs/}^{*}$), which are classified as non - dissipative, since the associated maximum energy expense is on average $Q_{kin} \sim 6.5$ MeV, corresponding to the excitation of ^{16}O bound states. For measured $Q_{kin} < -15.7$ MeV events, the (n, α, α, ^{15}O) channel opens and the Q_{kin} distribution becomes continuous, because of the missing kinetic energy of the emitted neutron in the energy balance. Events of this kind are called dissipative.

In the comparison between data and calculations it is found that the statistical model largely underestimates the percentage of non - dissipative events, predicted to be the (9 ± 1)% with respect to the experimental (37 ± 5)% of all triple coincidences events. Given the low energy dissipation characterizing these events, this may be attributed to the contamination of direct (transfer / pick-up) reactions, in competition with fusion - evaporation in the experimental sample. More surprising is that, once these events are excluded from the analysis and the comparison to calculations is restricted among dissipative events, still a deviation from the expected statistical behavior can be observed. This discrepancy is found to be related to a branching ratio discrepancy for the channels with a single and with two α's in coincidence with an oxygen residue: the shape of the α energy spectrum is rather well reproduce by our calculations in both cases, but the sum of the two processes is not correctly reproduced. Experimentally, (63 ± 5)% of the total cross section for completely reconstructed dissipative decays with a α particle and an oxygen fragment in the outgoing channel is absorbed by (α, α, $^{16}O^{*}$) channels, where the oxygen is excited above its neutron emission threshold, while according to the theoretical predictions these channels should represent only (10 ± 1)% of this class of events. This findings indicate that cluster correlations associated to the $^{12}C + ^{12}C$ system persist up to higher center - of - mass energies than previously expected, leading to a non - statistical behavior in the decay of the highly excited ^{24}Mg.

Isotopic Distributions and Neutron Detection

The finding of a branching ratio discrepancy between data and calculations for the channel (n, α, α, ^{15}O) necessarily translates into a discrepancy concerning the oxygen isotopic distribution. Unfortunately, because of the low energy regime of heavier fragments, the information on their mass is not directly accessible in this experiment. However, due to the completeness of the detection, this information can be deduced by means of a calorimetry balance. In each event, the excitation energy can be estimated as:

$$E^{*}_{cal}(A_{res}) = \sum_{i}^{Nc} E_i^{CM} + N_n(A_{res}) \cdot \langle E_n^{CM} \rangle + Q(A_{res}) \quad (1)$$

where N_c (N_n) and E_i^{CM} ($\langle E_n^{CM} \rangle$) are respectively the charged products (neutron) multiplicity and their center - of - mass kinetic energies, and Q is the decay Q - value.

The average neutron energy can be estimated as the measured average proton energy with the subtraction of the Coulomb barrier. All other quantities involving neutrons entering Eq. 1 (n multiplicity and Q - value) are univocally determined once a hypothesis on the mass of the residue A_{res} is done. The mass minimizing the quantity $|E_{cal}^{*}(A_{res}) - E^{*}_{fus}|$, where E^{*}_{fus} = 61.4 MeV is the compound excitation energy from energy balance in the entrance channel, can be considered as the better estimate of the residue mass. Results for this procedure concerning the experimental oxygen isotopic distribution are shown in Fig. 1 for the whole set of selected events, and compared to calculations. A shift towards n - poorer oxygen isotopes is evident in the experimental sample with respect to statistical model expectations, even starting from N = Z reaction partners.

It is worthwhile to stress that the lack of neutron detection is the only uncertainty source in the energy balance of Eq. 1. Our procedure shows that n detection, combined with the completeness of the measurement, allows us to achieve the isotopic identification of low energy fragments, even without a time - of - flight measurement. In this sense, efforts on the development of new neutron detectors [5] should be undertaken, along with the advancement in the planning and running of exotic beam facilities.

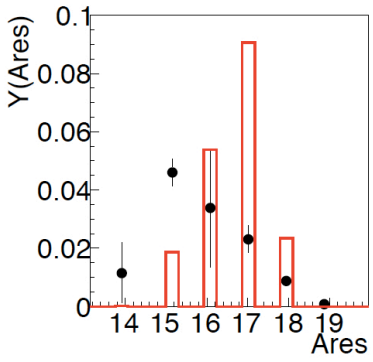

FIGURE 1. Reconstruction from experimental data (see text for details on the procedure, black dots) and statistical model prediction (red histograms) for the oxygen isotopic distribution in the outgoing channel for the ^{12}C (95 MeV) + ^{12}C reaction. Oxygen is detected at forward angles ($5° \leq \theta \leq 18°$) in coincidence with LCP at ($30° \leq \theta \leq 150°$), the total charge of the entrance channel is collected.

REFERENCES

1. G. Baiocco, PhD Thesis, Università di Bologna and Université de Caen Basse-Normandie (2012) http://amsdottorato.cib.unibo.it/4295/
2. R. Charity *et al.*, *Phys. Rev. C* **67,** 044611(2003); L. F. Canto *et al.*, *Phys. Rep.* **424**, 1 (2006) and references therein, S. Adhikari *et al.*, *Phys. Rev. C* **74**, 024602 (2006).
3. G. Baiocco *et al.*, arXiv:1301.5990 [nucl-ex].
4. F. Gramegna *et al.*, *Nucl. Instr. Meth. A* **389**, 474 (1997); F. Gramegna *et al.*, *IEEE Nucl. Science Symposium*, Rome, October 2004; A. Moroni *et al.*, *Nucl. Instr. Meth. A* **556**, 516 (2006).
5. T. Marchi *et al.*, *Proceeding of the 13th Varenna Conference on Nuclear Reaction Mechanisms*, CERN Proceedings series, 2012.

Explosive Nucleosynthesis with ISOL Beams

A. M. Laird[a]

[a]*Department of Physics, University of York, Heslington, York, UK*

ASTROPHYSICAL PROCESSES INVOLVING LIGHT NUCLEI

Short-lived nuclei play crucial roles in most explosive astrophysical environments, such as novae, X-ray bursts and supernovae. In the case of light nuclei, it is often a few individual reaction rates, involving these exotic nuclei, which determine the energy generation rates and the path of nucleosynthesis. The main reaction processes for light, short-lived nuclei are the hot-CNO cycle, the αp-process, and the rapid proton capture (rp-)process.

In novae, the hot-CNO cycles are the dominant processes. Here, the explosion is driven by thermonuclear runaway on the surface of a white dwarf star, following accretion of hydrogen-rich matter from a companion star. The reaction pathway lies close to stability and reaches up to ^{40}Ca. Processed material is ejected and enriches the interstellar medium with, in particular, ^{13}C, ^{15}N and ^{17}O. Moreover, novae are the only explosive system where the nuclear reaction rate data used in the models are largely experimentally determined.

In X-ray bursts, the higher temperatures reached results in breakout from the hot-CNO cycles into the αp- and rp-processes. Again, the explosion is driven by thermonuclear runaway following accretion from a companion, but here the progenitor is a neutron star rather than a white dwarf. The reaction pathway lies further from stability and consequently is less well defined as many of the key parameters of the nuclei involved are unknown. The pathway may reach up to the mass 100 region but, due to the strong gravitational field of the neutron star, very little if any material is ejected.

Supernovae fall into two categories: thermonuclear supernovae, which, like novae and X-ray bursts, occur in binary systems; and core collapse supernovae, which are the final stage of massive star evolution. In both cases, thousands of reactions are involved and sensitivity studies of these explosions are only now becoming possible.

EXPERIMENTAL STUDIES WITH ISOL BEAMS

The use of ISOL beams for nuclear astrophysics measurements was pioneered by the Centre de Recherches du Cyclotron (CRC), at Louvain-la-Neuve in Belgium, during the late 80s. This facility produced a variety of proton-rich beams, including ^{13}N, ^{15}O, ^{18}F, ^{18}Ne and ^{19}Ne, and in many cases delivered beam intensities which are

still unmatched by other ISOL facilities today. The driver was a 200 μA proton beam at 30 MeV, delivered by the CYCLONE 30 cyclotron onto the production target. The second cyclotron, CYCLONE 110, post-accelerated the reaction products and provided high-resolution mass separation. The experimental techniques, such as resonant elastic scattering [1], which proved to be such powerful tools at the CRC are still commonly exploited today. Similarly, the highly segmented silicon strip detector arrays developed for this facility are now widely used for many astrophysics and structure applications at laboratories around the world.

What is currently feasible - Direct Measurements

Direct measurements involving short-lived nuclei are necessarily performed in inverse kinematics, and the forward focusing of the reaction products can bring some experimental benefits to counter the low beam intensities available. The target in most cases is either hydrogen or helium, and so gas targets are often required. The energies of interest, corresponding to the Gamow window for the reaction under investigation, are typically between 0.1 and 3 MeV/u. Beam intensities available at these energies are usually in the region of 10^5-10^8 pps.

Recoil separators, such as DRAGON at the TRIUMF Laboratory, and the DRS at Oak Ridge National Laboratory, are ideal for studying radiative capture reactions, and a number of flagship experiments [2,3], e.g. with ^{21}Na, ^{26}Al, ^{17}F and ^{18}F, have already been performed at these facilities.

Highly-segmented silicon strip arrays have been used very effectively to study both (p,α) and (α,p) reactions, using both foil and gas targets. In the former case, the forward focusing of both reaction products allows high efficiency coincident measurements to be performed, providing very clean event identification [4,5].

What is currently feasible - Indirect Measurements

Arguably the most powerful technique currently used for indirect nuclear astrophysics studies with ISOL beams is resonant elastic scattering [6,7]. Measurements can be performed with as little as a few 10^4 pps, and a large centre of mass energy scan can be achieved using the thick target technique. Simultaneous measurements of multiple channels are also possible and, using R-matrix theory, robust level parameters can be extracted. More recently, resonant inelastic scattering has also proven effective in particular cases [8,9].

Transfer reactions are also useful tools for extracting level information, but to date there have been limited relevant measurements using ISOL beams. Again the beam intensity is the main limitation, as upwards of 10^6 pps is required. A successful proton transfer reaction study has been performed [10], but there have been no alpha transfer measurements for nuclear astrophysics.

FUTURE PROGRAMME

If further high intensity beams become available at HIE-ISOLDE (CERN), ISAC (TRIUMF) and SPIRALII (GANIL), then measurements of many key reactions should be achievable within the next 5-10 years. Investment in beam development at existing and future facilities will be critical to the success of the scientific programme. In the longer term, the push will be for more proton-rich beams. Low energy beams (less than 2 MeV/u) will be required with intensities in excess of 10^7 pps, and high purity. Good beam emittance, and timing and energy resolution will also be required. To fully exploit the new beams available, a suite of experimental facilities will be needed but in most cases existing separator and detector systems will be sufficient.

SUMMARY

It is around 25 years since the first nuclear astrophysics measurements were performed with ISOL beams, and in this time significant progress has been made, particularly in novae and X-ray studies. Many of the experimental techniques and detector systems used then are still crucial tools today but the main limitation comes from beam availability and intensity. The direction of future ISOL programmes in nuclear astrophysics will be critically influenced by the availability of intense proton-rich radioactive beams.

REFERENCES

1. Th. Delbar et al., Nucl. Phys. A542 (1992) 263.
2. S. Bishop et al., Phys. Rev. Lett. **90,** 162501 (2003).
3. K. Chipps et al., Phys. Rev. Lett. 102, 152502 (2009)
4. D. Bardayan et al., PRL89, 262501 (2002)
5. C. E. Beer et al., Phys Rev. C83, 042801 (2011)
6. C. Ruiz et al., Phys. Rev. C**71,** 025802 (2005)
7. D. J. Mountford, et al., Phys. Rev. C 85, 022801(R) (2012)
8. Dalouzy et al., Phys. Rev. Lett. 102, 162503 (2009)
9. J. J. He et al., Phys. Rev. C80, 042801 (2009)
10. Adekola et al., Phys. Rev. C(R)83, 052801 (2011)

Three-nucleon forces and exotic nuclei

A. Schwenk

Institut für Kernphysik, Technische Universität Darmstadt, 64289 Darmstadt, Germany and ExtreMe Matter Institute EMMI, GSI Helmholtzzentrum für Schwerionenforschung GmbH, 64291 Darmstadt, Germany

Abstract. Neutron-rich nuclei become increasingly sensitive to three-nucleon (3N) forces. These components of nuclear forces are at the forefront of theoretical developments based on chiral effective field theory (EFT). We discuss our understanding of 3N forces and their impact on exotic nuclei, and show how new measurements constrain 3N forces. Three-nucleon forces therefore provide an exciting link between theoretical and experimental frontiers.

Chiral EFT and 3N forces.– Chiral EFT provides a systematic expansion of nuclear forces based on quantum chromodynamics [1], where nucleons interact via pion exchanges and short-range contact interactions. The EFT opens up a powerful approach to investigate many-body forces and their impact on neutron-rich nuclei and neutron-rich matter [2]. This results from the consistency of NN and 3N interactions, which predicts the two-pion-exchange parts of 3N forces at next-to-next-to-leading order, N^{2}LO, leaving only two low-energy couplings c_D, c_E that encode pion interactions with short-range NN pairs and short-range three-body physics. Moreover, all 3N and 4N forces at the next order, N^{3}LO, are predicted. We have shown that for systems of only neutrons, the c_D, c_E parts of 3N forces do not contribute because of the Pauli principle and the coupling of pions to spin [3]. Therefore, chiral EFT predicts all three-neutron and four-neutron forces to N^{3}LO. At the same time, 3N forces are a frontier in the physics of nuclei and nucleonic matter in stars. This leads to a forefront connection of 3N forces with the exploration of exotic nuclei at rare isotope beam facilities worldwide.

Three-nucleon forces and neutron-rich nuclei.– Three-nucleon forces play a key role for understanding and predicting exotic nuclei and for the formation and evolution of shell structure. As shown in Fig. 1, chiral 3N forces lead to repulsive contributions to the interactions among excess neutrons that change the location of the neutron dripline from ^{28}O (with NN forces only) to the experimentally observed ^{24}O [4, 5]. This presents the first explanation of the oxygen anomaly based on nuclear forces. This 3N-force mechanism was recently confirmed in large-space calculations [6, 7, 8]. Moreover, as expected for normal Fermi systems [9], we have shown that the contributions from residual three-valence-nucleon interactions are small in the shell model, but amplified in the most neutron-rich nuclei [10].

While the magic numbers $N = 2, 8, 20$ are generally well understood, $N = 28$ is the first standard magic number that is not reproduced in microscopic theories with NN forces only. In first studies for calcium isotopes [11, 12], it was shown that 3N forces are key to explain the $N = 28$ magic number, leading to a high 2^+ excitation energy. Moreover, chiral 3N forces improve the agreement with experimental masses,

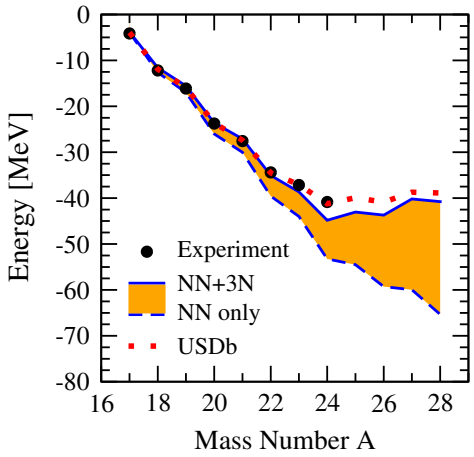

FIGURE 1. Ground-state energies of the neutron-rich oxygen isotopes relative to ^{16}O. The experimental energies of the bound isotopes $^{17-24}$O and phenomenological USDb energies are included for comparison. Results are shown based on NN forces only and with N^{2}LO 3N forces (NN+3N). The impact of chiral 3N forces is highlighted in orange. For details see Ref. [5].

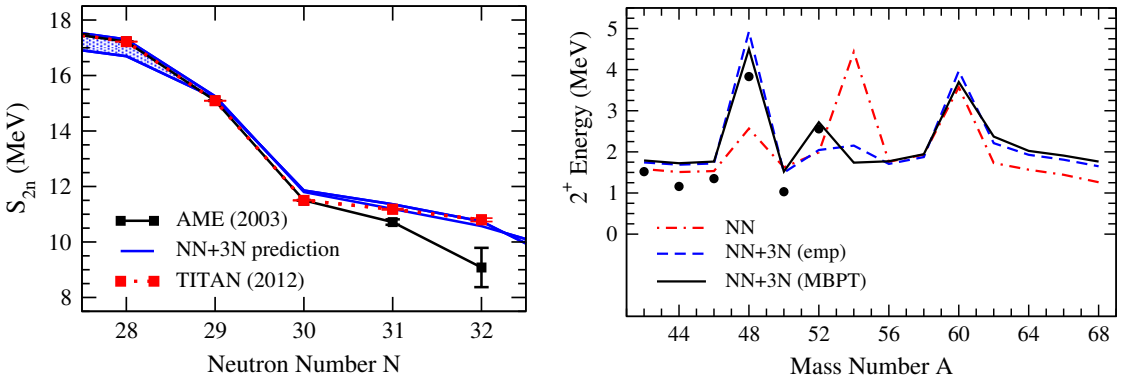

FIGURE 2. Left panel: Two-neutron separation energy S_{2n} of the neutron-rich calcium isotopes, with experimental energies from the AME 2003 atomic mass evaluation. We also show the new precision mass measurements for ^{51,52}Ca from TITAN, which disagree significantly with the indirectly measured masses of AME 2003. Our predictions based on NN+3N forces are in excellent agreement with these masses and with the flat S_{2n} behavior from ^{50}Ca to ^{52}Ca. For details see Ref. [13]. Right panel: 2^+ energy in the even calcium isotopes with and without 3N forces compared with experiment (dots from ENSDF). The excitation energies are calculated to ^{68}Ca in an extended $pfg_{9/2}$ valence space, using both empirical (emp) and calculated (MBPT) single-particle energies. For details see Ref. [14].

and as shown in Fig. 2 predict a flat behavior of the two-neutron separation energy from ^{50}Ca to ^{52}Ca, in excellent agreement with new precision TITAN Penning-trap mass measurements [13]. The 2^+ excitation energy in the even calcium isotopes with and without 3N forces, based on the same calculations as for the masses, is shown in Fig. 2 [14]. This predicts a 2^+ energy in ^{54}Ca (recently investigated at RIKEN) of $1.7-2.2$ MeV. Finally, we have presented first results with 3N forces for the ground and excited states of proton-rich nuclei along the $N=8$ (see Fig. 3) and $N=20$ isotones to the proton dripline [15].

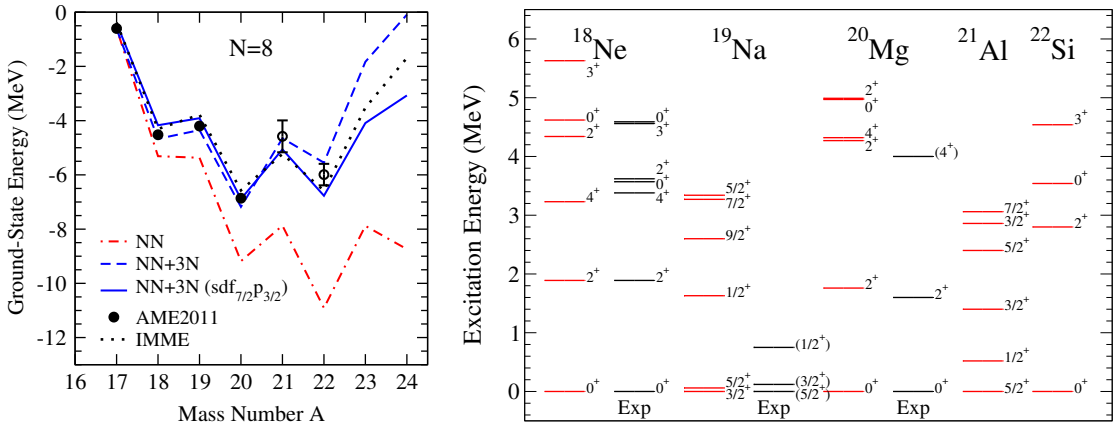

FIGURE 3. Left panel: Ground-state energies of $N = 8$ isotones relative to ^{16}O. Experimental energies (AME2011 with extrapolations as open circles) and energies from the isobaric multiplet mass equation (IMME) are shown. NN-only results in the *sd* shell are compared to calculations based on NN+3N forces in both *sd* and $sdf_{7/2}p_{3/2}$ valence spaces with calculated (MBPT) single-particle energies. Right panel: Excitation energies of $N = 8$ isotones calculated with NN+3N forces in the $sdf_{7/2}p_{3/2}$ valence space, compared with experimental data where available. For details see Ref. [15].

Neutron matter and symmetry energy.– As shown in Fig. 4, the same chiral 3N forces are repulsive in neutron matter and dominate the uncertainty of the properties of neutron-rich matter [3]. The predicted neutron-matter energy provides tight constraints for the symmetry energy (see the right panel of Fig. 4) and predicts the neutron skin thickness of ^{208}Pb to 0.17 ± 0.03 fm [16], in excellent agreement with a recent determination from the complete electric dipole response [17]. In addition, our calculations based on chiral EFT interactions constrain the properties of neutron-rich matter below nuclear densities to a much higher degree than is reflected in current neutron star modeling [16]. Combined with the heaviest $2M_\odot$ neutron star, our results constrain the radius of a typical $1.4M_\odot$ star to $R = 9.7 - 13.9$ km [18]. The predicted radius range is due, in about equal amounts, to the uncertainty in 3N (and higher-body) forces and to the extrapolation to high densities. To improve our understanding of neutron matter further, we have recently performed the first complete N^{3}LO calculation of neutron matter including NN, 3N and 4N forces [20, 21], which leads to bands consistent with our previous results [3].

ACKNOWLEDGMENTS

I would like to thank J. Dilling, A. T. Gallant, K. Hebeler, J. D. Holt, T. Krüger, J. M. Lattimer, J. Menéndez, T. Otsuka, C. J. Pethick, J. Simonis, T. Suzuki, and I. Tews, who contributed to the results presented in this talk. This work was supported by the BMBF under Contract No. 06DA70471, the DFG through Grant SFB 634, the ERC Grant No. 307986 STRONGINT, and the Helmholtz Alliance HA216/EMMI.

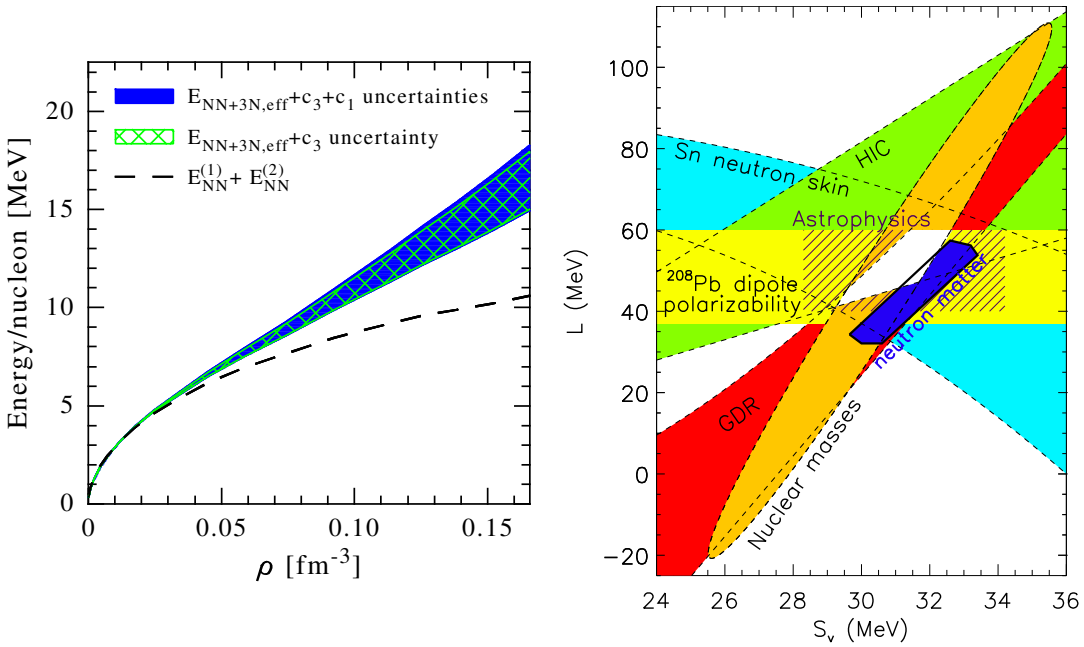

FIGURE 4. Left panel: Energy per particle E/N of neutron matter as a function of density ρ. The blue band is based on evolved N^{3}LO NN potentials and N^{2}LO 3N forces; the dashed line gives the NN-only energy. The range of the band is due to uncertainties in the c_1 and c_3 coefficients of 3N forces. For details see Ref. [3]. Right panel: Constraints for the symmetry energy S_v and its density derivative L. The blue region shows our neutron-matter constraints (based on the left panel), in comparison to bands from different empirical extractions [19]. The white area gives the overlap region of the different empirical ranges. For details see Ref. [18].

REFERENCES

1. E. Epelbaum, H.-W. Hammer, and U.-G. Meißner, *Rev. Mod. Phys.* **81**, 1773 (2009).
2. H.-W. Hammer, A. Nogga, and A. Schwenk, *Rev. Mod. Phys.* **85**, 197 (2013).
3. K. Hebeler and A. Schwenk, *Phys. Rev. C* **82**, 014314 (2010).
4. T. Otsuka, T. Suzuki, J. D. Holt, A. Schwenk, and Y. Akaishi, *Phys. Rev. Lett.* **105**, 032501 (2010).
5. J. D. Holt, J. Menéndez, and A. Schwenk, *Eur. Phys. J. A* **49**, 39 (2013).
6. G. Hagen *et al.*, *Phys. Rev. Lett.* **108**, 242501 (2012).
7. H. Hergert, S. Binder, A. Calci, J. Langhammer, and R. Roth, arXiv:1302.7294.
8. A. Cipollone, C. Barbieri, and P. Navrátil, arXiv:1303.4900.
9. B. Friman and A. Schwenk, in *From Nuclei to Stars: Festschrift in Honor of Gerald E. Brown*, Ed. S. Lee (World Scientific, 2011) arXiv:1101.4858.
10. C. Caesar, J. Simonis *et al.*, arXiv:1209.0156.
11. J. D. Holt, T. Otsuka, A. Schwenk, and T. Suzuki, *J. Phys. G* **39**, 085111 (2012).
12. G. Hagen *et al.*, *Phys. Rev. Lett.* **109**, 032502 (2012).
13. A. T. Gallant *et al.*, *Phys. Rev. Lett.* **109**, 032506 (2012).
14. J. D. Holt, J. Menéndez, and A. Schwenk, arXiv:1304.0434.
15. J. D. Holt, J. Menéndez, and A. Schwenk, Phys. Rev. Lett. **110**, 022502 (2013).
16. K. Hebeler, J. M. Lattimer, C. J. Pethick, and A. Schwenk, *Phys. Rev. Lett.* **105**, 161102 (2010).
17. A. Tamii *et al.*, *Phys. Rev. Lett.* **107**, 062502 (2011).
18. K. Hebeler, J. M. Lattimer, C. J. Pethick, and A. Schwenk, arXiv:1303:4662.
19. J. M. Lattimer and Y. Lim, arXiv:1203.4286.
20. I. Tews, T. Krüger, K. Hebeler, and A. Schwenk, *Phys. Rev. Lett.* **110**, 032504 (2013).
21. I. Tews, T. Krüger, K. Hebeler, and A. Schwenk, arXiv:1304.2212.

Dynamic core excitation efects in the scattering of halo nuclei

R. de Diego[*], A. M. Moro[†], J. A. Lay[†], R. Crespo[*,**] and J. M. Arias[†]

[*]*Centro de Física Nuclear, Universidade de Lisboa, Av. Prof. Gama Pinto 2, 1649-003 Lisboa, Portugal*
[†]*Departamento de FAMN, Universidad de Sevilla, Apartado 1065, E-41080 Sevilla, Spain*
[**]*Departamento de Física, Instituto Superior Técnico, Universidade Técnica de Lisboa, Av. Prof. Cavaco Silva, Taguspark, 2780-990 Oeiras, Portugal*

Abstract. We investigate the role of core excitation in the structure and dynamics of two-body halo nuclei by studying the breakup of ^{11}Be on protons at an incident energy of 63.7 MeV/nucleon. To describe the reaction, we use the XCDCC formalism, which incorporates these core excitation effects, in both the structure of the weakly-bound projectile, as well as in the reaction dynamics.

Keywords: halo nuclei; breakup; core excitation
PACS: 24.50.+g, 25.60.Gc,27.20.+n, 25.40.Ep

INTRODUCTION

Over the last decade, breakup reactions have played an important role in the study of weakly-bound systems like halo nuclei. Generally, these quantum collisions have been described within a three-body model and the coupling to the unbound states of the projectile (treated as a two-body system) should be taken into account. Under this approach, the Continuum-Discretized Coupled-Channels (CDCC) method [1], originally developed to describe the effect of breakup channels in deuteron scattering, has proved to be a very efficient tool and it has been applied successfully to investigate different loosely-bound nuclei, such as ^{6}Li, ^{7}Li, ^{11}Be or ^{8}B, for example.

In its standard formulation, the CDCC method considers that the weakly-bound projectile is composed of two or more inert clusters, without considering possible admixtures of different core states in the structure of the projectile or transitions between them.

In this contribution, we use an extension of the CDCC method for two-body projectiles, proposed in [2]. There, the continuum of the projectile was described by using a generalization of the standard binning method. Instead of this, we make use of a pseudo-state description of the projectile. This formalism is applied to the breakup of ^{11}Be on a proton target 63.7 MeV/nucleon and compared with a DWBA calculation, which takes also into account the effect of core excitation but within a no-recoil approximation.

THEORETICAL FORMALISM: STRUCTURE AND DYNAMICS

Structure of the halo nucleus: Particle-rotor model

Regarding the structure of the halo nucleus, we use the particle-rotor model so the Hamiltonian is given by:

$$H_p(\vec{r},\xi) = T(\vec{r}) + V_{vc}(\vec{r},\xi) + h_c(\xi) \tag{1}$$

where $\vec{r}$ is the relative coordinate between the valence and the core, ξ denote the internal degrees of freedom of the core, $T(\vec{r})$ the core-valence kinetic energy operator, V_{vc} the valence-core interaction, and $h_c(\xi)$ the intrinsic Hamiltonian of the core. The states of the system are computed by using the THO method [3]. In this method the Hamiltonian is diagonalized in an appropriate set of functions so the eigenstates are expanded in a truncated basis:

$$\phi^{THO}_{i,\alpha,J_p}(\vec{r},\xi) = R^{THO}_{i,\alpha}(r)\left[Y_{(\ell s)j}(\hat{r}) \otimes \varphi_I(\xi)\right]_{J_p} \quad i = 1,..,N \tag{2}$$

where the label α denotes the set of quantum numbers $\{\ell, s, j, I\}$, with ℓ (valence-core orbital angular momentum) and s (spin of the valence) both couple to j (total angular momentum). The spin of the projectile J_p is given by the coupling between j and I (intrinsic spin of the core). The states related to the valence-core relative motion are described by the functions $R^{THO}_{i,\alpha}(r)$ (radial part) and $Y_{(\ell s)j}(\hat{r})$ (angular part) while the functions $\varphi_I(\xi)$ describe the core states.

The eigenstates of the Hamiltonian (1) in a truncated THO basis will be given by $\Phi^{(N)}_{n,J_p} = \sum_{i=1}^{N}\sum_{\alpha} C^n_{i,\alpha}\phi^{THO}_{i,\alpha,J_p}$, where N is the number of basis states, n is an index identifying each eigenstate, and $C^n_{i,\alpha}$ are the coefficients for the expansion of the states of the system in the truncated THO basis.

The negative eigenvalues of the Hamiltonian (1) are identified with the energies of the bound states whereas the positive ones correspond to a discrete representation of the continuum spectrum.

Core excitation: XCDCC method

Once the projectile wave functions have been obtained, we proceed to solve the scattering problem. We consider a three-body Hamiltonian (3) and we express the three-body wave functions $\Psi^{M_T}_{J_T}$ in terms of the set $\{\Phi^{(N)}_{n,J_p}\}$:

$$H(\vec{R},\vec{r},\xi) = T(\vec{R}) + H_p(\vec{r},\xi) + V_{ct}(\vec{R},\vec{r},\xi) + V_{vt}(\vec{R},\vec{r}) \tag{3}$$

$$\Psi^{M_T}_{J_T}(\vec{R},\vec{r},\xi) = \sum_{\beta} F^{J_T}_{\beta}(R)\left[Y_L(\hat{R}) \otimes \Phi^{(N)}_{n,J_p}(\vec{r},\xi)\right]^{M_T}_{J_T} \tag{4}$$

where, in addition to the projectile coordinates $\vec{r}$ and $\vec{\xi}$, we have the relative coordinate $\vec{R}$ between the center of mass of the projectile and the target (assumed to be structureless). The different quantum numbers are labeled by $\beta = \{L, J_p, n\}$, where L (projectile-target orbital momentum) and J_p both couple to the total spin of the three-body system J_T.

By inserting (4) in the Schrödinger equation a system of coupled differential equations is obtained and the main ingredient is given by the coupling potentials:

$$U^{J_T}_{\alpha,\alpha'}(R) = \langle \alpha; J_T | V_{ct}(\vec{R},\vec{r},\xi) + V_{vt}(\vec{R},\vec{r}) | \alpha'; J_T \rangle \tag{5}$$

The nuclear and Coulomb contributions are treated simultaneously under this scheme. However, in our case, the Coulomb contribution can be neglected because we consider a proton target and the excitation is mainly due to the nuclear interaction.

APPLICATION TO ^{11}BE BREAKUP

Now we apply the XCDCC model in first order (equivalent to the DWBA formalism) to the breakup of ^{11}Be on protons at 63.7 MeV/nucleon. This reaction has been previously analysed in a no-recoil DWBA framework with core excitation [4]. The calculated angular distributions, integrated in the relative energy intervals E =0-2.5 MeV and E =2.5-5.0 MeV, were found to describe reasonably well the data of [5]. Furthermore, it was shown the importance of core excitation to the breakup cross section, specially in the second energy interval, which contains the $3/2^+$ resonance. This is due to the dominance of the $^{10}\mathrm{Be}(2^+) \otimes \nu s_{1/2}$ configuration as stated in Table 1, which collects the spectroscopic factors for the ground state $1/2^+$ and the resonances $5/2^+$ (E_x =1.78 MeV) and $3/2^+$ (E_x =3.41 MeV) of ^{11}Be in the particle-rotor model, assuming a permanent axial deformation in the ^{10}Be core with β_2=0.67 [6].

TABLE 1. Spectroscopic factors for the ground and resonant states $5/2^+$ and $3/2^+$ of ^{11}Be, according to the particle-rotor model.

State	$\|0^+ \otimes (\ell s) j\rangle$	$\|2^+ \otimes s_{1/2}\rangle$	$\|2^+ \otimes d_{5/2}\rangle$
$1/2^+$ (g.s.)	0.86	–	0.12
$5/2^+$ (1.78 MeV)	0.70	0.18	0.11
$3/2^+$ (3.41 MeV)	0.16	0.74	0.08

The fragment-target potentials are those used in [4] and we focus on the excitation of the two resonances. In Fig.1 the calculated breakup angular distributions as a function of the center-of-mass scattering angle are plotted. The left and right panels correspond, respectively, to the $5/2^+$ and $3/2^+$ resonances. The solid lines show the results in the no-recoil DWBA framework with core excitation similar to the calculation of [4], but using a continuum representation in terms of THO pseudo-states instead of continuum bins (these two basis representations give almost identical results). The open circles correspond to the present XCDCC computation with the pseudostates basis and, as we can see, they are found to be very close to the no-recoil calculations.

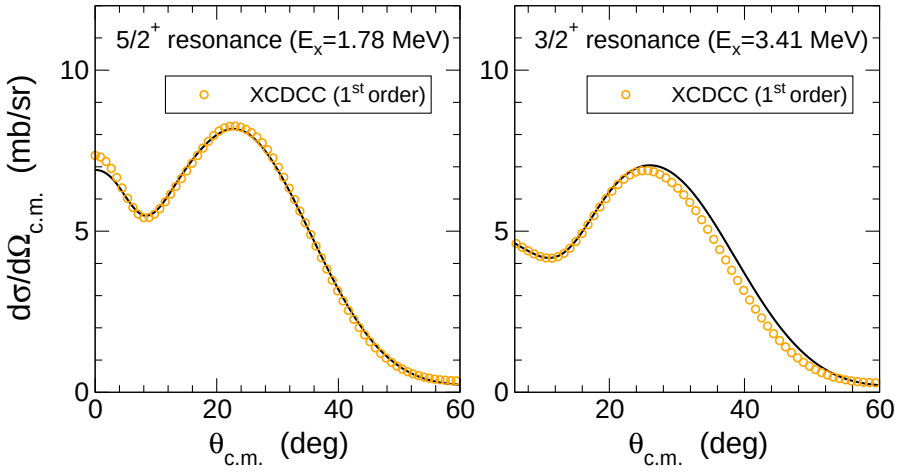

FIGURE 1. Angular distribution for the breakup of ^{11}Be on protons at 63.7 MeV/nucleon. The left and right panels correspond, respectively, to the $5/2^+$ and the $3/2^+$ resonances. The DWBA calculations using the no-recoil model are given by the solid lines. The open circles correspond to a XCDCC calculation taking into account recoil effects.

SUMMARY AND CONCLUSIONS

We have investigated the effect of core excitation in the breakup of halo nuclei. We have shown that the THO basis combined with the XCDCC method can provide a suitable framework which takes into account the core deformation in the structure of the two-body halo nuclei, as well as the dynamic core excitation during the collision, with a reduced number of functions (once the convergence has been assessed). The model has been applied to the resonant breakup of ^{11}Be on protons at an incident energy of 63.7 MeV/nucleon.

From these calculations, we may conclude that core excitation effects might be also important in other reactions induced by loosely-bound projectiles with deformed constituents. The proposed approach goes beyond the no-recoil approximation and it could describe core excitation effects in those situations in which the assumption of the no-recoil model (possibility of neglecting core-recoil) is not fulfilled.

We must notice that all calculations rely on the Born approximation, and higher order couplings are ignored. These calculations are in progress and will be presented elsewhere.

ACKNOWLEDGMENTS

This work has been partially supported by the Spanish Ministerio de Ciencia e Innovación under contracts No. FPA2009-07653 and FIS2011-28738-C02-01, and by the Spanish Consolider-Ingenio 2010 Programme CPAN (CSD2007-00042). R.D.D. and R.C. are supported by the FCT grants SFRH/BPD/78606/2011 and PTDC/FIS/103902/2008, respectively. J.A.L. acknowledges a research grant by the Ministerio de Ciencia e Innovación.

REFERENCES

1. N. Austern, Y. Iseri, M. Kamimura, M. Kawai, G. Rawitscher, and G. J. Yahiro, *Phys. Rep.* **154**, 125 (1987).
2. N. C. Summers, F. M. Nunes, and I. J. Thompson, *Phys. Rev. C* **74**, 014606 (2006).
3. J. A. Lay, A. M. Moro, J. M. Arias, and J. Gómez-Camacho, *Phys. Rev. C* **85**, 054618 (2012).
4. A. M. Moro, and R. Crespo, *Phys. Rev. C* **85**, 054613 (2012).
5. A. Shrivastava, et al., *Phys. Lett. B* **596**, 54 (2004).
6. F. M. Nunes, J. A. Christley, I. J. Thompson, R. C. Johnson, and V. D. Efros, *Nucl. Phys. A* **609**, 43 (1996).

Discontinuity of BBG self-consistent solutions and role on low-energy elastic scattering

F. A. Isaule* and H. F. Arellano*,†

*Department of Physics - FCFM, University of Chile, Av. Blanco Encalada 2008, Santiago, Chile
† CEA, DAM, DIF, F-91297 Arpajon, France

Abstract. Microscopic optical model potential in momentum space can be casted as the sum of two terms, one given by the Kerman-McManus-Thaler (KMT) folding of the off-shell scattering matrix and another depending on the gradient of the *in-medium* nucleon-nucleon effective interaction, modeled by the Brueckner-Bethe-Goldstone (BBG) *g* matrix for infinite nuclear matter. Thus, *g*-matrices based on self-consistent single-particle fields are needed at all densities ranging form zero to a maximum value given by the isoscalar density of the target. However, accurate self-consistent calculations in the Brueckner-Hartree-Fock (BHF) approximation lead to a discontinuity/coexistence in the self-consistent single-particle potentials at Fermi momenta below $k_F = 0.3$ fm^{-1}. In this work we present preliminary results accounting for this discontinuity and implied low-density self-consistent solutions. Total cross sections for nucleon elastic scattering become sensitive to these effects at beam energies below $\sim$40 MeV.

Keywords: Optical model, nucleon scattering, effective interactions, g-matrix, nuclear matter
PACS: 24.10.Ht 21.60.-n 25.60.Bx 25.40.Cm

A primary goal behind microscopic optical model potentials (OMP) for nucleon scattering, is that of providing a link between the two-nucleon interaction in free space with a one-body operator describing the transit of a nucleon through a composite system. The degree of understanding of the scattering process is inferred from the level coherence between measurements obtained in experimental facilities and predictions made by theory. From a theoretical point of view, the construction of a microscopic OMP faces many challenges at various levels, one of them being that of constructing an effective interaction able to retain leading-order correlations of interacting nucleons (fermions) in a many-body environment. It is at this stage where the BBG *g*-matrix has played a pivotal role. Its use has typically been implemented by means of local density-dependent effective interactions [1], an approximation aimed to simplify the involved structure of the OMP when the genuine off-shell *g* matrix is used. The effort in this work is not only to avoid such approximation but also to assess implications resulting from accurate evaluations of the *g* matrix, particularly its associated self-consistent single-particle potentials in the continuous choice.

The interaction between a nucleon with energy E and a nucleus can be described by means of an OMP which in momentum space is expressed as

$$U(\boldsymbol{k}',\boldsymbol{k};E) = \int d\boldsymbol{p}'\, d\boldsymbol{p}\, \langle \boldsymbol{k}'\boldsymbol{p}' \mid \hat{T}(E) \mid \boldsymbol{k}\,\boldsymbol{p} \rangle_{\mathscr{A}}\, \hat{\rho}(\boldsymbol{p}',\boldsymbol{p})\,. \tag{1}$$

Here $\hat{T}$ represents a two-body effective interaction which, in general, contains information about the discrete spectrum of the many-body system. The one-body mixed density

$\hat{\rho}(\boldsymbol{p}',\boldsymbol{p})$ accounts for the ground-state of the target. The evaluation of optical potentials considering all these elements is far from feasible even with current computational capabilities. Part of the difficulties is avoided by treating separately the ground-state of the target and the nucleon-nucleon (*NN*) effective interaction. A remaining challenge is the Fermi motion of the target nucleons implied by the $d\boldsymbol{p}\,d\boldsymbol{p}'$ integration.

Following Ref. [2], intrinsic medium contributions in the structure of the optical potential can be disentangled from their free-space counterpart in $\hat{T}$ following a general analysis of its momentum-space structure. The matrix elements of $\hat{T}$ in coordinate space are denoted with $\langle \boldsymbol{r}'\boldsymbol{s}' \mid \hat{T} \mid \boldsymbol{r}\,\boldsymbol{s}\rangle$, where the 'prior' coordinates of each particle are denoted by $\boldsymbol{r}$ and $\boldsymbol{s}$, respectively, while $\boldsymbol{r}'$ and $\boldsymbol{s}'$ refer to the 'post' coordinates of the same particles. These vectors define the *mean coordinate* $\boldsymbol{z}$, given by the average

$$\boldsymbol{z} = \tfrac{1}{4}(\boldsymbol{r}+\boldsymbol{s}+\boldsymbol{r}'+\boldsymbol{s}')\,.$$

As shown in the cited reference, a reduced two-nucleon interaction modeled by the density-dependent BBG g matrix, needs to be evaluated at this site z, where the local density is $\rho(z)$. After some analysis described in Ref. [2], Eq. (1) for U yields

$$U(\boldsymbol{k}',\boldsymbol{k};E) = U_0(\boldsymbol{k}',\boldsymbol{k};E) + U_1(\boldsymbol{k}',\boldsymbol{k};E)\,,$$

with U_0 the full-folding optical potential based on the free t-matrix (KMT contribution). The medium-dependent contribution U_1, in turn, is given by

$$U_1(\boldsymbol{k}',\boldsymbol{k};E) = \frac{1}{2\pi^2}\int d\boldsymbol{p}\,d\boldsymbol{p}'\hat{\rho}(\boldsymbol{p}',\boldsymbol{p})\int_0^\infty z^3 dz \frac{j_1(zK_\perp)}{zK_\perp}\left(-\frac{\partial g_z}{\partial z}\right). \tag{2}$$

Here g_z is evaluated at off-shell at relative momenta $\frac{1}{2}(\boldsymbol{k}'-\boldsymbol{p}')$ and $\frac{1}{2}(\boldsymbol{k}-\boldsymbol{p})$, total momentum $\boldsymbol{k}'+\boldsymbol{k}$ and starting energy ω consistent with the energy of the beam. Actual evaluations of the OMP are made considering the reduced interaction g_z as the nuclear matter g matrix in the BBG theory. Here the coordinate z defines the density $\rho(z)$ at which g_z is evaluated. As shown in Ref. [2], this model reproduces as a particular case the *in-medium* folding model of Arellano, Brieva and Love [3] if one assumes a Slater approximation for the mixed density (ABL folding).

In BBG theory for symmetric nuclear matter the g matrix depends on the density of the medium, characterized by the Fermi momentum k_F, and a starting energy ω. To lowest order in the BHF approximation, when only two-body correlations are taken into account, the g matrix satisfies

$$g(\omega) = v + v\frac{Q}{\omega+i\eta-\hat{h}_1-\hat{h}_2}g(\omega)\,, \tag{3}$$

with v the bare interaction between nucleons, $\hat{h}_i$ the single-particle energy of nucleon i ($i=1,2$), and Q the Pauli blocking operator. The solution to this equation enables the evaluation of the mass operator

$$M(k;E) = \sum_{|\boldsymbol{p}|\le k_F}\langle \tfrac{1}{2}(\boldsymbol{k}-\boldsymbol{p})|g_{\boldsymbol{K}}(E+e_p)|\tfrac{1}{2}(\boldsymbol{k}-\boldsymbol{p})\rangle\,, \tag{4}$$

where $\boldsymbol{K}$ is the total momentum of the interacting pair, $\boldsymbol{K} = \boldsymbol{k} + \boldsymbol{p}$, and $e_p = p^2/2m + U(p)$, the single-particle energy defined in terms of an auxiliary field U. The nucleon mass m is taken as the average of proton and neutron masses. In the BHF approximation the single-particle potential is given by the on-shell mass operator,

$$U(k) = \Re e M(k; e_k) \, , \tag{5}$$

a self-consistency requirement which can be achieved iteratively. In Ref. [4] it is reported a thorough study on self-consistent solutions for these self-consistent fields. A key element in this study is the explicit treatment of di-nucleon bound states during the self-consistency search. As a result, it is found two families of self-consistent solutions. One of them describes unbound solutions and the other bound ones. In Fig. 1 we show self-consistent solutions for the single-particle fields based on the Argonne v_{18} potential. On the left we show a set of solutions for $k_F \geq 0.35$ fm^{-1}, denoted U_{II}, featuring the usual aspect of solutions reported elsewhere. On the right, for $k_F \leq 0.35$ fm^{-1}, two families (I and II) of self-consistent solutions are shown, both meeting the self-consistency requirement expressed by Eq. (5). The density range where these solutions coexist corresponds to $0.13 \leq k_F \leq 0.28$, in units of fm^{-1}. These Fermi momenta represent low nuclear densities located on the surface of the nucleus.

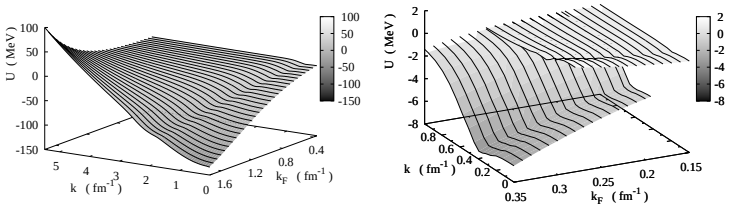

FIGURE 1. Left: Self-consistent solutions $U_{k_F}(k)$ as functions of k_F and k for the Argonne v_{18} potential in the bound phase II. Right: Solutions I and II in the coexistence range in k_F.

To each of the two families of self-consistent fields, U_I and U_{II}, corresponds a set of solutions for the g matrix, g_I and g_{II}, respectively. In an attempt to explore these solutions in the context of optical potentials, we have represented the g matrix as function of k_F in the form

$$g[k_F] = \Theta(k_C - k_F) \times g_I[k_F] + \Theta(k_F - k_C) \times g_{II}[k_F] \, , \tag{6}$$

with k_C a Fermi momentum in the region of coexistence. Certainly other prescriptions can be investigated following more rigorous arguments, or aimed to assess how sensitive is the optical potential to the use of alternative combinations of coexisting solutions.

Following Ref. [5], we have evaluated optical potentials for nucleon elastic scattering from ^{12}C and ^{16}O. The *NN* interaction is the Argonne v_{18} potential, from which off-shell g matrices are calculated at various densities. The applications presented in this report use $k_C = 0.25$ fm^{-1} in Eq. (6). These matrices are then used, with no localization whatsoever, to obtain non-local optical potentials to get scattering observables.

In Fig. 2 (left frame) we show the reaction cross section σ_R for p+^{16}O and p+^{12}C elastic scattering as function of the beam energy. Solid curves represent results based on

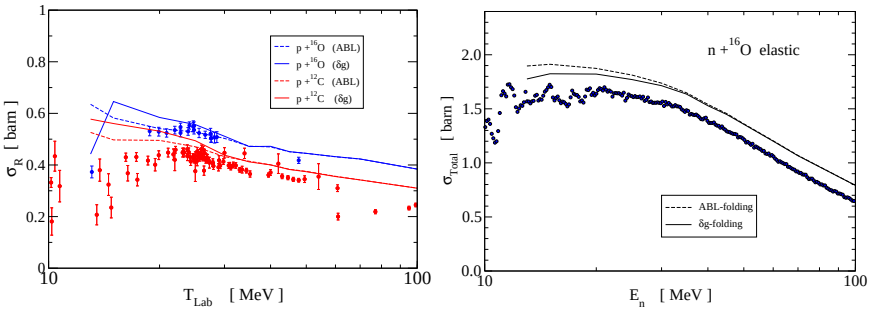

FIGURE 2. Left: Reaction cross section for proton elastic scattering from ^{16}O (blue curves) and ^{12}C (red curves), based on δg-folding (continuous curves) and ABL-folding (dashed curves). Data from Ref. [6]. Right: Total cross section for neutron elastic scattering from ^{16}O. The same convention as in the previous plot is adopted for the curve patterns. Data from Ref. [7]

δg-folding, using the exact one-body mixed density from shell-model wavefunctions. Dashed curves are obtained using ABL-folding, where the radial density is used to evaluate the potential. Differences between the two approaches to evaluate the optical potential appear below 40 MeV, becoming more pronounced at the lower energies. Additionally, the ABL approximation exhibits better agreement with the data than the δg approach. In Fig. 2 (right frame) we show the total cross section σ_T for $n+^{16}$O elastic scattering as function of the beam energy. Here again differences appear below 40 MeV, although the δg-approach agrees better with the data than ABL. We also note that theory overestimates σ_T by about 0.15 barn, almost uniformly.

In summary, we have performed microscopic OMP in momentum space considering high precision g matrices in BBG theory. Special attention has been placed on the account for coexisting solutions of single-particle fields at low densities. From this study we conclude that nucleon elastic scattering at low energies is sensitive to medium effects on the surface of nuclei. Under the assumption that the g matrix is discontinuous in the range of coexisting solutions of the single-particle fields, the effect of such discontinuity shows up in reaction and total cross sections below 40 MeV nucleon energy (40 MeV/A ion energy). At these energies shell-structure effects become relevant, as evidenced when comparing ABL vs δg approaches. Considering that the effects investigated here occur at low densities (surface), the findings we report here might be relevant for the study of nuclear reactions involving exotic structures.

H.F.A acknowledges partial funding from FONDECYT under Grant No 1120396.

REFERENCES

1. K. Amos, P. J. Dortmans, H. V. von Geramb, S. Karataglidis, and J. Raynal, Adv. in Nucl. Phys. **25**, 275 (2000).
2. H. F. Arellano and E. Bauge, Phys. Rev. C **76**, 014613 (2007).
3. H. F. Arellano, F. A. Brieva, and W. G. Love, Phys. Rev. C **52**, 301 (1995).
4. H. F. Arellano and J.-P. Delaroche, submitted to Phys. Rev. C.
5. F. J. Aguayo and H. F. Arellano, Phys. Rev. C **78**, 014608 (2008).
6. R. F. Carlson, Atomic Data and Nucl. Data Tables **63**, 93-116 (1996).
7. R. W. Finlay *et al.*, Phys. Rev. C **47**, 237 (1993).

On the Origin of Nuclear Clustering

Marek Płoszajczak[a]

[a]*Grand Accelerateur National d'Ions Lourds (GANIL), CEA/DSM-CNRS/IN2P3, BP 5027, F-14076 Caen Cedex 05, France.*

INTRODUCTION

The nuclear Shell Model (SM) in which the one-body behavior is supplemented by configuration-mixing effects of residual two-body interaction, describes nucleus as a Closed Quantum System (CQS) where nucleons occupying bound orbits are isolated from the environment of scattering states and decay channels. In its modern version, SM calculates nuclear properties in *ab initio* manner [1], using realistic interactions which reproduce the nucleon-nucleon scattering data [2,3].

The validity of such a CQS framework depends on the dissociation energy. The configuration-mixing effects in weakly bound or unbound nuclear states cannot be treated as a small perturbation atop the mean field, and involve effects of the coupling to decay channels [4]. Phenomena such as the anomalous behavior of elastic cross-sections and the associated overlap integral near threshold states in multi-channel coupling [5], the isospin and mirror symmetry-breaking threshold effects [6], the resonance trapping [7,8] and super-radiance phenomenon [9], the modification of spectral fluctuations [10], and deviations from Porter-Thomas resonance width distribution [8,11], are all unique manifestations of the continuum coupling. For a description of these diverse phenomena it was necessary to create theories which unify structure and reactions. Examples of these attempts are the Shell Model Embedded in the Continuum (SMEC) [12] and the Gamow Shell Model (GSM) [13,14]. *Ab initio* calculations that use a proper asymptotic behavior of wave functions include also the No-Core Shell Model (NCSM) coupled with the Resonating Group Method [15] and the Coupled Cluster approach generalized in the complex-energy plane using the Berggren basis [16].

We assert that the appearance of cluster states in the vicinity of their respective cluster decay thresholds is another direct consequence of an openness of the nuclear many-body system and, as such, cannot be predicted by the standard SM [17].

NEAR-THRESHOLD CLUSTER STATES

The cluster states are closely related to the nature of a nearby cluster-decay threshold. The challenging problem is how to separate generic and specific features of this intricate many-body phenomenon. The energetic order of particle emission thresholds, and their nature, is given by the N- and Z-dependence of the nuclear

binding energy, *i.e.*, it depends on specific properties of the nuclear Hamiltonian. The appearance of specific decay channels involving both kinds of nucleons, and the absence of stable nuclei entirely composed of like nucleons, is a direct consequence of the isospin structure of the nuclear force. On the other hand, the phenomenological rule that cluster correlations are seen in the vicinity of the respective cluster emission threshold is unlikely a consequence of specific properties of nuclear forces and calls for a generic explanation.

The comprehensive understanding of the universal occurrence of clustering and its properties is absent in the CQS formulation of the nuclear many-body problem. The commonly used Cluster Model (CM) [18] is an *a posteriori* approach that *assumes* effective building blocks (clusters). *A priori* approaches, like the nuclear SM approach, simply fail to predict cluster states at around cluster-decay thresholds. A well-known formal correspondence between Slater determinants of single-particle harmonic oscillator wave functions, used in many CQS SM frameworks, and CM wave functions [19], is of limited use when it comes to a proper treatment of decay thresholds and asymptotic behavior of wave functions.

Ikeda *et al.* [20] remarked that α-cluster states can be found in the proximity of α-particle decay thresholds. A plausible explanation of this phenomenological rule has been in terms of the collective coupling of SM states via the decay channel(s) [17]. Actually, the conjecture of Ikeda can be formulated more generally [17]; namely, the coupling to a nearby particle/cluster decay channel induces particle/cluster correlations in Continuum Shell Model (CSM) wave functions which are the imprint of this channel. In other words, clustering is a generic near-threshold phenomenon in OQS which does not originate from any particular property of the nuclear forces or any dynamical symmetry of the nuclear many-body problem. This generalized conjecture holds for *all* kinds of clustering, including unstable clusters such as dineutron or ^{8}Be.

The real-energy CSM (SMEC) using Feshbach projection formalism [12] offers a convenient framework in which generic features of clustering can be discussed. In this framework, the description of internal dynamics includes couplings to the environment of decay channels, and is modelled by the energy-dependent effective Hamiltonian which is non-Hermitian for energies above the first particle-decay threshold. The continuum-coupling term in this Hamiltonian generates effective many-body interactions in the internal space, even if it has two-body character in the full space [21].

The coupling to decay channels results in the anti-Hermitian component. The interplay between Hermitian and anti-Hermitian components of the effective Hamiltonian is a source of collective near-threshold phenomena in the ensemble of SM states [17] and leads to the binding energy stabilization. In particular, the anti-Hermitian mixing tends to concentrate the continuum coupling in a single state (aligned state) of the OQS, an archetype of the cluster state, which captures most of the continuum coupling, and, above the decay threshold, exhausts most of the decay width.

The continuum-coupling correlation energy of the SM eigenstate depends on the structure of the SM eigenstate and the nature of the decay channel. The correlation energy is peaked at the threshold only for the coupling to the l=0 neutron decay channel [21]. For higher partial waves and/or for charged particles, the centrifugal

Coulomb barriers shift the maximum of the correlation energy above the threshold. Even though the continuum-coupling correlation energy is a small fraction of the total binding energy, it profoundly impacts the configuration mixing leading to instabilities of certain SM eigenstates near the channel threshold.

The continuum-coupling induced mixing of SM states diminishes with increasing proton number, *i.e.*, the increased Coulomb barrier in heavier nuclei suppresses correlation energy close to particle-decay threshold and, therefore, prevents the clustering. This generic tendency does not depend on the nature of the decay threshold

OUTLOOK

Clustering is one of the most complex phenomenon known to the structure of atomic nuclei. A comprehensive description of clustering goes beyond standard SM and CM frameworks. We argue that clustering is a direct consequence of the collective mixing of SM eigenstates via the aligned state which captures most of the continuum coupling and carries many characteristics of the decay channel. Above the decay threshold, the aligned state becomes a broad resonance.

The mechanism responsible for the creation of the aligned near-threshold state is mathematically similar to the formation mechanism of collective super-radiant [7] or trapped states [8,9]. However, the physical domain of aligned states is not restricted to the region of large density of resonances in the continuum. It can even correspond to a bound state at energy below the lowest decay threshold. Collectivity of the aligned state is a fingerprint of instability in the ensemble of all SM states having the same quantum numbers and coupled to the same decay channel. Quantitatively, manifestations of this instability depend on the strength of the continuum coupling, the density of SM states, and the nature of the decay channel [17].

Neutral-cluster configurations are expected to show up primarily *below* the threshold, due to the rapid growth of the decay width with energy. Here, spectacular examples are one- and two-neutron halos in light nuclei. Favorable conditions for the charged-cluster configurations are *above* the charged-cluster emission threshold. The Hoyle resonance in ^{12}C represents is a good example of such a continuum-correlated collective state. Several narrow α-cluster resonances are known in *p*- and s*d*-shell nuclei from the valley of beta stability. Exotic forms of clustering, such as ^{3}H-, dineutron-, and ^{3}He-clustering, are expected close to neutron and proton drip lines, respectively.

To learn more about an interplay between internal (Hermitian) and external (anti-Hermitian, via the continuum) configuration mixing, it will be necessary to develop a vigorous experimental program searching for coalescing resonances. An excellent example is the 2+ doublet of narrow (Γ~100 keV) resonances in ^{8}Be at the excitation energies 16.63 MeV and 16.92 MeV, respectively. These two resonances, which have approximately the structure of ^{7}Li+p and ^{7}Be+n threshold configurations [22], are seen below one-nucleon emission thresholds. Above these thresholds, one finds a nearly degenerate, both in energy and width, doublet of 3+ resonances. More experimental data on exotic clustering and double-poles of S-matrix would be necessary to stimulate intense studies of the continuum-coupling induced

configuration mixing by comparing *ab initio* No-Core GSM and NCSM for the same with realistic chiral interactions [23].

REFERENCES

1. P. Navratil, S. Quaglioni, I. Stetcu, and B. R. Barrett, J. Phys. G: Nucl. Part. Phys. **36**, 083101 (2009).
2. E. Epelbaum, H.W. Hammer, and U.G. Meissner, Rev. Mod. Phys. **81**, 1773 (2009).
3. R. Machleidt, and D. Entem, Phys. Rep. **503**, 1 (2011).
4. J. Dobaczewski, N. Michel, W. Nazarewicz, and M. Płoszajczak, Prog. Part. Nucl. Phys. **59**, 432 (2007).
5. E. P. Wigner, Phys. Rev. **73**, 1002 (1948);
   N. Michel, W. Nazarewicz, and M. Płoszajczak, Phys. Rev. C **75**, 031301 (2007).
6. J. B. Ehrman, Phys. Rev. **81**, 412 (1951);
   R. G. Thomas, Phys. Rev. **88**, 1109 (1952);
   N. Michel, W. Nazarewicz, and M. Płoszajczak, Phys. Rev. C **82**, 044315 (2010).
7. P. Kleinwächter, and I. Rotter, Phys. Rev. C **32**, 1742 (1985);
   V.V. Sokolov, and V.G. Zelevinsky, Phys. Lett. B **202**, 10 (1988).
8. S. Drożdż, J. Okołowicz, M. Płoszajczak, and I. Rotter, Phys. Rev. C **62**, 24313 (2000).
9. R. H. Dicke, Phys. Rev. **93**, 99 (1954);
   N. Auerbach, and V. G. Zelevinsky, Rep. Prog. Phys. **74**, 106301 (2011).
10. A. I. Baz, Soviet Phys.-JETP **6**, 709 (1957);
    R. G. Newton, Phys. Rev. **114**, 1611 (1959).
11. P. E. Kohler, F. Bečvař, M. Krtička, J. A Harvey, and K. H. Guber, Phys. Rev. Lett. **105**, 072502 (2010); G. L. Celardo, N. Auerbach, F. M. Izrailev, and V. G. Zelevinsky, Phys. Rev. Lett. **106**, 042501 (2011).
12. K. Bennaceur, F. Nowacki, J. Okołowicz, and M. Płoszajczak, Nucl. Phys. A **651**, 289 (1999);
    J. Okołowicz, M. Płoszajczak, and I. Rotter, Phys. Rep. **374**, 271 (2003).
13. N. Michel, W. Nazarewicz, M. Płoszajczak, and K. Bennaceur, Phys. Rev. Lett **89**, 042502 (2002);
    N. Michel, W. Nazarewicz, M. Płoszajczak, and J. Okołowicz, Phys. Rev. C **67**, 054311 (2003);
    R. Id Betan, R.J. Liotta, N. Sandulescu, and T. Vertse, Phys. Rev. Lett. **89**, 042501 (2002);
    N. Michel, W. Nazarewicz, M. Płoszajczak, and T. Vaertse, J. Phys. G: Nucl. Part. Phys. **36**, 013101 (2009).
14. G. Papadimitriou, J. Rotureau, N. Michel, M. Płoszajczak and B. R. Barrett, arXiv:1301.7140.
15. S. Quaglioni, and P. Navrátil, Phys. Rev. C **79**, 044606 (2009);
    S. Baroni, P. Navrátil, and S. Quaglioni, Phys. Rev. Lett. **110**, 022505 (2013).
16. G. Hagen, D. J. Dean, M. Hjorth-Jensen, and T. Papenbrock, Phys. Lett. B **656,** 169 (2007).
17. J. Okołowicz, M. Płoszajczak, and W. Nazarewicz, Prog. Theor. Phys. Supplement **196**, 230 (2012);
    J. Okołowicz, W. Nazarewicz, and M. Płoszajczak, Fortschr. Phys., **61**, 66 (2013).
18. J. A. Wheeler, Phys. Rev. **52**, 1083 (1937);
    J. Hiura and I. Shimodaya, Prog. Theor. Phys. **30**, 585 (1963); *ibid.* **36**, 977 (1966);
    R. Tamagaki and H. Tanaka, Prog. Theor. Phys. **34**, 191 (1965).
19. K. Wildermuth, Nucl. Phys. **31**, 478 (1962);
    I. Rotter, Nucl. Phys. A **135**, 378 (1969);
    K. T. Hecht, Phys. Rev. C **16**, 2401 (1977).
20. K. Ikeda, N. Takigawa, and H. Horiuchi, Prog. Theor. Phys. Suppl Extra number, 464 (1968).
21. Y. Luo, J. Okołowicz, M. Płoszajczak, and N. Michel, arXiv:nucl-th/0211068;
    J. Okołowicz, M. Płoszajczak, and Y. Luo, Acta Physica Polonica B **39**, 389 (2007).
22. F. Hintenberger et al., Nucl. Phys. A **299**, 397 (1978).
23. G. Papadimitriou, J. Rotureau, B.R. Barrett, Ch. Forssén, and M. Płoszajczak, in preparation (2013).

Clusters, Halos, And S-Factors In Fermionic Molecular Dynamics [1]

Hans Feldmeier and Thomas Neff

GSI Helmholtzzentrum für Schwerionenforschung GmbH, Darmstadt

Keywords: exotic nuclear structure, Fermionic Molecular Dynamics, cluster, proton halo, S-factor
PACS: 21.10, 21.60, 23.20, 24.10, 25.55

FERMIONIC MOLECULAR DYNAMICS (FMD)

In the FMD approach we employ Gaussian wave packets

$$\langle \mathbf{x}|q\rangle = \exp\left\{-\frac{(\mathbf{x}-\mathbf{b})^2}{2a}\right\} \otimes \big|\, \chi^{\uparrow}, \chi^{\downarrow} \,\big\rangle \otimes \big|\, \xi \,\big\rangle \tag{1}$$

as single-particle basis states. The complex parameters **b** encode the mean positions and momenta of the wave packets and a the widths of the wave packets. The spins can assume any direction, isospin is ± 1 denoting a proton or a neutron. Intrinsic many-body basis states are Slater determinants

$$\big|\, Q \,\big\rangle = \mathscr{A}\left\{ \big|\, q_1 \,\big\rangle \otimes \ldots \otimes \big|\, q_A \,\big\rangle \right\} \tag{2}$$

that reflect deformation or clustering and break the symmetries of the Hamiltonian with respect to parity, rotation and translation. To restore the symmetries the intrinsic basis states are projected on parity, angular momentum and total linear momentum

$$\big|\, Q; J^{\pi} MK; \mathbf{P}=0 \,\big\rangle = \hat{P}^{\pi} \hat{P}^{J}_{MK} \hat{P}^{\mathbf{P}=0} \,\big|\, Q \,\big\rangle. \tag{3}$$

In a full FMD calculation the many-body Hilbert space is spanned by a set of N projected intrinsic basis states $\{\big|\, Q^{(a)}; J^{\pi} MK; \mathbf{P}=0 \,\big\rangle, a = 1, \ldots, N\}$. By diagonalizing the Hamiltonian in this set of non-orthogonal basis states the amplitudes of the various configurations contained in the many-body eigenstate are determined.

Starting from the realistic Argonne V18 interaction [1] we derive a phase-shift-equivalent effective low-momentum interaction using the unitary correlation operator method (UCOM). The basic idea of the UCOM approach is to explicitly include short-range central and tensor correlations by means of a unitary operator [2, 3, 4]. No-core shell model calculations show that the two-body UCOM interaction gives a good description of *s*- and light *p*-shell nuclei [4], indicating that the neglected induced 3-body forces cancel to a certain extent the missing genuine 3-body forces.

[1] Supported by the ExtreMe Matter Institute EMMI

CLUSTER STATES IN ^{12}C

The structure of the second 0^+_2 state in ^{12}C, the famous Hoyle state, is still one of the hottest topics in nuclear structure. In [5] we investigated its structure with a model space consisting of FMD configurations obtained by variation and a full set of three-α configurations and found that the Hoyle state has a very dilute and extended three-α structure. This is illustrated in Fig. 1 where we show the intrinsic FMD basis states that have the largest overlap with the ground state and the Hoyle state.

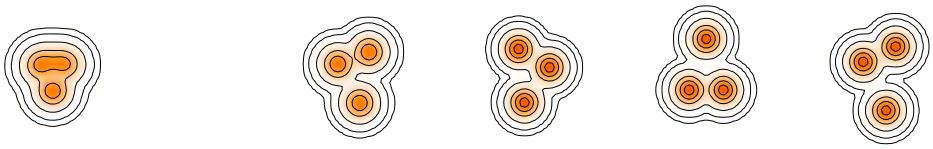

FIGURE 1. Left: intrinsic FMD basis state that has the largest overlap with the ground state. Right: the four intrinsic FMD basis states that have the largest overlap with the Hoyle state.

We used these many-body wave functions also to calculate the transition form factor from the ground state to the Hoyle state and compared it directly to electron scattering data [5, 6]. The good agreement of calculation and experiment is a strong confirmation for a spatially extended cluster structure of the Hoyle state. Also the second 2^+_2 above the Hoyle state and the third 0^+_3 exhibit very extended α-cluster structures with large point radii. Overall, the results are very similar to those in [7, 8].

Radii	Exp	FMD	Transitions	Exp	FMD
$r_{\text{charge}}(0^+_1)$	2.47(2) fm	2.53 fm	$M(E0, 0^+_1 \to 0^+_2)$	5.4(2) fm^2	6.53 fm^2
$r(0^+_1)$		2.39 fm	$B(E2, 2^+_1 \to 0^+_1)$	7.6(4) e^{2}fm^4	8.69 e^{2}fm^4
$r(0^+_2)$ Hoyle state		**3.38** fm	$B(E2, 2^+_1 \to 0^+_2)$	2.6(4) e^{2}fm^4	3.83 e^{2}fm^4
$r(0^+_3)$ Hoyle like		**4.62** fm			
$r(2^+_1)$		2.50 fm			
$r(2^+_2)$ Hoyle like		**4.43** fm			

NEON ISOTOPES AND TWO-PROTON HALO

The charge radii of the neon isotopes, which have been measured in Ref. [9], do not show the usual monotonic increase with mass number, see Fig. 2. The FMD model explains this by substantial changes in the ground-state structure. It attributes the large charge radius of ^{17}Ne to an extended two-proton halo with an s^2 component of about 40%, r.h.s. of Fig. 2. In ^{18}Ne the radius is smaller due to a significantly smaller s^2 component. The radius increase for ^{19}Ne is caused by the admixture of ^{16}O - ^{3}He and ^{15}O - ^{4}He cluster configurations in the tail of the wave function. These admixtures are related to the known deformation properties and decrease with growing neutron number.

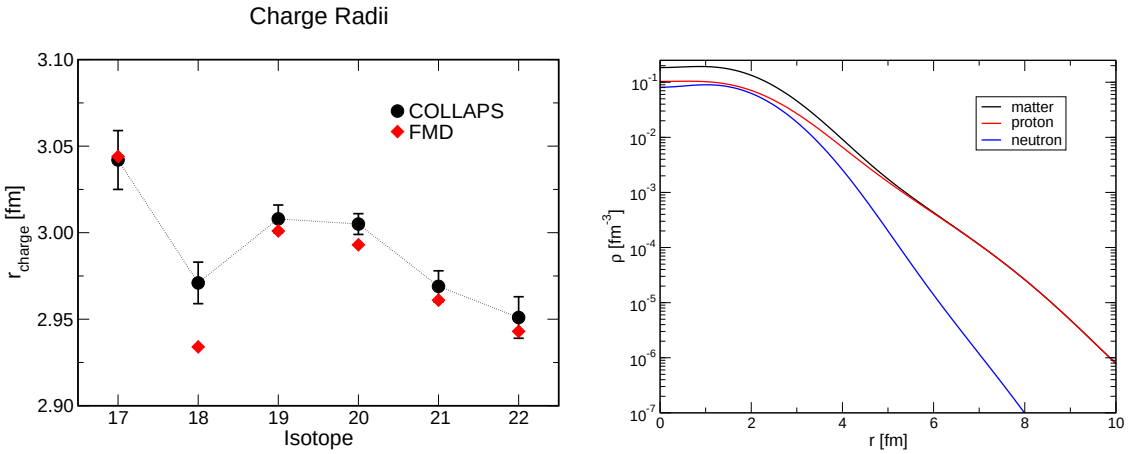

FIGURE 2. Left: charge radii of Ne isotopes measured by COLLAPS und calculated with FMD [9] Right: two-proton halo in ^{17}Ne, matter and proton point densities.

RADIATIVE CAPTURE REACTION ^{3}He$(\alpha,\gamma)^7$Be

Another application of the FMD approach is the calculation of the ^{3}He$(\alpha,\gamma)^7$Be radiative capture reaction [16]. As this reaction plays an important role in the solar proton-proton chains and determines the production of ^{7}Be and ^{8}B neutrinos [17, 18], it has been studied extensively from the experimental side in recent years [10, 11, 12, 13, 14]. However, it is still not possible to reach the low energies relevant for solar burning in experiment. From the theory side this reaction has been investigated using simple potential models, where ^{3}He and ^{4}He are treated as point-like particles interacting via an effective nucleus-nucleus potential, e.g., [19] or microscopic cluster models, e.g., [20, 21] where the ^{7}Be bound and scattering states are constructed from microscopic ^{3}He and ^{4}He clusters interacting via an effective nucleon-nucleon interaction. *Ab-initio* calculations using variational Monte Carlo [22] and no-core shell model wave functions [23] were used to calculate asymptotic normalization coefficients for the bound states

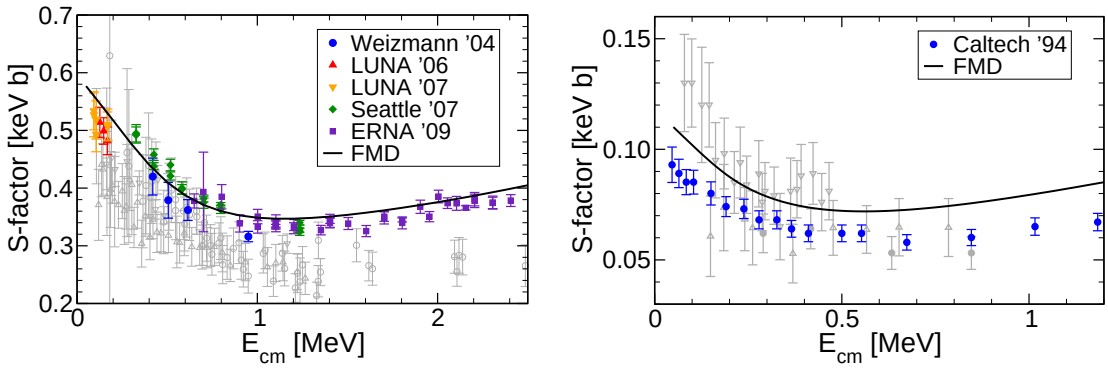

FIGURE 3. *S*-factor for capture reaction - left: ^{3}He$(\alpha,\gamma)^7$Be, recent data [10, 11, 12, 13, 14] colored symbols, older data gray symbols - right: ^{3}H$(\alpha,\gamma)^7$Li, recent data [15] colored, older data gray symbols.

but relied on potential models for the scattering phase shifts.

In the FMD calculation we divided the many-body Hilbert space into an external region, where the scattering states are antisymmetrized products of ^{3}He and ^{4}He clusters in their FMD ground states at various distances, and an interaction region, where FMD configurations were obtained by variation after projection on spin-parity $1/2^+$, $3/2^+$, $5/2^+$ and $3/2^-$, $1/2^-$, $7/2^-$, $5/2^-$. A constraint on the radius of the intrinsic states was used to vary the distance between the clusters. Using the microscopic *R*-matrix method [24] boundary conditions for bound and scattering states were implemented by matching to Whittaker and Coulomb functions at the channel radius (a = 12 fm).

The capture cross section was calculated from electromagnetic transition rates between the microscopic many-body scattering and bound and states. The result for the total cross section for the ^{3}He$(\alpha,\gamma)^7$Be capture, shown in form of the astrophysical *S*-factor in the left part of Fig. 3 agrees very well with the recent data, both in absolute normalization and in the energy dependence. The calculated energy dependence of the *S*-factor in the isospin mirror reaction ^{3}H$(\alpha,\gamma)^7$Li agrees well with the data (right hand side of Fig. 3), but the absolute cross section is larger then the data by Brune *et al.* by about 15%. This is surprising as the FMD results for the ^{7}Li bound states and the scattering phase shifts are of similar quality as those for ^{7}Be.

REFERENCES

1. R. B. Wiringa, V. G. J. Stoks, and R. Schiavilla, *Phys. Rev. C* **51**, 38 (1995).
2. H. Feldmeier, T. Neff, R. Roth, and J. Schnack, *Nucl. Phys.* **A632**, 61 (1998).
3. T. Neff, and H. Feldmeier, *Nucl. Phys.* **A713**, 311 (2003).
4. R. Roth, T. Neff, and H. Feldmeier, *Prog. Part. Nucl. Phys.* **65**, 50 (2010).
5. M. Chernykh, H. Feldmeier, T. Neff, P. von Neumann-Cosel, and A. Richter, *Phys. Rev. Lett.* **98**, 032501 (2007).
6. M. Chernykh, H. Feldmeier, T. Neff, P. von Neumann-Cosel, and A. Richter, *Phys. Rev. Lett.* **105**, 022501 (2010).
7. M. Kamimura, *Nucl. Phys.* **A351**, 456 (1981).
8. Y. Funaki, A. Tohsaki, H. Horiuchi, P. Schuck, and G. Röpke, *Phys. Rev. C* **67**, 051306(R) (2003).
9. W. Geithner, T. Neff, G. Audi, K. Blaum, P. Delahaye, H. Feldmeier, S. George, C. Guénaut, F. Herfurth, A. Herlert, S. Kappertz, M. Keim, A. Kellerbauer, H.-J. Kluge, M. Kowalska, P. Lievens, D. Lunney, K. Marinova, R. Neugart, L. Schweikhard, S. Wilbert, and C. Yazidjian, *Phys. Rev. Lett.* **101**, 252502 (2008).
10. B. S. Nara Singh, M. Hass, Y. Nir-El, and G. Haquin, *Phys. Rev. Lett.* **93**, 262503 (2004).
11. D. Bemmerer, et al., *Phys. Rev. Lett.* **97**, 122502 (2006).
12. F. Confortola, et al., *Phys. Rev. C* **75**, 065803 (2007).
13. T. A. D. Brown, et al., *Phys. Rev. C* **76**, 055801 (2007).
14. A. Di Leva, et al., *Phys. Rev. Lett.* **102**, 232502 (2009).
15. C. R. Brune, R. W. Kavanagh, and C. Rolfs, *Phys. Rev. C* **50**, 2205 (1994).
16. T. Neff, *Phys. Rev. Lett.* **106**, 042502 (2011).
17. E. G. Adelberger, et al., *Rev. Mod. Phys.* **70**, 1265 (1998).
18. E. G. Adelberger, et al., *Rev. Mod. Phys.* **83**, 195 (2011).
19. B. T. Kim, T. Izumoto, and K. Nagatani, *Phys. Rev. C* **23**, 33 (1981).
20. K. Langanke, *Nucl. Phys.* **A457**, 351 (1986).
21. T. Kajino, *Nucl. Phys.* **A460**, 559 (1986).
22. K. M. Nollett, *Phys. Rev.* **C63**, 054002 (2001).
23. P. Navrátil, V. G. Gueorguiev, J. P. Vary, W. E. Ormand, and A. Nogga, *Phys. Rev. Lett.* **99**, 042501 (2007).
24. P. Descouvemont, and D. Baye, *Rep. Prog. Phys.* **73**, 036301 (2010).

Study of pairing and clusterisation in light nuclei through nuclear break-up

Marlène Assié[a], Jean-Antoine Scarpaci[b] and D. Lacroix[c]

[a]*Institut de Physique Nucléaire, and Université Paris Sud 11, UMR 8608, Bât 100, 15 rue Georges Clémenceau, 91406 Orsay, France.*
[b]*Centre de Spectrométrie Nucléaire et de Spectrométrie de Masse (CSNSM), IN2P3-CNRS and Université Paris Sud 11, UMR 8609, Bât. 104, 91405 0rsay Campus, France*
[c] *GANIL, Bd Henri Becquerel, BP 55027, 14076 Caen Cedex 5, France*

.

NUCLEAR BREAK-UP REACTIONS

Nuclear break-up occurs at few tens of MeV per nucleon. Among all other inelastic processes leading to the emission of one nucleon, the nuclear break-up, also called Towing Mode is characterized by the emission of a nucleon from the target on the same side as the projectile with an intermediate velocity and a large angle with respect to the beam axis. Knock-out reactions lead to a nucleon emitted around 90 deg. while pick-up break-up reactions lead to forward emission.The mechanism is understood the following way: when the projectile passes by the target, the nucleon inside the target feels its nuclear potential and is towed to be emitted to the continuum. This picture is confirmed by a theoretical model solving the time dependent Schrödinger equation (TDSE) for the wave function of a nucleon inside the potential of target when the projectile potential passes by.

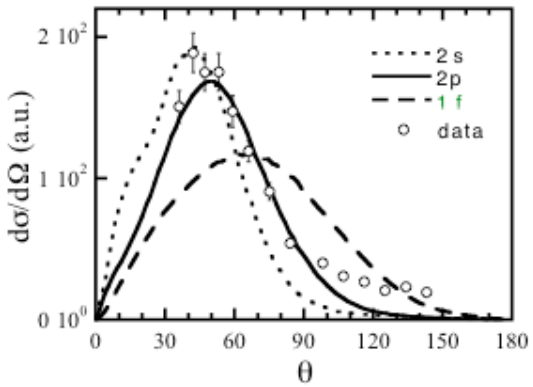

FIGURE 1 : Angular distribution of neutrons from the ^{40}Ar+^{58}Ni experiment compared to TDSE calculations for 3 different wave functions.

The nuclear break-up was brought out in the ^{40}Ar+^{58}Ni @ 44 MeV/A reaction where the neutron or proton knock-out was measured [1]. In addition to the statistical decay, a contribution was highlighted in the forward region. The angular distribution extracted for each excited state populated in the daughter nucleus showed very good

agreement with the TDSE calculations (see Fig. 1). Therefore nuclear break-up is sensitive to the initial wave function (quantum numbers) of the nucleon inside the target and can be used as a tool to probe nuclear structure. Several examples of utilization of nuclear break-up will be shown below such as configuration mixing, pairing correlation and clusterization into alpha particles.

PROBING CONFIGURATION MIXING

The ground state of ^{11}Be is known to be a superimposition of two configurations that is to say (i) a ^{10}Be in its ground state and a neutron in the $2s_{1/2}$ and (ii) a ^{10}Be in its first deformed 2^+ state with a neutron in the $1d_{5/2}$. The configuration mixing was estimated by breaking up the ^{11}Be and detecting the emitted neutron and the possibly emitted gamma together with the residual projectile. The energy distributions obtained compared to TDSE calculations enabled to extract a spectroscopic factor for the (i) configuration of S_{2s} = 0,47± 0,04 and for the (ii) configuration of S_{1d}= 0,50 ± 0,20 [2].

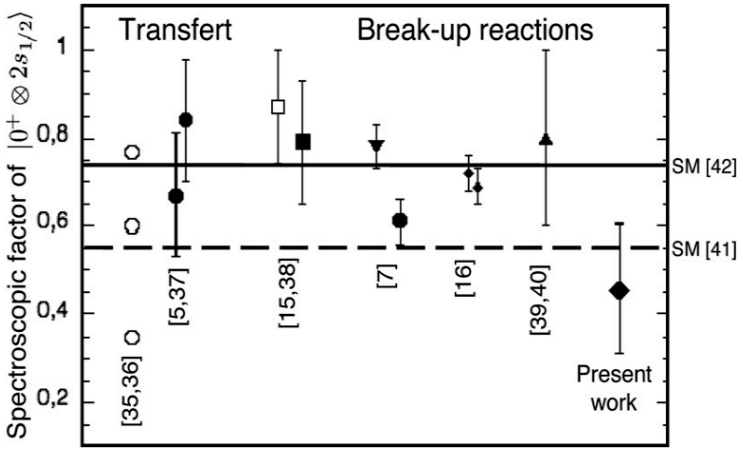

FIGURE 2 : Comparaison of S(2s) with previous experiments. See references in [2].

A good agreement is obtained for the S_{2s} spectroscopic factor with previous experiment (see Fig. 2) although the TDSE model does not take into account interferences between the two types of configurations.

PROBING ALPHA CLUSTERIZATION IN NUCLEI

Several nucleons can be towed in the nuclear break-up process and particularly alpha particles. In the case of symmetric matter, the formation of alpha clusters in the ground state of the N=Z nuclei should increase the cross-section of alpha emission from the nuclear break-up.

The experiment was performed at GANIL with the reaction $^{40}Ca+^{40}Ca$ at 50 MeV/A. The projectile was identified with the SPEG spectrometer and the emitted alpha with the INDRA array. The missing mass spectrum of ^{36}Ar shows several excited states. For each of them the angular distribution of the emitted alphas can be extracted experimentally. Then, it can be compared to the TDSE calculation for the wave function of an alpha particle and an adjusted potential to reproduce ^{40}Ca rotational bands. This schematic calculation reproduces surprisingly well the width of the experimental curves.

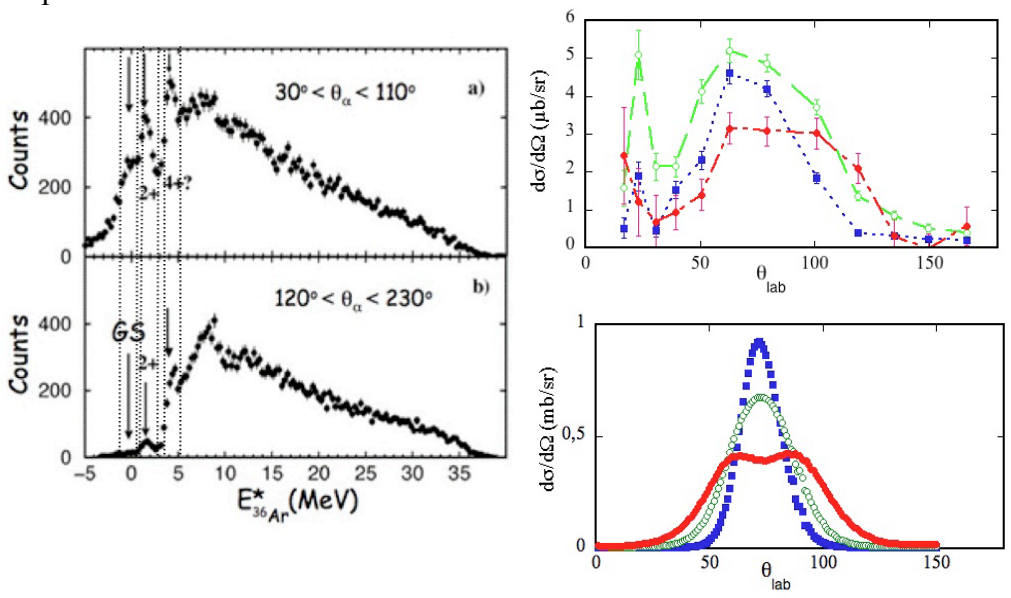

FIGURE 3 : (Left) Missing mass spectra for ^{36}Ar for an alpha particle detected forward (top) and backward (bottom). (Right top) Experimental angular distributions associated to each excited state in ^{36}Ar. (Right bottom) Expected angular distribution from the TDSE calculations [3].

A spectroscopic factor of 1.2% was extracted for the alpha clusterization in the ground state of ^{40}Ca. This is in agreement with shell model calculations [4] but not with the measurement of Umeda et al [5].

PROBING PAIRING CORRELATIONS IN LIGHT NUCLEI

In the case of very light nuclei close to driplines, pairing plays an important role and particularly for borromean nuclei where the binding is insured by pairing. As nuclear break-up is sensitive to the wave function of the nucleons and also to spatial configuration, it can be a powerful tool to investigate pairing.

In the case of ^{6}He, two configurations are expected from the three-body model: (i) a di-neutron configuration where the two neutrons lie close to each other and (ii) a cigar configuration where the neutrons are on opposite side with respect to the alpha core. In the first case (i) nuclear break-up should lead to the emission of the two neutrons

together at large angle whereas in case (ii) one neutron will be towed and the second one be emitted in the direction of the beam as ^{5}He is not bound. The distribution of relative angle between the two emitted neutron should then give the information on the spatial correlation between the neutrons in the halo.

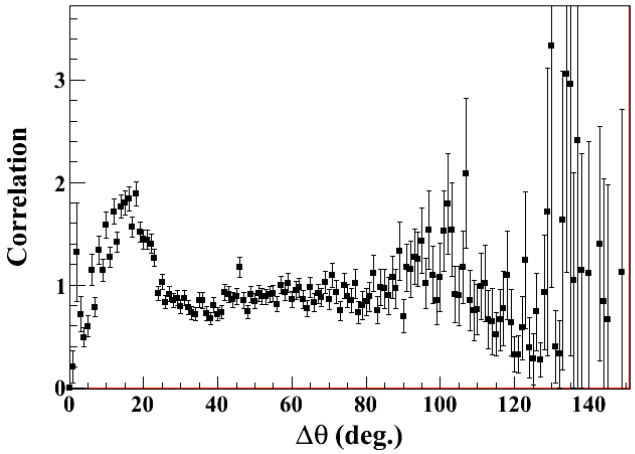

FIGURE 4 : Correlation function obtained from the experimental data. When it is close to 1, no correlation is seen and any deviation is a signature of correlation. A strong correlation is seen for small angles corresponding to di-neutron configuration.

The break-up of ^{6}He on ^{208}Pb was studied at GANIL using the Neutron Wall and the EDEN neutron detectors coupled to an annular Silicon stripped detector. Correlation functions were extracted experimentally (see Ref.[7] for more details). In order to compare the experimental results a new theoretical model has been developed. This reaction model TDDM^{P} is a beyond mean-field model including pairing correlations [6]. It confirms that nuclear break-up is sensitive to the different configurations in ^{6}He and seems to show that most part of the experimental distribution is reproduced by the di-neutron configuration.

CONCLUSION

Several studies with nuclear break-up show that it is a powerful tool to investigate nuclear clusterization. This mechanism requires post-accelerated beams such as the EURISOL ones. In the next coming years, efforts will be devoted to the study of cluterization into the B chain where AMD calculations predict strong clusterization.

REFERENCES

1. J.A. Scarpaci *et al., Physics Letters B* **428**, 241 (1998).
2. V.Lima *et al*., *Nuclear Physics A* **795,** 1 (2007).
3. J-A. Scarpaci *et al*, *Phys. Rev. C* **82** 031301(R) (2010).
4. Chung et al. *Phys. Lett. B* **79**, 381, (1978).
5. Umeda et al. *Nucl. Phys. A* **429**, 88 (1984).
6. M. Assié and D. Lacroix, *Phys. Rev. Lett.* **102**, 202501 (2009)
7. M. Assié *et al, Eur. Phys. J. A* **42,** 441 (2009).

Direct Reactions with Exotic Nuclei

Alexandre Obertelli

CEA Saclay, IRFU/Service de Physique Nucléaire, 91191 Gif-sur-Yvette cedex, France

1- Nuclear structure from direct reactions

In nuclear reactions, some processes leave the final nucleus in a state that retains recollections of the initial wave function. These reactions, for which few degrees of freedom were modified, are called direct [1]. This gives to direct reactions, in addition to their selectivity, the strong advantage to allow a quantitative investigation of the ground-state properties of atomic nuclei.

Different direct reaction mechanisms are used depending on the incident energy. Often encountered are nucleon transfer reactions at low incident energy, generally in a regime between 5 and 50 MeV/nucleon, and knockout reactions at relativistic energies, typically above 150 MeV/nucleon to minimize indirect contributions to the direct cross section.
The electron-induced stripping reaction *(e,e'p)* is considered to be the reference stripping measurement from stable nuclei. As an electromagnetic probe, *(e,e'p)* is considered to be well understood when restricted to large momentum transfer. In this case, small corrections have to be taken into account for final state interaction with the proton in the exit channel [2]. Charge density and intrinsic momentum distributions of protons in stable nuclei have been well studied this way. The neutron component of nuclei requires a nuclear probe. Transfer and *(p,2p)* reactions have been benchmarked with *(e,e'p)* and found to be consistent for stable nuclei when treated as direct mechanisms and analyzed within a DWBA framework [3].

Information extracted from the analysis of direct reaction cross sections has driven our understanding of the nuclear shell structure and their usefulness is unanimously recognized. The spectroscopic strength obtained from pickup and stripping reactions are indeed necessary to quantify the amount of correlations in a given nucleus and offer the possibility to address, when extracted from cross sections within a given theoretical framework, the question of uncorrelated single-particle energies E_{sp} [4]

$$E_{sp} = \Sigma_{\mu} SF_{\mu}^{+} E_{\mu} + \Sigma_{\nu} SF_{\nu}^{-} E_{\nu}$$

Where $SF^{+(-)}$ are the so-called spectroscopic factors extracted from the pickup (stripping) cross sections. The non-observable nature of spectroscopic factors and single-particle energies restricts their use to being model dependent. However they are still necessary and allow for a depiction of nuclear structure [5,6].

From the early 90s, direct reactions have been widely used as a selective probe for the structure of unstable nuclei. The spectroscopy of radioactive ions can only be reached in inverse kinematics and laboratories such as GANIL, REX-ISOLDE at CERN, RIKEN and the NSCL, have successfully devoted a significant part of their research programs to in-beam spectroscopy in inverse kinematics.

2- Spectroscopic strength from one-nucleon stripping

The distribution of spectroscopic strength in nuclei can be extracted from direct-reaction cross section measurements, assuming a modeling of the reaction mechanism.

Recently, a compilation of one-nucleon removal at intermediate energies from *sd*-shell exotic nuclei showed that the measured cross sections for knocking out a valence nucleon in a very asymmetric nucleus (such as a neutron in ^{32}Ar, ^{28}Ar and ^{24}Si) are about four times smaller than predictions from state-of-the-art calculations [7]. On the other hand, at low energy, a study of the *(p,d)* neutron transfer on the proton-rich ^{34}Ar and on the neutron-rich ^{46}Ar provides experimental spectroscopic factors in agreement with large-basis shell model calculations to within 20% [8]. These findings which are in agreement with a previous systematic study of transfer reactions [9] are inconsistent with the trend observed in knockout. Therefore, it is suggested that these two probes lead systematically to different spectroscopic factors. The origin of this difference has to be understood.

A recent study of the nucleon removal from ^{14}O and ^{16}C ($\Delta S = |S_n - S_p|$ close to 20 MeV) at intermediate energies lower than 100 MeV nucleon has shown that the applicability of the sudden approximation and the eikonal theory for nucleon removal depends on both the incident beam energy and the binding energy of the removed nucleon [10]. The applicability of the eikonal formalism to the previously deeply-bound nucleon removal was questioned. Indeed, one may question the rôle of dissipation in deeply-bound nucleon removal [11].

The corresponding transfer stripping reactions *(d,t)* and *(d,^{3}He)* from the same ^{14}O nucleus at 18 MeV/nucleon performed at GANIL [12] and analyzed within the framework of coupled reaction channel formalism with a set of optical potentials, matter radii and spectroscopic factors did not show any systematic reduction for deeply-bond nucleon stripping at variance with [7]. This is in agreement with the first analysis of [8].

A more systematic study of deeply-bound nucleon removal reactions from weakly bound nuclei will definitely help understanding the limits of current direct reaction models.

3- Long-range correlations via two nucleon stripping

Two-body correlations are also a key aspect of nuclear structure. It can be probed via direct reactions. Momentum and spatial correlations in the nucleus have been investigated at all incident energies with different reaction mechanisms in the past.
The two neutron transfer has been widely used in both direct and indirect kinematics and is known to be sensitive to configuration transitions, such as shape transitions [13] or pairing in light [14,15] or heavy nuclei [16].
Two-nucleon knockout has been more recently introduced to probe correlations [17,18] and a dedicated formalism has been developed showing a strong sensitivity to two-body correlations of the intermediate-energy inclusive knockout [19]. At variance with transfer, the two-nucleon knockout probes only the spatial correlations. The fast two-neutron stripping and two-neutron transfer may then be seen as complementary probes for two-body correlations.
Still at intermediate energies, the incomplete transfer or towing mode [20] has been also used to investigate correlations in two neutron halos [21].
At relativistic incident energies, exclusive quasi free scattering with large momentum transfer can be seen as a perfect probe and should be investigated further.

In the case of proton-neutron T=0 correlations, deuteron transfer can be seen an efficient tool [22]. Some work have been performed in that direction along the N=Z line [23] but these studies are still marginal due to difficult interpretation of the absolute cross sections in terms of proton-neutron correlations.

In all these approaches, the effect of final state interactions on the observables is central and should be further investigated. To address this question, a careful benchmarking program of all relevant technics on the same physics case and, if possible, at different incident energies seems unavoidable.

4- New detection systems dedicated to direct reactions with radioactive beams

The construction of new facilities or upgrade of existing machines dedicated to radioactive-ion beam studies parallels the development of a new instrumentation with increased sensitivity to probe the spectroscopy of the most exotic nuclei. This increase in sensitivity can be obtained via a higher luminosity, a larger energy range of detection and a better energy resolution, alternatively an efficient combination of several probes, such as gamma and particle spectroscopy. In most cases, each of these developments is adapted to the accelerators and hence to given incident energy regime, typically low energies for transfer reactions (GANIL, REX-ISOLDE, FRIB,…) or relativistic energies for quasi-free scattering like experiments (RIKEN, FAIR,…).

At low incident energy, the European community has strongly pursued two directions in view of SPIRAL2: the ACTAR Time Projection Chamber [24] as a follow up of the MAYA detector [25] first developed at GANIL and the GASPARD Si-based telescope array [26] compact enough to fit inside a photon-detection array such as PARIS [27]

or AGATA [28] partly issued from the MUST2-array developments [29]. These instrumentations were primarily developed to be used at SPIRAL2 and HIE-ISOLDE for transfer and inelastic scattering experiments. These new devices are complemented by the development of the very thin pure hydrogen target CHyMENE [30].
In the US, a complementary approach is being followed and focused on the use of magnetic field. The leading projects focusing on transfer and inelastic scattering studies are AT-TPC [31], a TPC located inside a solenoid, and HELIOS [32], a novel setup using Si detectors inside a solenoid that allows an unreached energy resolution when very thin targets are used. A cautious analysis of the reason(s) why Europe is not pursuing such a direction should be undertaken.

At relativistic energies, several large-acceptance spectrometers and associated detection have been or are being developed for direct reactions at new and future facilities: SAMURAI [33] at RIBF, R3B [34] at FAIR. New generation scintillator arrays with high granularity, currently under study, should bring in a not so distant future a higher efficiency and enhanced resolution.

In-beam gamma spectroscopy should gain at least an order of magnitude, depending on the setup considered, with the use of the H_2 target – vertex tracker MINOS [35].

It is believed that direct reactions with hydrogen will provide in the future, benchmark data for the understanding of nuclear dynamics at both low energy and relativistic energy. Indeed, in view of more reliable results from reaction analysis, one may advocate that hydrogen induced reactions, when applicable to a specific study, should be favored to heavy targets whose structure can only add more complexity in the system [36].

On the theory side, a more consistent treatment of nuclear structure and the reaction mechanism is required. Such consistent calculations at an *ab initio* level are today performed for light systems at very low incident energy. Such *brute force* approach is considered inadequate for transfer or knockout.

5- Summary and outlook

Direct reactions have provided the physics community at large a sizeable part of the information required to reach our present understanding of the nuclear shell structure. Shell evolution with isospin and in-medium correlations can be effectively investigated via transfer and fast nucleon removal. It is considered here that direct reactions will be a corner-store of studies performed at upcoming new-generation radioactive beam facilities.

The study of highly exotic nuclei with very low binding energy requires a careful selection of approaches, a handful of which were initially developed for stable nuclei. Further, even though not seen as very appealing for structure studies, a proper benchmark for reaction models seems unavoidable to estimate the theoretical

uncertainties. Redundancy of a measurement at two different incident energies and the systematical use of two different experimental techniques are possible directions to follow. In that sense, a LINAC-based machine with a rather easy change of incident energy should be a definite asset.

The European community is developing several innovative detectors dedicated to direct reactions. They have distinct advantages, some improve the detection thresholds and allow the measurement of low-energy recoil reactions while others increase the compactness of the system and allow the combination of gamma and particle detection with high efficiency.

The near future should not be held within what is already under development. Colliders with exotic beams should offer new probes for nuclear structure. *(e,e'p)* reactions with exotic nuclei or nucleon annihilation from the interaction with antiprotons could be seen as a possible and exciting future possibilities where both new nuclear reaction models with innovative technical developments will allow a deeper understanding of nuclear mechanisms and structure.

REFERENCES

[1] Direct Nuclear Reactions, G. R. Satchler, Oxford University Press, 1983.
[2] C. Barbieri, D. Rohe, I. Sick, L. Lapikas, Physics Letters B **608**, 47-52 (2005).
[3] G.J. Kramer, H.P. Blok, L. Lapikas, Nuclear Physics A **679**, 267 (2001).
[4] M. Baranger, Nuclear Physics A **149**, 225 (1970).
[5] R. J. Furnstahl, H.-W. Hammer, Physics Letters B **531**, 203 (2002).
[6] T. Duguet, G. Hagen, Physical Review C **85**, 034330 (2012).
[7] A. Gade *et al.*, Physical Review C **77**, 044306 (2008).
[8] J. Lee *et al.*, Physical Review Letters **104**, 112701 (2010).
[9] M. B. Tsang *et al.*, Physical Review Letters **102**, 062501 (2009).
[10] F. Flavigny *et al.,* Physical Review Letters 108, 252501 (2012).
[11] C. Louchart *et al.,* Physical Review C 83, 011601 (2011).
[12] F. Flavigny *et al.,* accepted in Physical Review Letters (2013).
[13] P. D. Duval, D. Goutte, M. Vergnes, Physics Letters B **124**, 297 (1983).
[14] I. Tanihata *et al.,* Physical Review Letters **100**, 192502 (2008).
[15] G. Potel, F. Barranco, E. Vigezzi, R. A. Broglia, Physical Review Letters **105**, 172502 (2010).
[16] G. Potel *et al.,* Physical Review Letters **107**, 092501 (2011).
[17] K. Yoneda *et al.,* Physics Letters B **499**, 233-237 (2001).
[18] K. Yoneda *et al.,* Physical Review C **74**, 021303 (2006).
[19] E.C. Simpson, J.A. Tostevin, Physical Review C **79**, 024616 (2009).
[20] D. Lacroix, J.-A. Scarpaci, Ph. Chomaz, Nuclear Physics A **658**, 273-281 (1999).
[21] M. Assié, D. Lacroix, Physical Review Letters **102**, 202501 (2009).
[22] P. Van Isacker, D. D. Warner, A. Frank, Physical Review Letters 94, 162502 (2005).
[23] P. Fröbich, Physics Letters B 37, 338 (1971).
[24] http://pro.ganil-spiral2.eu/spiral2/instrumentation/actar-tpc
[25] C.E. Demonchy *et al*., Nucl. Instr. Meth. in Res. Phys. A **573**, 145-148 (2007).
[26] http://gaspard.in2p3.fr/index.html
[27] http://paris.ifj.edu.pl
[28] S. Akkoyun *et al.,* Nucl. Instr. Meth. in Res. Phys. A **688**, 26-58 (2012).
[29] E.C. Pollacco *et al.,* Nucl. Instr. Meth. in Res. Phys. A **421**, 471-491 (1999).
[30] A. Gillibert *et al.,* to be published in European Physics Journal A (2013).

[31] http://www.nscl.msu.edu/exp/sr/attpc
[32] A. H. Wuosmaa *et al.,* Nucl. Instr. Meth. in Res. Phys. A **580**, 1290-1300 (2007).
[33] Y. Shimizu *et al.,* Journal of Physics, Conference Series, **312**, 052022 (2011).
[34] http://www.gsi.de/work/forschung/nustarenna/kernreaktionen/activities/r3b.htm
[35] MINOS, European Research Council Starting Grant – 258301 (2010-2015).
[36] A. Obertelli, T. Uesaka, European Physics Journal A **47**, 105 (2011).

Trojan Horse Method: Application to Radioactive Ion Beam reactions

Claudio Spitaleri and Silvio Cherubini

Dipartimento di Fisica e Astronomia, Università di Catania,
INFN- Laboratori Nazionali del Sud, Catania. Italy

TROJAN HORSE METHOD: BASIC THEORY

The Trojan Horse Method (THM) has been used to measure nuclear reaction cross sections, between charged particles at sub-Coulomb energies, related to fundamental astrophysical problems at ultra low energies as an alternative to extrapolation techniques in particularly complex cases or when such measurement are even beyond the experimental feasibility [1-3]. This method has been presented in many previous cases both for non-resonant and resonant cross sections. Recently, it has also been applied to the measurement of cross sections of neutron induced reactions [4,5]. Here we will give a short description of the method and report on its application to the measurement of cross sections of reactions involving radioactive nuclei.

The THM allows to extract the bare nucleus astrophysical S_b(E)-factor without any contribution due to coulomb effects such as the cross section suppression [6] and the electron screening enhancement [7,8], that affect direct measurements at very low energies.

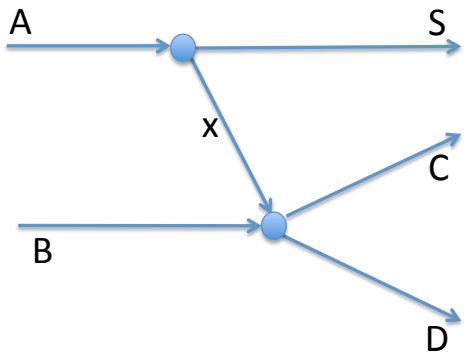

Fig.1 Diagram representing the quasi-free process A (B,C D)S. The upper vertex describes the virtual break-up of the THM-nucleus A into the clusters x (participant) and S (spectator).

The quasi-free A (B,C D)S reaction can be described by a Feynman diagram (Fig. 1). The diagram represents the dominant process (pole approximation), while other graphs (triangle graphs) indicating re-scattering between the reaction products, are neglected [9,10]. This diagram describes basically a transfer reaction to the continuum where the THM-nucleus A breaks up into a nucleus *"x"* ("participant" cluster) that is transferred to B originating the B(x,C)D virtual reaction while the nucleus "*S*" acts as a spectator ("spectator" cluster) in the process. The nucleus *"A"* should have a strong *"x + S*" cluster structure.

In this method the quasi-free (QF) contribution to the cross section of the three-body reaction A + B → C + D + S [11,12], measured at energies well above the Coulomb barrier, is selected to extract a charged particle two-body reaction cross section x + B → C + D at astrophysical energies.

In the impulse approximation (IA) the three body reaction cross section is proportional to the cross section of the binary reaction [13]. Following the Plane Wave Impulse Approximation (PWIA), simpler approximation, the three body reaction can be factorized into two terms corresponding to the vertices of Fig. 1 and it is given by:

$$\frac{d^3\sigma}{d\Omega_C d\Omega_D dE_C} \propto (KF)\varphi(p_S)^2 \left(\frac{d\sigma}{d\Omega}\right)_{x+B--C+D}^{HOES}$$

where:

i-is the half-off-energy-shell differential cross section for the binary reaction B(x,C)D at the center of mass energy "E" given in post-collision prescription ("PCP") by $E_{cm} = E_{CD} - Q_{x+B->C+D}$ where $Q_{B(x,C)D}$ is the *Q-value* for the *B(x,C)D* reaction and is the E_{C-D} relative energy of particles *C* and *D* in the exit channel .

ii- (KF) is a kinematical factor containing the final state phase-space factor and it is a function of the incident particle *B*, of the two detected particles *C* and *D* and of the spectator *S* [14],

iii- $\phi(p_S)^2$ is the Fourier transform of the radial wave function for the $\chi(r)$ inter-cluster motion usually described in terms of Hulthén functions depending on the *"x-S"* system properties.

In a coplanar geometry, to completely determine the kinematical properties of the "S" spectator-particle, in particular its momentum distribution, three out of four kinematical variables of the outgoing particles, the energies E_C and E_D and the emission angles θ_C and θ_D of the two particles *C* and *D,* must be measured. The resulting two-dimensional energy spectrum $(E_C\text{-}E_D)$ obtained from such a measurement is usually reduced to a one-dimensional spectrum by projecting the coincidence yield onto one of the energy axes E_C or E_D (see [15,16]. Beam energies have been carefully chosen:

i- to optimize the kinematical conditions for the presence of quasi-free mechanism under the assumptions of the IA;

ii- to overcome the Coulomb barrier $(E_{(A-B)})^{C.B.}$ in the entry channel.

Thus, particle *"A"* is brought inside the nuclear interaction zone to induce the relevant reaction *B(x,C)D*. The QF kinematical conditions must be chosen in such a way that relative energy E_{x-B} can span the astrophysical region of interest below the Coulomb barrier $(E_{x-B)}^{C.B.}$.

This is possible because the initial projectile velocity is compensated for by the binding energy of particle *"x"* inside "*A"* ([15,16] and references therein). Thus, the center of mass energy E_{cm} can be very low. The applicability of the pole approximation is limited to small p_{xS} region within the prescription given by Shapiro [10]: $0 \leq p_S \leq k_S$ with p_S being the hoff energy shell momentum of the cluster "x" when it interacts with the particle "B", and "k_S" defined by the relation $k_S = \sqrt{2\mu_{xS}B_{xS}}$ where μ_{xS} is the reduced mass of the *xS* system.

^{18}F(p,α)^{15}O : A TEST CASE

The THM was applied for the first time to a ^{18}F(p,α)^{15}O reaction induced by ^{18}F Radioactive Ion Beam (RIB) using the three body reaction ^{18}F(d,α^{15}O)n to infer information on the process at relevant energy. The ^{18}F beam was produced at the CRIB separator of the Center for Nuclear Study (CNS) of the University of Tokyo at RIKEN campus in Wako, Japan. The beam tracks were reconstructed, particle by particle, using two PPACs. The secondary target was made of a thin CD2 foil. The detector setup was based on a modular detectors array ASTRHO developed at the INFN Laboratori Nazionali del Sud.

A large solid angle detector is used in order to recover, at least in part, the possibility of accumulating a statistics high enough to study the processes of interest at 38 keV in the 19F-p center of mass energy.

The data analysis of a THM experiment mainly consists in these steps: identification of ^{18}F(d,α^{15}O)n reaction of interest, selection of the event corresponding to the quasi-free reaction channel, extraction of the two body cross section of astrophysical interest.

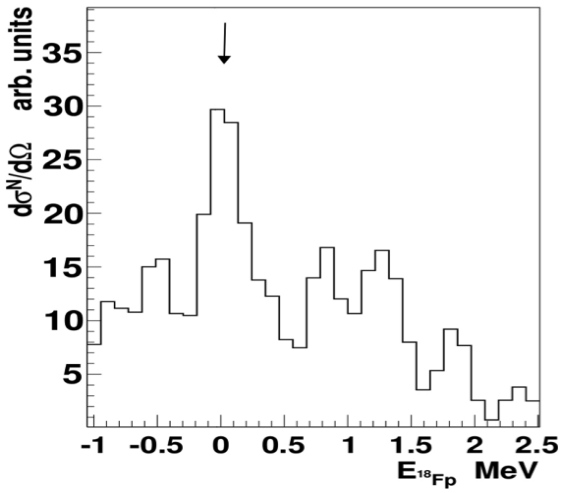

FIGURE 2. The nuclear cross section spectrum in function of the p-^{18}F cm energy for the events that pass the conditions described in the text. The arrow indicate the expected position 0f 19Ne level at 6.437 MeV.

The selection of events that come from the quasi-free channel in the $^{18}F(d,\alpha^{15}O)n$ reaction was also performed and the rest of the analysis was done by imposing a cut on the momentum of the spectator particle: only events where this momentum was lower than 40 MeV/c were accepted.

Assuming the events selected according to the previous procedure are actually coming from the quasi-free contribution to the reaction yield, then one can apply the formula described above to obtain the cross section of interest for the $^{18}F(p,\alpha)^{15}O$ process at astrophysical energies.

The result of this experiment is shown in Figure 2. The histogram represents the preliminary results of nuclear cross section for $^{18}F(p,\alpha)^{15}O$ measured by THM down to zero energies.

This result gives us confidence that a new THM experiment with increased statistics will be helpful in the study of the problem of ^{18}F destruction in Novae.

REFERENCES

1. C. Spitaleri et al., *Phys. Atom. Nucl.* 74, 1725 (2011).
2. S. Cherubini, V. N. Kondratyev, M. Lattuada, C. Spitaleri, D. Miljanic, M. Zadro, and G. Baur. Astrophys.J., 457, 855, (1996).
3. C. Spitaleri *Interaction of High-Energy Particles with Nuclei*, International School of Physics Enrico Fermi, Course , Ed. by A. Bracco and E. Nappi. Ericson, p. 210 (Academic Press, New York, 2011).
4. M. Gulino et al. *Phys. Rev, C* 87, 012801(R) (2013)
5. M.Gulino et al. *J. Phys, G Nucl. Part. Phys*, 37, 125105 (2010)
6. A. Tumino et al., *Phys. Rev. Lett*. 98, 252502 (2007).
7. H. Assenbaum, K. L. Langanke, and C. Rolfs, *Z. Phys.A* 327, 461 (1987).
8. F. Strieder, C. Rolfs, C. Spitaleri, and P. Corvisiero, *Naturwissenschaften* 88, 461 (2001).
9. I. S. Shapiro, *Sov. Physics Uspechi* 10, 515 (1968)
10. I. S. Shapiro, *Interaction of High-Energy Particles with Nuclei*, International School of Physics "Enrico Fermi", Course 38, Ed. by E. O. Ericson, p. 210 (Academic Press, New York, 1967), p. 210.
11. G. Baur, *Phys. Lett. B* 178, 135 (1986).
12. C. Spitaleri, *Problems of Fundamental Modern Physics*, Vol. II, Ed. by R. Cherubini, P. Dalpiaz, and B. Minetti (World Sci., 1990), p. 21.
13. G. F. Chew and G. C. Wick, *Phys. Rev.* 85, 636 (1952).
14. P. G. Fallica, et al., *Lett. Nuovo Cimento* 22, 547 (1978).
15. C.Spitaleri et al. *Phys. Rev. C* 60 037601(1999)
16. C. Spitaleri et al. *Phys. Rev. C* 69 055806 (2004)

Reaction and Structure effects on the Breakup of ^{15}C on a proton target

R. Crespo*, E. Cravo† and A. Deltuva**

*Departamento de Física, Instituto Superior Técnico, Universidade Técnica de Lisboa, Taguspark, Av. Prof. Cavaco Silva, Taguspark, 2780-990 Porto Salvo, Oeiras, Portugal,Centro de Física Nuclear da Universidade de Lisboa, Av. Prof. Gama Pinto 2, 1649-003 Lisboa, Portugal

†Centro de Física Nuclear da Universidade de Lisboa, Av. Prof. Gama Pinto 2, 1649-003 Lisboa, Portugal

** Centro de Física Nuclear da Universidade de Lisboa, Av. Prof. Gama Pinto 2, 1649-003 Lisboa, Portugal

Abstract. The breakup of a one-neutron halo ^{15}C on a proton target is studied assuming that the halo nucleus is well described by an inert ^{14}C(0^+) core and a valence neutron with unity spectroscopic factor. ^{14}C ground state transverse momentum distributions for the p(^{15}C,^{14}C) n p reaction at 54 MeV/u are calculated using the few-body Faddeev/Alt-Grassberger-Sandhas (Faddeev/AGS) reaction framework. The sensitivity of the calculated observables on the core-valence neutron interaction and in particular the introduction of an imaginary component is analysed. The effect of higher order multiple scattering distortion effects is also investigated.

Keywords: Direct Reactions
PACS: 24.50.+g, 25.60.Gc,27.20.+n

INTRODUCTION

Breakup reaction studies are a usefull tool to extract spectrocopic information about Halo nuclei, by comparing the calculated cross sections with the experimental data. This relies on a tight control on the reaction theory and on the structure input information.

From the reaction point of view, an accurate estimation of distortion effects on the incident and exit channels has to be considered in the low energy regime. We shall be addressing this point in the present manuscript.

From the structure point of view an important and unexplored issue so far is to know to what extent the absence of the full structure knowledge and some unknown components of the projectile and its energy spectrum might affect the reaction observables. In general, the valence neutron-core interaction is chosen to be local, L-dependent and the parameters of the interaction adjusted such that it reproduces the known experimental energy spectrum (ground state, excited and resonant states). The interaction for all other states might contain a small imaginary component to take into account possible dissipation effects. In this manuscript we also analyse the dependence of the observables on the valence neutron-core interaction. We shall make use of the few-body Faddeev/Alt-Grassberg-Sandhas (Faddeev/AGS) reaction framework [1, 2] , but introducing as in [3] an imaginary component in some of the partial waves of the valence-core interaction.

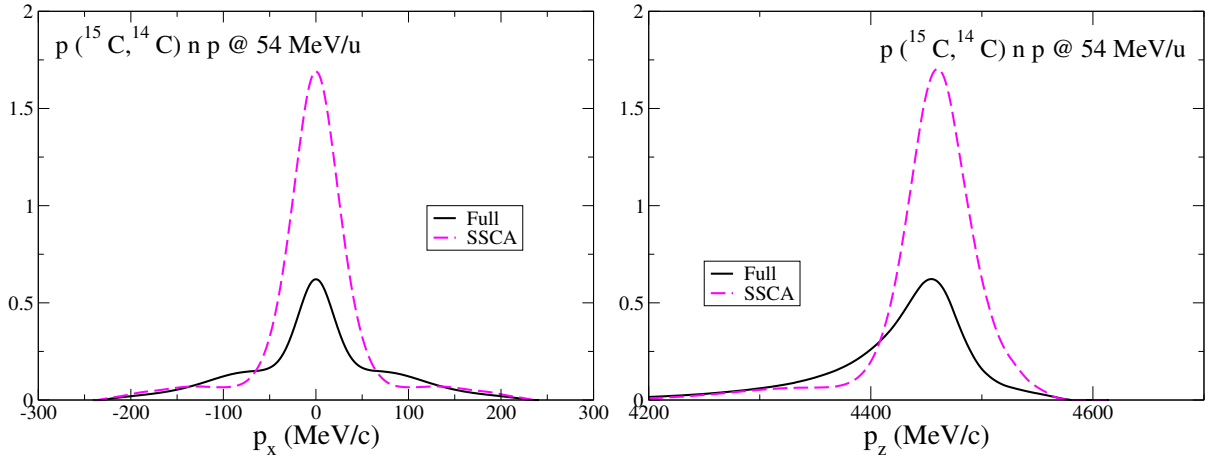

FIGURE 1. ^{14}C ground state transverse momentum P_x distributions in the p(^{15}C,^{14}C) n p reaction at 54 MeV/u. The curves correspond to the single scattering approximation (dashed line) and to the full Faddeev calculation (solid line).

THE REACTION FRAMEWORK

According to The Faddeev/AGS reaction framework [1, 2], one needs to evaluate the operators $U^{\beta\alpha}$, whose on-shell matrix elements are the transition amplitudes. These operators are obtained by solving the three-body AGS integral equations

$$U^{\beta\alpha} = \bar{\delta}_{\beta\alpha} G_0^{-1} + \sum_{\gamma} \bar{\delta}_{\beta\gamma} t_\gamma G_0 U^{\gamma\alpha} \,, \tag{1}$$

with $\alpha,\beta,\gamma = (1,2,3)$, ($\beta = 0$ in the final breakup state) and where we use the odd-man-out notation for the three interacting particles (1,2,3). In this Equation $\bar{\delta}_{\beta\alpha} = 1 - \delta_{\beta\alpha}$ and the pair transition operator is

$$t_\gamma = v_\gamma + v_\gamma G_0 t_\gamma \,, \tag{2}$$

where G_0 is the free resolvent $G_0 = (E + i0 - H_0)^{-1}$, and E is the total energy of the three-particle system in the center of mass (c.m.) frame. The breakup observables are calculated from the on-shell matrix elements of the AGS operators. The solution of the Faddeev/AGS equations can be found by iteration. The first term of the series is known as the single scattering.

RESULTS

In Fig. 1 we show the calculated ^{14}C ground state transverse and longitudinal momentum distributions. The solid line represents the calculated observable using the Faddeev/AGS equations. The transverse momentum distribution is symmetrical while the longitudinal momentum distribution exhibits a pronounced asymmetry with an increased width intensity at low core momenta. The single scattering approximation (dashed line) overestimates significantly the full calculation indicating that higher order destructive distortion

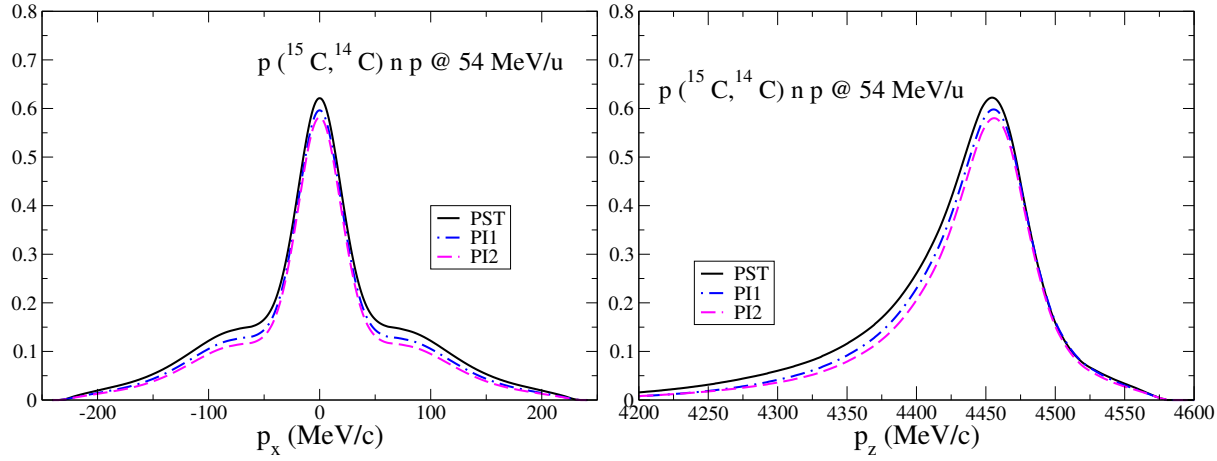

FIGURE 2. ^{14}C ground state transverse momentum P_x (a) and longitudinal momentum $P_{||}$ (b) distributions in the p(^{15}C,^{14}C) n p reaction at 54 MeV/u. The curves correspond to different n-^{14}C interactions as described in the text.

effects are very important at this energy. In addition, the longitudinal momentum distribution in the single scattering approximation is less asymmmetrical indicating that the longitudinal momentum distribution at low core momenta probe higher order distortion effects.

In Fig. 2 we show the calculated ^{14}C ground state transverse and longitudinal momentum distributions using the Faddeev/AGS equations. The solid, dashed-dotted and dashed lines correspond to the PST, PI1 and PI2 n-Core interactions as described in [3]: (i) PST a standard real interaction taken from [4] (ii) PI1 where the interaction for the S-, P- and D-waves are kept the same as in the PST interaction and where the even and odd partial waves (with $L > 2$) are modified to include an imaginary component with strength equal to 25% of the real part. (iii) PI2 identical to PI1 but where the P-wave is also modified to include an imaginary component. As shown in the figure, the changes of the calculated momentum distributions due to the modification of the n-Core interaction are not very significant.

SUMMARY AND CONCLUSIONS

We have calculated the breakup of a one-neutron halo nucleus ^{15}C on a proton target at 54 MeV/u incident energy using the few-body Faddeev/AGS reaction framework. The sensitivity of the calculated ^{14}C ground state transverse and longitudinal momentum distributions on the core-valence neutron interaction and on higher order multiple scattering distortion effects is analysed. We have shown that the longitudinal momentum distribution exhibits a pronounced asymmetry with an increased width intensity at low core momenta due to higher order multiple scattering distortion effects. In addition, we have also shown that the single scattering approximation overestimates significantly the full calculation indicating that higher order destructive distortion effects are very important at this energy. Finally, we have shown that changes of the calculated momentum

distributions due to the modification of the n-Core interaction are not very significant.

ACKNOWLEDGMENTS

The authors are supported by the Fundação para a Ciência e Tecnologia (FCT) grant PTDC/FIS/103902/2008. A.D. is partially supported by the FCT grant PTDC/FIS/65736/2006.

REFERENCES

1. L. D. Faddeev, Zh. Eksp. Theor. Fiz. **39**, 1459 (1960) [Sov. Phys. JETP **12**, 1014 (1961)].
2. E. O. Alt, P. Grassberger, and W. Sandhas, Nucl. Phys. B **2**, 167 (1967).
3. E. Cravo, R. Crespo, A. Deltuva, to be published in Phys. Rev. C (2013).
4. A. Deltuva, Phys. Rev. C **79**, 054603 (2009).

Theoretical models for reactions involving exotic nuclei

P. Descouvemont

Physique Nucléaire Théorique et Physique Mathématique, C.P. 229,
Université Libre de Bruxelles (ULB), B 1050 Brussels, Belgium

Abstract. Recent calculations within the CDCC and eikonal methods are presented. We briefly describe the methods, and apply them to the ^{11}Be+^{64}Zn elastic scattering and to the ^{11}Li breakup on ^{208}Pb.

INTRODUCTION

Reaction theories play a fundamental role in the study of exotic nuclei [1]. These nuclei present unusual properties, such as a large rms radius, or low breakup thresholds. At low energies (i.e. close to the Coulomb barrier), the Continuum Discretized Coupled Channel (CDCC) method represents an accurate tool for the treatment of elastic scattering and breakup reactions [2, 3]. It was originally developed to describe deuteron-induced reactions. Owing to the low breakup energy of the deuteron, it was shown that the inclusion of breakup thresholds are one of the main characteristics of exotic nuclei. This makes the CDCC method well suited to the description of reactions involving exotic nuclei, such as ^{11}Be or ^{6}He.

At high energies, the Glauber model [4], using the eikonal approximation [5], provides an accurate description of various processes: elastic scattering, inclusive reactions, or breakup. The first calculations were based on the adiabatic approximation, where the projectile is assumed to remain in its ground state. Recent developments, using the Dynamical eikonal approximation [6] or the CDCC-eikonal method [7] allow to go beyond the adiabatic approximation, and to include excited states of the projectile. The relative simplicity of the eikonal approximation makes possible two-body and three-body breakup calculations, with a correct treatment of scattering boundary conditions [8, 9].

THEORETICAL FRAMEWORK

Introduction

Let us consider a system made of a target (assumed to be in its ground state) and of a projectile described by a cluster structure. This structure involves N constituents (in practice $N = 2$ or 3) with coordinates $\boldsymbol{r}_i$. If $\boldsymbol{R}$ is the target-projectile coordinate, the

Hamiltonian of the system is written as

$$H = H_0(\boldsymbol{r}_i) + T_R + \sum_{i=1}^{N} V_{ti}(\boldsymbol{r}_i, \boldsymbol{R}), \tag{1}$$

where $H_0(\boldsymbol{r}_i)$ is associated with the projectile, T_R is the projectile target kinetic energy, and V_{ti} are two optical potentials describing the interaction between the target and the constituents of the projectile.

The CDCC method

In CDCC calculations, the first step is to diagonalize H_0 as

$$(H_0 - E_T)\Phi_k^{jm} = E_k^j \Phi_k^{jm}, \tag{2}$$

where E_T is the threshold energy, j is the spin of the projectile, and k the excitation level. States with $E_k^j < 0$ correspond to physical states, and positive eigenvalues simulate breakup effects. The total wave function in partial wave $J\pi$, associated with (1) is then expanded as

$$\Psi^{JM\pi} = \sum_{jkL} u_{jkL}^{J\pi}(R) \left[\Phi_k^j \otimes Y_L(\Omega_R)\right]^{JM}, \tag{3}$$

where L is the projectile-target angular momentum (the spin of the target is neglected). Inserting (3) in the Hamiltonian (1) provides the standard coupled-channel system

$$-\frac{\hbar^2}{2\mu}\left[\frac{d^2}{dR^2} - \frac{L(L+1}{R^2}\right] u_c^{J\pi} + \sum_{c'} V_{cc'}^{J\pi}(R) u_{c'}^{J\pi} = (E - E_k^j) u_c^{J\pi}, \tag{4}$$

where c stands for $c = (j,k,L)$, and where the relative energy E is defined from the threshold E_T. Potentials $V_{cc'}^{J\pi}(R)$ are obtained from matrix elements of the interaction between basis functions. The scattering matrix is finally calculated by using the R-matrix method [10, 11].

The eikonal approximation

In the eikonal approximation, the wave function is not expanded in partial waves. It is factorized as $\Phi(\boldsymbol{R}, \boldsymbol{r}_i) = e^{iKZ}\hat{\Phi}(\boldsymbol{R}, \boldsymbol{r}_i)$. This factorization is introduced in Eq. (1) with the adiabatic approximation that consists in replacing H_0 by the projectile ground-state energy E_0 [5]. We introduce the impact parameter by $\boldsymbol{R} = (\boldsymbol{b}, Z)$. Then, defining $\Psi^{J_0 M_0 \pi_0}$ as the ground-state wave function of the projectile, the eikonal wave function, valid at high energies, is given by

$$\hat{\Phi}_{\text{eik.}}(\boldsymbol{b}, Z, \boldsymbol{r}_i) = \Psi^{J_0 M_0 \pi_0}(\boldsymbol{r}_i) \exp\left(-\frac{i}{\hbar v}\int_{-\infty}^{Z} dZ' \sum_{i=1}^{N} V_{ti}(\boldsymbol{r}_i, \boldsymbol{b}, Z')\right), \tag{5}$$

where v is the relative velocity between the target and the projectile. From wave function (5), elastic and breakup cross sections can be determined [12, 8, 9].

APPLICATIONS

^{11}Be+^{64}Zn elastic scattering

The ^{11}Be+^{64}Zn elastic cross section has been recently measured [13] at $E_{cm} = 24.5$ MeV, i.e. near the Coulomb barrier. It shows significant differences with respect to ^{9,10}Be+^{64}Zn, which is interpreted as an evidence for a halo structure in ^{11}Be [13, 14]. The cross section is determined in the CDCC formalism (see Ref. [15] for detail) and is displayed in Fig. 1. For the ^{10}Be+n system, we adopt $l_{\max} = 2$ and introduce pseudostates up to 30 MeV. These conditions provide a fair compromise between optimal conditions and reasonable computing limits. As expected, the single-channel calculation overestimates the data in the range $\theta = 20^\circ - 40^\circ$, but is below the data for $\theta > 40^\circ$. Introducing the $1/2^-$ first excited state reduces the overestimation near $\theta \approx 40^\circ$, but does not improve the general shape of the cross section. Conversely the inclusion of continuum states provides a fair agreement with experiment.

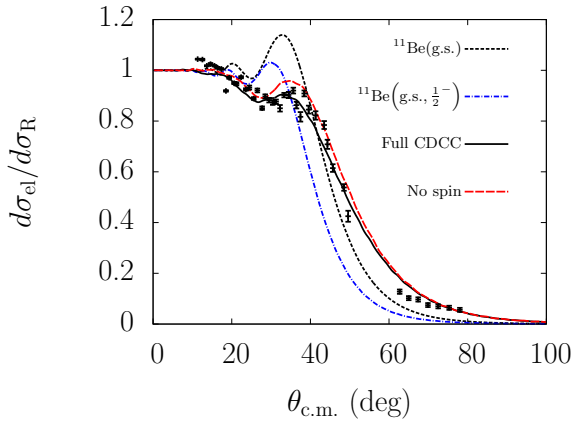

FIGURE 1. CDCC calculations compared to the experimental data of Ref. [13]. ^{11}Be(g.s.) and ^{11}Be(g.s.,1/2$^-$) correspond to one-channel (the ground state only) and two-channel calculations (the ground state and the first excited state) respectively.

^{11}Li+^{208}Pb breakup

The ^{11}Li+^{208}Pb breakup cross section is computed in the eikonal formalism (see Ref. [9] for detail) and is displayed in Fig. 2, where we compare the calculation with experiment [16]. In agreement with experiment, we find a peak near 0.5 MeV, which corresponds to a 1^- three-body resonance. Including the 0^+ and 2^+ contributions increases the total cross section beyond 1 MeV, in better agreement with the experimental data. In the literature, calculations of breakup cross sections of halo nuclei often use

the equivalent photon method [17]. This approximation assumes a dipole breakup process, and ignores other contributions. In contrast, the present eikonal description of the breakup reaction is more accurate, since it allows a quantitative evaluation of other partial wave contributions.

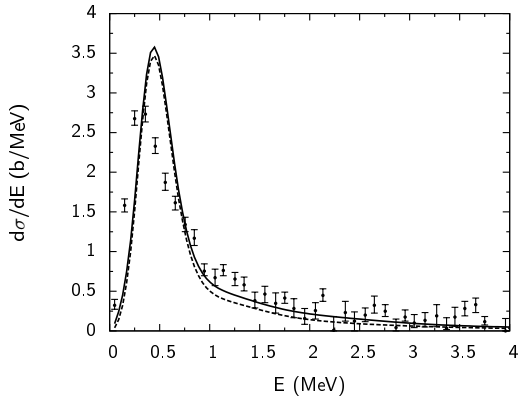

FIGURE 2. Total breakup cross section (full line) and 1^- contribution (dashed line) convoluted with the detector response. Experimental data are taken from Ref. [16].

CONCLUSION

We have presented recent applications of the CDCC and eikonal methods to reactions involving exotic nuclei. Owing to the low binding energy, the projectile wave functions must include many breakup channels to reach convergence. A challenge for future works in this field is to make use of microscopic descriptions of the projectile [18].

REFERENCES

1. A. S. Jensen, K. Riisager, D. V. Fedorov, and E. Garrido, *Rev. Mod. Phys.* **76**, 215 (2004).
2. M. Kamimura et al., *Prog. Theor. Phys. Suppl.* **89**, 1 (1986).
3. N. Austern et al., *Phys. Rep.* **154**, 125 (1987).
4. R. J. Glauber, *High energy collision theory, in Lectures in Theoretical Physics, Vol. 1*, Interscience, New York, 1959.
5. Y. Suzuki, R. G. Lovas, K. Yabana, and K. Varga, *Structure and Reactions of Light Exotic Nuclei*, Taylor & Francis, London, 2003.
6. G. Goldstein, D. Baye, and P. Capel, *Phys. Rev. C* **73**, 024602 (2006).
7. K. Ogata, M. Yahiro, Y. Iseri, T. Matsumoto, and M. Kamimura, *Phys. Rev. C* **68**, 064609 (2003).
8. D. Baye, P. Capel, P. Descouvemont, and Y. Suzuki, *Phys. Rev. C* **79**, 024607 (2009).
9. E. C. Pinilla, P. Descouvemont, and D. Baye, *Phys. Rev. C* **85**, 054610 (2012).
10. P. Descouvemont, and D. Baye, *Rep. Prog. Phys.* **73**, 036301 (2010).
11. T. Druet, D. Baye, P. Descouvemont, and J.-M. Sparenberg, *Nucl. Phys. A* **845**, 88 (2010).
12. P. Capel, D. Baye, and Y. Suzuki, *Phys. Rev. C* **78**, 054602 (2008).
13. A. Di Pietro et al., *Phys. Rev. Lett.* **105**, 022701 (2010).
14. A. Di Pietro et al., *Phys. Rev. C* **85**, 054607 (2012).
15. T. Druet, and P. Descouvemont, *Eur. Phys. J. A* **48**, 147 (2012).
16. T. Nakamura et al., *Phys. Rev. Lett.* **96**, 252502 (2006).
17. C. Bertulani, and G. Baur, *Phys. Rep.* **163**, 299 (1988).
18. P. Descouvemont, and M. Dufour, *Clusters in Nuclei, Vol.2*, Springer, 2012.

Toward the Ab-initio Description of Medium Mass Nuclei

C. Barbieri[*], A. Cipollone[*,**], V. Somà[‡,§], T. Duguet[¶,‖] and P. Navrátil[††]

[*]*Department of Physics, University of Surrey, Guildford GU2 7XH, UK*
[†]*Dipartimento di Fisica, Università "Sapienza", I-00185 Roma, Italy*
[**]*INFN, Sezione di Roma, Piazzale Aldo Moro 2, I-00185 Roma, Italy*
[‡]*Institut für Kernphysik, Technische Universität Darmstadt, 64289 Darmstadt, Germany*
[§]*ExtreMe Matter Institute EMMI, GSI Helmholtzzentrum für Schwerionenforschung GmbH, 64291 Darmstadt, Germany*
[¶]*CEA-Saclay, IRFU/Service de Physique Nucléaire, F-91191 Gif-sur-Yvette, France*
[‖]*National Superconducting Cyclotron Laboratory and Department of Physics and Astronomy, Michigan State University, East Lansing, MI 48824, USA*
[††]*TRIUMF, 4004 Wesbrook Mall, Vancouver, British Columbia, V6T 2A3, Canada*

Abstract. As ab-initio calculations of atomic nuclei enter the A=40-100 mass range, a great challenge is how to approach the vast majority of open-shell (degenerate) isotopes. We add realistic three-nucleon interactions to the state of the art many-body Green's function theory of closed-shells, and find that physics of neutron driplines is reproduced with very good quality. Further, we introduce the Gorkov formalism to extend *ab-initio* theory to semi-magic, fully open-shell, isotopes. Proof-of-principle calculations for ^{44}Ca and ^{74}Ni confirm that this approach is indeed feasible. Combining these two advances (open-shells and three-nucleon interactions) requires longer, technical, work but it is otherwise within reach.

Keywords: Green's functions theory; ab-initio; nuclear structure; similarity renormalization group
PACS: 31.10.+z,31.15.Ar

Introduction. Microscopic first principle predictions of atomic nuclei are highly desirable since they can unambiguously guide research of exotic isotopes. These could also help in constraining extrapolations to higher mass regions [1] and to extreme proton-neutron asymmetries [2], including regions close to the driplines where experimental data is unlikely to become available in the foreseeable future.

Ab-initio methods such as coupled-cluster (CC) [3], in-medium similarity renormalization group (IMSRG) [4] or Dyson self-consistent Green's function [5, 6] (Dyson-SCGF) have accessed medium-mass nuclei up to A$\sim$60 on the basis of realistic two-nucleon (2N) interactions. However, it has become clear that three-nucleon forces (3NFs) play a major role in determining crucial features of exotic isotopes, such as the evolution of magic numbers and the position of driplines [7, 8, 9]. Realistic 2N and 3N interactions based on chiral perturbation theory have recently been evolved to low cut-offs, retaining both induced and pre-existing 3NFs [10, 11]. Proper implementations of similar hamiltonians within the above many-body theories will be required to eventually achieve quantitative predictions of medium-mass isotopes.

A second (and major) challenge to ab-initio theory is that current implementations of the above methods are limited to doubly closed (sub-)shell nuclei and their immediate neighbors [3, 6]. As one increases the nuclear mass, longer chains of truly open-shell

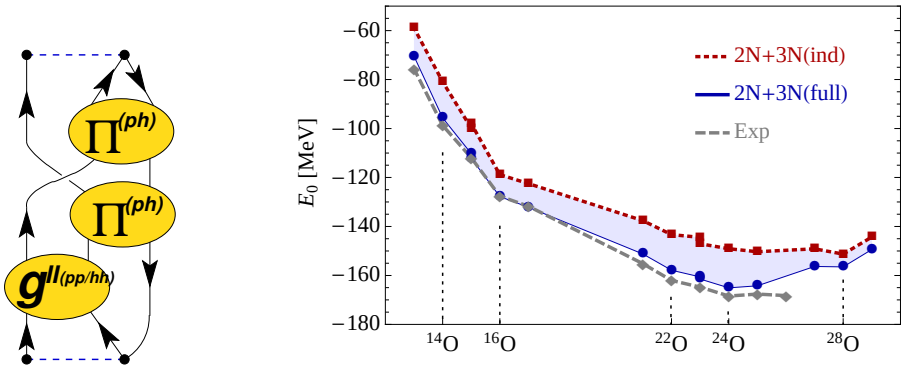

FIGURE 1. *Left:* Example of a particle-vibration coupling diagram entering the FTDA/ADC(3) self energy. *Right:* Binding energies of oxygen isotopes obtained from a SRG evolved NN+3N interactions with cutoff λ=1.88 fm^{-1}. Squares (dots) refer to induced-only (full) three-nucleon interactions and are compared to experiment (diamonds). Binding energies of even-N isotopes are obtained through the corrected Koltum sum rule (3). Odd-N energies are inferred from addition and separation energies, as obtained from the poles of the propagator (1).

nuclei connecting isolated doubly closed-shell ones emerge and cannot be accessed with existing approaches. Many-body techniques that could tackle genuine (at least) singly open-shell systems would immediately extend the reach of ab-initio studies from a few tens to several hundreds of mid-mass nuclei. A manageable way to fill this gap was recently proposed in Refs. [12, 13] by extending SCGF to Gorkov formalism and will be discussed in the following. This talk reports on recent progress on the above topics.

Three-nucleon interactions. We employ Green's function (or propagator) theory, where the object of interest is the single particle propagator [14],

$$g_{\alpha\beta}(\omega) = \sum_n \frac{\langle\Psi_0^A|c_\alpha|\Psi_n^{A+1}\rangle\langle\Psi_n^{A+1}|c_\beta^\dagger|\Psi_0^A\rangle}{\omega-(E_n^{A+1}-E_0^A)+i\eta} + \sum_k \frac{\langle\Psi_0^A|c_\beta^\dagger|\Psi_k^{A-1}\rangle\langle\Psi_k^{A-1}|c_\alpha|\Psi_0^A\rangle}{\omega-(E_0^A-E_k^{A-1})-i\eta}\,, \quad (1)$$

where $|\Psi_n^{A+1}\rangle$, $|\Psi_k^{A-1}\rangle$ are the eigenstates, and E_n^{A+1}, E_k^{A-1} the eigenenergies of the $(A\pm1)$-nucleon system. Therefore, the poles of the propagator reflect nucleon addition and separation energies. The propagator is calculated for finite closed-shell nuclei by first solving spherical Hartree-Fock (HF) equations. The HF state is then used as a reference state for the Faddeev Tamm-Dancoff (FTDA) method [a.k.a. ADC(3)] of Refs. [6]. The FTDA method completely accounts for particle-vibration diagrams as shown in Fig. 1.

We employ the intrinsic hamiltonian $H_{int} \equiv H - T_{c.m.} = \hat{U}+\hat{V}+\hat{W}$, where the kinetic energy of the center of mass has been subtracted and $\hat{U}$, $\hat{V}$ and $\hat{W}$ are the one-, two-, and three-nucleon components, respectively. Form this, we generate one- and two-nucleon density dependent interactions with matrix elements,

$$u_{\alpha\beta}^{(3NF)} = \frac{1}{2}\sum_{\gamma\sigma\mu\nu}\frac{1}{(2\pi i)^2}\int_{C\uparrow}d\omega_1\int_{C\uparrow}d\omega_2\; w_{\alpha\mu\nu,\beta\gamma\sigma}\,g_{\gamma\mu}(\omega_1)\,g_{\sigma\nu}(\omega_2)\,,$$

TABLE 1. Predicted matter radii (in fm) for ^{16}O and ^{44}Ca form SRG evolved 2N-only interactions and by including induced and full 3NF. Experiment are charge radii.

	2NF only	**2+3NF(ind.)**	**2+3NF(full)**	**Experiment**
^{16}O:	2.10	2. 41	2.38	2.718±0.210 [19]
^{44}Ca:	2.48	2.93	2.94	3.520±0.005 [20]

$$v^{(3NF)}_{\alpha\beta,\gamma\delta} \;=\; \sum_{\mu\,\nu} \frac{1}{2\pi i} \int_{C\uparrow} d\omega \;\; w_{\alpha\beta\mu,\gamma\delta\nu}\, g_{\nu\mu}(\omega)\;. \tag{2}$$

These definition extend the normal ordering approach of Ref. [11] by contracting with fully correlated propagators, as opposed to a mean-field reference state. The matrix elements $u^{(3NF)}_{\alpha\beta}$ and $v^{(3NF)}_{\alpha\beta,\gamma\delta}$ are then added to the existing 1N and 2N forces with the caveat that only interaction irreducible diagrams are retained to ensure the correct symmetry factors in the diagrammatic expansion [15].

After obtaining the sp propagator $g(\omega)$ the total binding energy can be calculated as usual through the Koltun sum rule which—due the the presence of 3NF—acquires the corrected form

$$E^A_0 = \sum_{\alpha\,\beta} \frac{1}{4\pi i} \int_{C\uparrow} d\omega \;\; \left[u_{\alpha\beta} + \omega\delta_{\alpha\beta}\right]\, g_{\beta\alpha}(\omega) \;-\; \frac{1}{2}\langle\Psi^A_0|\hat{W}|\Psi^A_0\rangle\;. \tag{3}$$

Eq. (3) is still an exact equation. However, it requires to evaluate the expectation value of the 3NF part of the hamiltonian $<\hat{W}>$ which is calculated here to first order in $\hat{W}$.

Calculations for closed sub-shell oxygen isotopes were performed for the chiral N^{3}LO 2NF [16] and N^{2}LO 3NF [17] with the cutoff of 400 MeV as introduced in Ref. [11]. These were evolved to a cutoff $\lambda = 1.88\,\mathrm{fm}^{-1}$ using free-space similarity renormalization group (SRG) [18]. We employed large model spaces of up to 12 harmonic oscillator shells with frequency $\hbar\omega$=20 MeV. Results for the induced 3NF are obtained from the SRG evolution of the original 2NF only and are indicated by red squares in Fig. 1. These are to be considered analogous to predictions of the sole N^{3}LO 2NF and systematically under bind the oxygen isotopes. Adding full 3NFs, that include in particular the two-pion exchange Fujita-Miyazawa contribution, reproduces experimental binding energies throughout the isotopic chain and the location of the neutron dripline. Table 1 shows that although SRG evolved 2NFs alone underestimate the nuclear radii, results improve with the inclusion of 3NFs.

Gorkov formalism for open-shell isotopes. The Gorkov's approach handles intrinsic degeneracies of open shell systems by allowing the breaking of particle number symmetry. One considers the grand canonical hamiltonian $\Omega_{int} = H_{int} - \mu_p\hat{Z} - \mu_n\hat{N}$ and constrains expectation values of proton and neutron number operators to the expected values. This allows defining a superfluid state which already accounts for pairing correlation and can be used as reference for Green's function diagrammatic expansion. The formalism for Gorkov self-consistent Green's function (Gorkov-SCGF) theory up to second order in the self-energy has been worked out in full in Ref. [12], for 2N interactions only. First results are reported in [13].

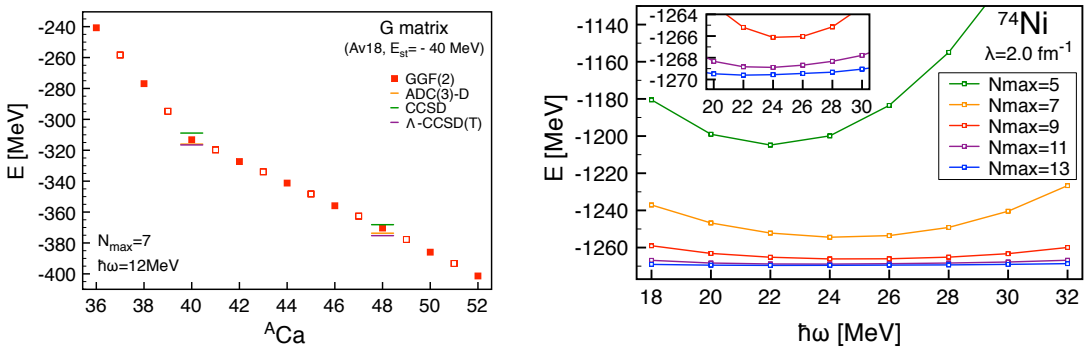

FIGURE 2. Results obtained from second-order Gorkov-SCGF *Left*: Binding energies of Ca isotopes for a fixed model space of eight shells. Gorkov propagators are calculated for even-A (filled symbols) while odd-A results (open symbols) are computed according to Ref. [21]. Closed-shell ^{40}Ca and ^{48}Ca are compared to CC and Dyson-SCGF results. *Right*: Binding energy ^{74}Ni as a function of the harmonic oscillator spacing $\hbar\omega$ and for an increasing size N_{max} of the single-particle model space.The insert shows a zoom on the most converged results.

The left panel in figure 2 displays the binding energies of calcium isotopes and compares them to single-reference CC and Dyson-SCGF for closed-shell ^{40}Ca and ^{48}Ca, using a G-matrix interaction at a fixed starting energy. Already at second-order in the self-energy, Gorkov-SCGF can provide comparable accuracy to CC singles and doubles (CCSD). Higher order corrections introduced by triples [Λ-CCSD(T)] are closely reproduced by Dyson-SCGF in the FTDA/ADC(3) approximation. Since the extension of Gorkov's formalism to ADC(3) schemes is within computational reach, this gives confidence that Gorkov-SCGF calculations can be improved to desired accuracy. The right panel displays good convergence properties, with respect to the model space, for isotopes as heavy as ^{74}Ni, using 2N SRG interactions with cutoff λ=2.0 fm^{-1}. These findings demonstrate the feasibility of first-principle calculations along full isotopic chains based on Gorkov-SCGF theory.

We further consider ^{44}Ca with the SRG, λ=2.0 fm^{-1}, interaction and add a crude estimate of 3NF by calculating the normal self-energy in a filling approximation. Full 3NFs are found to shift the neutron Fermi energy to -8.69 MeV, fairly close to the experiment. The neutron shell gap between the $0f_{7/2}$ and $0d_{3/2}$ is reduced from 12.9 MeV (2NF only) to 7.2 MeV (full 3NF). The gap between the centroids of their distributions [22] is 9.3 MeV, in agreement with data driven predictions of Ref. [23]. The calculated r.m.s. matter radius of 2.94 fm (Tab. 1) also improves with respect to 2NF only.

These are extremely encouraging results and confirm recent investigations of 3NFs [10, 11, 9]. It must be kept in mind that a correct microscopical extension to the Gorkov approach—to include missing 3NFs in both the anomalous and higher order self-energies—is still missing. This requires substantial work to develop and implement correctly the formalism and will be addressed in the coming future.

Acknowledgments. This work was supported by the UK's STFC Grants ST/I003363 and ST/J00005, by the German DFG through grant SFB 634 and Helmholtz Alliance Program, contract HA216/EMMI, and Canada's NSERC Grant No. 401945-2011.

Calculations were performed using HPC resources from GENCI-CCRT (Grant 2012-050707).

REFERENCES

1. J. Erler, et al., Nature **486**, 509 (2012).
2. S. Waldecker, C. Barbieri, and W. Dickhoff, Phys. Rev. C**84**, 034616 (2011).
3. G. R. Jansen, M. Hjorth-Jensen, G. Hagen, and T. Papenbrock, Phys. Rev. C**83**, 054306 (2011).
4. K. Tsukiyama, S. K. Bogner, and A. Schwenk, Phys. Rev. Lett. **106**, 222502 (2011).
5. W. H. Dickhoff and C. Barbieri, Prog. Part. Nucl. Phys. **52**, 377 (2004).
6. C. Barbieri et al., Phys. Rev. C 79, 064313 (2009); Phys. Rev. A **76**, 052503 (2007).
7. T. Otsuka, T. Suzuki, J. D. Holt, A. Schwenk, and Y. Akaishi, Phys. Rev. Lett. **105**, 032501 (20120).
8. J. D. Holt, T. Otsuka, A. Schwenk, and T. Suzuki, J. Phys. **G39**, 085111 (2012).
9. G. Hagen et al., Phys. Rev. Lett. **109**, 032502 (2012).
10. E. D. Jurgenson, P. Navrátil, and R. J. Furnstahl, Phys. Rev. Lett. **103**, 082501 (2009).
11. R. Roth et al., Phys. Rev. Lett. **109**, 052501 (2012).
12. V. Somà, T. Duguet, and C. Barbieri, Phys. Rev. C**84**, 064317 (2011).
13. V. Somà, C. Barbieri, and T. Duguet, (2012), arXiv:1208.2472 [nucl-th].
14. A. L. Fetter and J. D. Walecka, *Quantum Theory of Many-Particle Physics* (McGraw-Hill, 1971).
15. A. Carbone, A. Cipollone, C. Barbieri. A. Rios, A. Polls, in preparation.
16. D. R. Entem and R. Machleidt, Phys. Rev. C**68**, 041001(R) (2003).
17. P. Navrátil, Few-Body Syst. 41, 117 (2007).
18. S. K. Bogner, R. J. Furnstahl, and A. Schwenk, Prog. Part. Nucl. Phys. **65**, 94 (2010).
19. H. D. Wohlfahrt, et al., Phys. Rev. C**23**, 533 (1981).
20. W. Schütz, Z. Physik **A273**, 69 (1975).
21. T. Duguet, P. Bonche, P.-H. Heenen, and J. Meyer, Phys. Rev. C**65**, 014311 (2002).
22. T. Duguet and G. Hagen, Phys. Rev. C**85**, 034330 (2012).
23. R. J. Charity et al., Phys. Rev. C**76** 044314 (2007).

Ab initio approach to the structure of light nuclei

C. Forssén

Department of Fundamental Physics, Chalmers University of Technology, SE–412 96 Göteborg, Sweden.

Abstract. Over the last decade we have seen significant progress in several key areas that allow for a successful *ab initio* description of nuclear structure for light nuclei. This exciting trend in modern nuclear theory is now continuing with the evolution of methods to treat bound, scattering, and resonance states within a single, unified formalism. The development of such a capability is crucial for obtaining a fundamental understanding of the structure of exotic nuclear systems currently being investigated at radioactive beam facilities. Such methods would also form the foundation for a microscopic treatment of low-energy nuclear reactions on light nuclei.

Keywords: Theoretical nuclear physics
PACS: 21.30.-x,21.60.-n,21.10.-k,24.10.-i

INTRODUCTION

Scientific progress on three fronts finally allow us to make a serious attempt to systematically bridge the gap all the way from low-energy quantum chromodynamics (QCD) to nuclear structure. The three steps are: (1) The development of realistic nuclear forces using chiral effective field theory (EFT); (2) The development of computational many-body methods; and (3) The adaptation of realistic nuclear potentials to finite model spaces using unitary transformations. All three of these steps are based on breakthrough developments during approximately the past decade. The latter two components have been crucial for the progress in performing *ab initio* calculations for nuclear systems with more than four nucleons. An overview of this progress is presented in the recent review by Leidemann and Orlandini [1]. They also give a definition of *ab initio* methods:

- Consider an A-nucleon system described by a well defined microscopic Hamiltonian.
- *Ab initio* methods are those that solve the relevant quantum mechanical many-body equations without uncontrolled approximations.
- Controlled approximations, e.g. number of channels, are allowed as they can be increasingly improved to the point that convergence is reached for the observable.
- Converged results are considered precise *ab initio* results.

The comparison of precise *ab initio* results with experimental results then allows an indisputable answer as to whether or not the chosen Hamiltonian appropriately describes the nuclear dynamics. Any uncontrolled approximation in the calculation would disqualify any such conclusions. Quite naturally, precise *ab initio* results obtained with different *ab initio* methods, but with the same Hamiltonian as input, have to agree and are often referred to as benchmark results. However, not fully converged results

with error estimates are also useful, and we expect much work towards uncertainty quantification in the coming years.

NUCLEAR STRUCTURE FROM FIRST PRINCIPLES

The question of nuclear interactions has a long, and often obscure, history [2]. Unfortunately, QCD, the underlying theory of the strong interaction, is highly non-perturbative in the energy region characteristic of nuclear structure. This region is governed by nucleonic (and sometimes mesonic) degrees of freedom. This requires an effective theory, usually framed as chiral EFT, which is consistent with the symmetries of low-energy QCD and the separation of scales relevant to the low-energy nuclear many-body problem. Linking different scales is far from easy. Interactions derived from these low-energy theories carry also a dependence on an energy scale, defined in terms of an energy cutoff Λ, that separates the Hilbert space of interest from its higher-energy complement. The cutoff is usually chosen so that it is possible to reproduce nucleon-nucleon (NN) scattering phase shifts up to ~ 300 MeV laboratory kinetic energy, which requires $\Lambda \sim 500 - 700$ MeV. For details, we refer the reader to the recent reviews [3, 4].

Currently used *ab initio* approaches to the nuclear many-body problem ($A > 4$) include: coupled-cluster methods [5], quantum Monte Carlo applications [6], perturbative expansions [7], Green's function methods [8], correlation operator methods [9, 10], effective interaction for hyperspherical harmonics [11, 12], in-medium similarity renormalization group [13], lattice simulations [14], and the no core shell model [15, 16].

Nuclear ground-state properties

Binding energies and excitation spectra of light nuclei are standard observables that are computed in *ab initio* approaches. In addition, most of these calculations also provide wave functions of the various nuclear states. Therefore, it is in principle straight forward to evaluate other observables, such as charge and matter radii, magnetic and quadrupole moments, and electroweak transition strengths. Of particular interest are recent experimental campaigns for charge radii, electromagnetic moments, and B(E2) transition strengths. Such efforts allow to study chains of isotopes, from stable to dripline (and beyond), and to follow the evolution of nuclear structure.

Stepping into the continuum

As we approach the driplines, the vicinity of the continuum will become increasingly important. Couplings to the continuum environment will strongly influence nuclear structure. We say that we're dealing with open quantum systems.

In this final part of the contribtion I will mention ongoing efforts to incorporate the continuum into *ab initio* nuclear-structure calculations. This development is timely since the overarching scientific questions of modern nuclear structure are about very neutron-rich or proton-rich nuclei whose properties are impacted by a coupling to the particle

continuum of scattering and decaying states. Many nuclei of interest lie very close to particle emission thresholds, i.e., they are either short-lived or unstable. Such nuclei cannot be described in a closed quantum-system formulation.

It is therefore crucial that new theoretical methods are developed that allow for an accurate description of loosely bound and unbound nuclear states. The recently developed complex-energy Gamow Shell Model (GSM) [17] has proven to be a reliable tool in the description of nuclei, where continuum effects cannot be neglected. In the GSM, a many-body basis is constructed from a single-particle Berggren ensemble [18, 19, 20], which treats bound, resonant, and scattering states on equal footing. Recently, GSM calculations of loosely bound and unbound states in nuclei, starting from a realistic interaction and a Gamow-Hartree-Fock basis were reported [21]. However, an *ab initio* description of light, unstable nuclei within the GSM approach will require novel many-body truncation schemes. In Ref. [22] the Berggren basis was employed for the first time in coupled-cluster calculations of the helium isotopes, and there are promising attempts to include the Berggren basis in an NCSM-like framework [23].

Other approaces, such as the resonating group method [24], are also being developed for *ab initio* calculations and are already able to compute nuclear reaction observables. A recent review on the first-principles description of nuclear systems along the drip lines is given by Forssén *et al.* [25].

OUTLOOK

In this contribution, we have argued that modern many-body techniques are now capable of providing a reliable description of nuclear properties thanks to new conceptual insights as well as algorithmic and computational advances. It is important to realize that *ab initio* nuclear properties are dependent on the nuclear Hamiltonian used, and that the study of the performance of these interactions in light nuclear systems is one of the goals of nuclear *ab initio* methods. An important conclusion, which consistently emerges from these theoretical analyses, is that three-nucleon forces are crucial for both global nuclear properties and detailed nuclear structure, and that many-body correlations due to the coupling to the particle continuum are essential as one approaches particle drip lines.

There are ongoing efforts to extend the range of applicability of *ab initio* methods. In this context we have also seen a new generation of many-body methods; in particular those that can use realistic nuclear interactions from chiral EFT. Furthermore, much work is concentrated on understanding the uncertainties of results obtained in various many-body schemes, as well as the propagation of uncertainties from the nuclear interaction input [26]. We conclude that experimental data from radioactive beam facilities will continue to play an important role in this endeavour.

ACKNOWLEDGMENTS

I am very much indebted to all colleagues in the field of radioactive beam physics, both experiment and theory, for many stimulating discussions. The research leading to these results has received funding from the European Research Council under the European

Community's Seventh Framework Programme (FP7/2007-2013) / ERC grant agreement no. 240603, and by the Swedish Research Council (dnr. 2007-4078).

REFERENCES

1. W. Leidemann, and G. Orlandini, *Progress in Particle and Nuclear Physics* **68**, 158–214 (2013).
2. R. Machleidt, and I. Slaus, *Journal Of Physics G-Nuclear And Particle Physics* **27**, R69 (2001).
3. E. Epelbaum, and U.-G. Meißner, *Reviews of Modern Physics* **81**, 1773–1825 (2009).
4. R. Machleidt, and D. R. Entem, *Physics Reports* **503**, 1–75 (2011).
5. G. Hagen, T. Papenbrock, D. J. Dean, and M. Hjorth-Jensen, *Physical Review C* **82**, 034330 (2010).
6. S. C. Pieper, and R. B. Wiringa, *Annu. Rev. Nucl. Part. Sci.* **51**, 53–90 (2001).
7. M. Hjorth-Jensen, T. T. S. Kuo, and E. Osnes, *Physics Reports* **261**, 125–270 (1995).
8. W. H. Dickhoff, and C. Barbieri, *Progress in Particle and Nuclear Physics* **52**, 377–496 (2004).
9. R. Roth, H. Hergert, P. Papakonstantinou, T. Neff, and H. Feldmeier, *Physical Review C* **72**, 34002 (2005).
10. T. Neff, H. Feldmeier, and K. Langanke, *Progress in Particle and Nuclear Physics* **66**, 341–345 (2011).
11. N. Barnea, W. Leidemann, and G. Orlandini, *Physical Review C* **61**, 054001 (2000).
12. S. Bacca, N. Barnea, and A. Schwenk, *Physical Review C* **86**, 034321 (2012).
13. H. Hergert, S. K. Bogner, S. Binder, A. Calci, J. Langhammer, R. Roth, and A. Schwenk, *Physical Review C* **87**, 034307 (2013).
14. E. Epelbaum, H. Krebs, D. Lee, and U.-G. Meißner, *Physical Review Letters* **106**, 192501 (2011).
15. P. Navrátil, S. Quaglioni, I. Stetcu, and B. R. Barrett, *Journal Of Physics G-Nuclear And Particle Physics* **36**, 083101 (2009).
16. B. R. Barrett, P. Navrátil, and J. P. Vary, *Progress in Particle and Nuclear Physics* **69**, 131–181 (2013).
17. N. Michel, W. Nazarewicz, M. Płoszajczak, and T. Vertse, *Journal Of Physics G-Nuclear And Particle Physics* **36**, 013101 (2009).
18. T. Berggren, *Nuclear Physics* **A109**, 265–287 (1968).
19. T. Berggren, and P. Lind, *Physical Review C* **47**, 768–778 (1993).
20. P. Lind, *Physical Review C* **47**, 1903–1920 (1993).
21. G. Hagen, M. Hjorth-Jensen, and N. Michel, *Physical Review C* **73**, 064307 (2006).
22. G. Hagen, D. J. Dean, M. Hjorth-Jensen, and T. Papenbrock, *Physics Letters B* **656**, 169–173 (2007).
23. G. Papadimitriou, J. Rotureau, N. Michel, and B. R. Barrett, *ArXiv e-prints* (2013), 1301.7140.
24. S. Quaglioni, and P. Navrátil, *Physical Review C* **79**, 44606 (2009).
25. C. Forssén, G. Hagen, M. Hjorth-Jensen, W. Nazarewicz, and J. Rotureau, *Physica Scripta* **T152**, 014022 (2013).
26. A. Ekström, G. Baardsen, C. Forssén, G. Hagen, M. Hjorth-Jensen, G. R. Jansen, R. Machleidt, W. Nazarewicz, T. Papenbrock, J. Sarich, and S. M. Wild, *ArXiv e-prints* (2013), accepted for publication in Phys. Rev. Lett., 1303.4674.

The Future of Shell Model Techniques

Angelo Signoracci[a]

[a]*Centre de Saclay, IRFU/Service de Physique Nucléaire, F-91191 Gif-sur-Yvette, France*

INTRODUCTION

Nuclear shell structure, especially with its evolution away from stability, is used to explain experimental data and to justify proposed experiments with rare isotope beams. It is also the foundation for the nuclear shell model, which has been developed and employed for realistic calculations of nuclei up to $A \approx 100$ in the last decades. The nuclear shell model,[1] as a particular implementation of configuration interaction methods, utilizes a doubly-magic core as the particle vacuum, with the remaining valence nucleons filling a limited number of single particle orbits outside the core. In this way, a reduced Schrödinger equation is solved exactly in the limited valence space for energies and wavefunctions, where the latter can be written simply and manipulated easily with an appropriate choice of single particle basis. Observables can also be calculated, assuming that the operator structure is known and that the effective operators in the reduced model space can be determined. The shell model has been used to reproduce and predict observables such as energies, decay half-lives, electromagnetic transition strengths, etc., with good agreement to available experimental data.

The accuracy of the configuration interaction method depends on the determination of an effective interaction (and in principle effective operators), assuming an appropriate core and model space and sufficient computing resources. The effective interaction must incorporate effects from core excitations as well as from higher-energy orbits excluded from the valence model space. In the most common implementations of the nuclear shell model, empirical interactions, e.g. the USDB interaction[2] fit to energy data throughout the *sd* shell, have been used because the standard nuclear potentials are not amenable to the many-body perturbative techniques necessary to derive effective interactions. Such fitting procedures eliminate the connection to the underlying interactions and therefore limit the predictive power of calculations in the reduced model space, especially those which extend beyond the range of data used in the fit.

While decades of research have led to efficient shell model codes and reliable phenomenological effective interactions in standard model spaces, many improvements remain to be implemented, motivated by experimental interest away from stability and advances in other fields of nuclear structure. Four improvements are highlighted in this work which can be implemented in the coming decades.

IMPROVEMENTS IN SHELL MODEL TECHNIQUES

Derivation of Effective Interactions

The effective interaction generally determines the extent to which a shell model calculation reproduces low-lying nuclear states, and therefore its determination is of primary importance for shell model techniques. The practical need for accuracy with comparison to experiment has led to the parameterization of effective interactions (in whole or in part). While such a procedure will reproduce available experimental data optimally, it lacks predictive power away from known data, for instance towards the neutron dripline. Efforts to produce effective interactions in a more microscopic way have already begun, but should continue to develop in the coming decades.

The essential aspects of a more microscopic procedure for shell model calculations are:

(i) to begin with a microscopic nucleon-nucleon (*NN*) potential (e.g., N3LO[3])

(ii) to "soften" the potential, i.e. to decouple high-momentum modes from low-momentum behavior, by means of renormalization group (RG) methods

(iii) to perform many-body perturbation theory (MBPT) on the low-momentum interaction in order to produce an effective interaction in the reduced model space, in terms of single particle energies (SPE) and two-body matrix elements (TBME)

(iv) to calculate nuclear properties of interest with shell model codes in the reduced model space with the effective interaction and effective operators determined in a consistent way

Currently, there exist applications following this procedure,[4,5,6] which have various limitations. For one example, MBPT has not been formally developed for model spaces which span multiple oscillator shells, requiring ad hoc approximations to produce effective interactions. However, an extension of MBPT to multiple oscillator shells is underway.[7] Furthermore, effective interactions derived in this way reproduce neither empirical SPE nor the behavior of nuclei far from the core of the model space. Both issues can be improved with an accurate treatment of three-body forces.

Three-Body Forces

In fact, two types of many-body forces can be important in the derivation of an effective interaction in the reduced model space: (i) those existing naturally in the *A*-body system, which can be derived in a manner consistent with the *NN* potential (e.g., from chiral effective field theory in the case of the N3LO interaction) and (ii) those induced by the RG methods. Holt et al.[8,9] have shown that the inclusion of the former lead both to an improved description of SPE and to a reproduction of exotic oxygen isotopes from a repulsive contribution to TBME. Care must be taken, as Roth et al.[10] have recently shown that the latter contribution of many-body forces might not obey the standardly assumed hierarchy, i.e. $NN > NNN > NNNN$ ... In standard applications, the explicit three-body contribution of the three-body forces, when written in normal-ordered form, are at least an order of magnitude smaller than the effective one-body

and effective two-body terms.[11] As a result, the standard form of effective interactions (in terms of SPE and TBME) can still be utilized, along with standard shell model codes, in order to produce calculations with three-body forces. Holt et al. have shown that three-body forces, limited to the effective one-body and two-body components, contribute to an evolution of shell structure away from stability. Experimental interest in exotic nuclei currently require effective interactions which reproduce the behavior away from stability, and therefore the inclusion of three-body forces is an essential aspect of future research with shell model techniques, especially for effective interactions derived in a more microscopic manner from two-body interactions, as outlined in the prior subsection.

Evolution of Shell Structure

Single-nucleon shell structure is believed to correspond to a certain degree of reality in nuclear structure, in the sense that low-energy observables are expected to reflect its main features near the Fermi surface. However, quantities that are measured experimentally, e.g. the excitation energy and collective properties of the first 2^+ state in even-even nuclei, do not directly correspond to one particular single particle shell structure. Through theoretical methods, shell structure is accessed via effective single-particle energies (ESPEs), as described by Baranger.[12] As recently shown by Duguet and Hagen,[13] ESPEs are basis-independent but not observable, depending significantly on the resolution scale characterizing the Hamiltonian. A detailed definition of ESPEs and their properties, as well as further results and conclusions, can be found in a forthcoming publication.[14]

The concept of single-nucleon shell structure provides a simplified picture of nuclear systems and a valuable tool to analyze the behavior of complicated many-body observables in terms of simpler theoretical ingredients. However, the practical reconstruction of ESPEs is contaminated by theoretical uncertainties, due in part to incomplete spectroscopic data, and therefore an evaluation of uncertainties is necessary for meaningful discussion. The omission of states characterized by small spectroscopic strength and/or large excitation energies leads to a significant error in the reconstruction of ESPEs, even in doubly magic nuclei. The shell model presents an appropriate way to determine completely correlated ESPEs from many-body nuclear systems, and has been utilized to evaluate errors on the reconstruction of ESPEs. Because the results are not yet finalized, they will primarily be presented elsewhere.[14] To emphasize briefly the conclusions of the article, the standard approximations to assess the evolution of shell structure in nuclear physics result in errors on the order of 500 keV. Consistent methods must be employed and must focus on the relative behavior of ESPEs, with an evaluation of uncertainties, in order to have relevance in the discussion of shell structure.

Coupling to the Continuum

The shell model utilizes a discrete single particle basis which describes bound states, but cannot be used to represent the continuous states above the lowest-energy decay threshold. Especially for exotic nuclei, where the thresholds often occur at low

excitation energy, the treatment of resonant states is important even in an effective theory treating low-energy states. Multiple procedures have been developed in order to explicitly include coupling to the continuum, and to provide additionally a straightforward treatment of reaction processes.[15,16] Presently, standard shell model techniques are often used to calculate states above the threshold. With empirical interactions, relatively good agreement is often found for unbound states because continuum effects can be implicitly included by the interaction through the fit to data. The coupling to the continuum is often neglected as a result, even though the standard shell model does not treat it correctly; however, it will be more important in the case of microscopic interactions which are not constrained by nearby data, and especially for nuclei far from stability near the limits of experimental capabilities.

CONCLUSION

Shell model techniques are often used for accurate descriptions of light- and medium-mass nuclei. Many improvements in recent years have focused on computational advances or on utilizing recently measured data to update empirical interactions. The future of shell model techniques depends on merging computational progress with more microscopic components. Namely, effective interactions should be derived from microscopic potentials, including three-body forces at least at the one- and two-body level. Coupling to the continuum should be included for near- and above-threshold states, and evaluations of shell structure should be determined in a consistent way with the prescription of Baranger. Such progress should be prioritized and should be adopted in an integrated fashion, which requires a willingness to collaborate among the practitioners of shell model methods.

REFERENCES

1. E. Caurier et al., *Rev. Mod. Phys.* **77**, 427 (2005).
2. B. A. Brown and W. A. Richter, *Phys. Rev. C* **74**, 034315 (2006).
3. D. R. Entem and R. Machleidt, *Phys. Rev. C* **68**, 041001(R) (2003).
4. M. Hjorth-Jensen, T. T. S. Kuo, and E. Osnes, *Phys. Rept.* **261**, 125 (1995).
5. A. Signoracci, B. A. Brown, and M. Hjorth-Jensen, *Phys. Rev. C* **83**, 065803 (2011).
6. B.A. Brown, A. Signoracci, and M. Hjorth-Jensen, *Phys. Lett. B* **695**, 507 (2011).
7. N. Tsunoda, K. Takayanagi, M. Hjorth-Jensen, and T. Otsuka, in preparation.
8. J.D. Holt and A. Schwenk, arXiv:1108.2680.
9. J. D. Holt, T. Otsuka, A. Schwenk, and T. Suzuki, arXiv:1009.5984.
10. R. Roth et al., *Phys. Rev. Lett.* **109**, 052501 (2012).
11. S. C. Pieper, V. R. Pandharipande, R. B. Wiringa, and J. Carlson, *Phys. Rev. C* **64**, 014001 (2001).
12. M. Baranger, *Nucl. Phys. A* **149**, 225 (1970).
13. T. Duguet and G. Hagen, *Phys. Rev. C* **85**, 034330 (2012).
14. A. Signoracci and T. Duguet, in preparation.
15. N. Michel et al., *Phys. Rev. Lett.* **89**, 042502 (2002).
16. A. Volya and V. Zelevinsky, *Phys. Rev. C* **74**, 064314 (2006).

Study of the Pygmy Resonance within a New Microscopic Multiphonon Approach

N. Lo Iudice[*,†], D. Bianco [1,†], F. Knapp[**], P. Vesely[†], F. Andreozzi[*,†] and A. Porrino[*,†]

[*] *Dipartimento di Scienze Fisiche, Università di Napoli "Federico II" Monte S Angelo, Via Cintia I-80126 Napoli, Italy*

[†] *Istituto Nazionale di Fisica Nucleare, sezione di Napoli, Monte S Angelo, Via Cintia I-80126 Napoli, Italy*

[**] *Institute of Particle and Nuclear Physics, Charles University, V Holešovičkách 2, CZ-18000 Praha 8, Czech Republic*

Abstract. The electric dipole response in the neutron rich ^{20}O is investigated within a new equation of motion approach proposed recently which generates a basis of multiphonon states, built of quasiparticle Tamm-Dancoff phonons. Attention is focused on the low-lying excitations associated to the pygmy resonance.

Keywords: Electric dipole response, pygmy resonance, ^{20}O, microscopic multiphonon basis, equation of motion
PACS: 21.60.Ev,23.20.Js,24.30.Cz

The electric dipole mode has attracted recently a renewed interest. Attention has been focused on the excitations occurring in nuclei with neutron excess at the low-energy tail of the dipole giant resonance (GDR). These excitations are interpreted as a manifestation of a collective mode termed pygmy dipole resonance (PDR) generated by a translational oscillation of the neutron excess against a N=Z core. A list of experimental and theoretical papers may be found in Refs. [1, 2].

In the energy range of the PDR, other low-lying vibrational modes may come into play and contribute to the dipole strength. This issue can be clarified only by going beyond the mean-field level. In fact, the PDR was studied mainly in shell model (SM) [3] or in extensions of the quasiparticle random phase approximation (QRPA), like the quasiparticle phonon model (QPM) [2], QRPA plus phonon-coupling [4] and the relativistic time blocking approximation (RTBA) [5].

We propose here a study of the dipole response based on an equation of motion phonon method (EMPM) developed few years ago [6, 7], recast recently in a more consistent scheme [8]. The method consists in deriving a set of equations of motion which can be solved iteratively to generate a basis of multiphonon states, built of phonons created in particle-hole (*ph*) Tamm-Dancoff approximation (TDA). It applies to a Hamiltonian of general form and does not rely on any approximation except for the truncation of the multiphonon space.

---

[1] Present address : Ecole Normale Superieur (ENS) de Cachan, 61 av. du Président Wilson, Cachan - France

In its *ph* scheme, it was applied with success to study the $E1$ response in the heavy ^{208}Pb [9]. Here, a *qp* version suited to open shell nuclei is derived and employed to study the $E1$ response in the neutron rich ^{20}O by solving the eigenvalue problem in a space which covers up to three-phonon states. This large scale calculation will enable us to investigate the spreading of the GDR and to explore the low-lying excitations, associated to the PDR, which were observed in Coulomb excitation experiments [11, 12, 13] and investigated theoretically in SM [3] and in QRPA plus phonon-coupling [4].

BRIEF OUTLINE OF THE METHOD

As illustrated in Ref. [8], the main goal of the EMPM is to generate a basis of *n*-phonon states

$$|n;\beta>=\sum_{\lambda\alpha} C^{\beta}_{\lambda\alpha}\left\{O^{\dagger}_{\lambda}\times \mid n-1,\alpha>\right\}^{\beta}, \tag{1}$$

where $O^{\dagger}_{\lambda}$ is a quasiparticle TDA phonon operator acting on a $(n-1)$-phonon state $\mid n-1,\alpha>$, assumed to be known.

The key for generating such a basis is provided by the equations of motion

$$<n,\beta\mid\left\{\left[H,O^{\dagger}_{\lambda}\right]\times\mid n-1,\alpha>\right\}^{\beta}=\left(E_{\beta}-E_{\alpha}\right)<n,\beta\mid\left\{O^{\dagger}_{\lambda}\times\mid n-1,\alpha>\right\}^{\beta}. \tag{2}$$

The procedure followed in Ref. [8], we obtain the generalized eigenvalue equation

$$\sum_{\lambda'\alpha'}\mathscr{H}^{\beta}(\lambda\alpha,\lambda'\alpha')C^{\beta}_{\lambda'\alpha'}=E_{\beta}\sum_{\lambda'\alpha'}\mathscr{D}^{\beta}(\lambda\alpha,\lambda'\alpha')C^{\beta}_{\lambda'\alpha'}. \tag{3}$$

where the Hamiltonian has the composite form $\mathscr{H}=\mathscr{A}\mathscr{D}$, $\mathscr{D}$ is the metric matrix and

$$\mathscr{A}^{\beta}(\lambda\alpha,\lambda'\gamma)=(E_{\lambda}+E_{\alpha})\delta_{\lambda\lambda'}\delta_{\alpha\gamma}+\sum_{\sigma}W(\beta\lambda'\alpha\sigma;\gamma\lambda)\mathscr{V}^{\sigma}_{\lambda\alpha,\lambda'\gamma}. \tag{4}$$

Here E_{λ} and E_{α} are the energies of the TDA phonon of multipolarity λ and of the $(n-1)$-phonon state with quantum numbers α, W is a Racah coefficient, and $\mathscr{V}$ a phonon-phonon interaction potential. The close formal analogy with TDA was pointed out [8].

All quantities appearing in the eigenvalue equations are given by recursive formulas, which allow to solve Eq. (3) iteratively. The redundant states are eliminated by the procedure outlined in [6, 7], based on the Cholesky decomposition method.

A set of orthonormal multiphonon states $\{|0>,|\lambda>,\ldots|n,\alpha>\ldots\}$ is generated. The Hamiltonian is diagonal in each *n*-phonon block. The terms coupling different blocks are also given by recursive formulas. The Hamiltonian matrix so constructed is easily brought to diagonal form yielding the totality of eigenstates allowed by the dimensions of the multiphonon space. These eigenfunctions are linear combinations of $\{|0>,|\lambda>,\ldots|n,\alpha>\ldots\}$ phonon states. Thus, the multipole operator promotes forward and backward transitions among components differing by one phonon, as well as transitions among states with the same number of phonons.

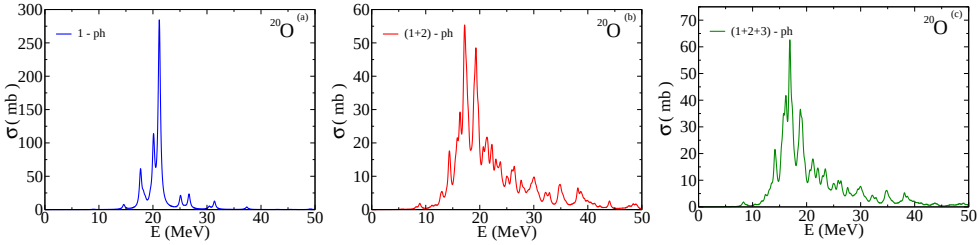

FIGURE 1. $E1$ cross sections in ^{20}O.

NUMERICAL APPLICATION: E1 RESPONSE IN ^{20}O.

We used a Brueckner G-matrix [14] derived from the CD-Bonn nucleon-nucleon potential [15] and a Nilsson Hamiltonian with the same parameters used for ^{16}O [8].

The TDA phonons were generated in a space which includes up to the (sdg) major shell. Among them, we selected the positive (negative) parity phonons of energies $E_\lambda \leq 25$ MeV ($E_\lambda \leq 30$ MeV) to generate the two- and three-phonon basis states. On the whole, the space includes up to 3p-3h configurations of energy $\sim 12\hbar\omega$ MeV. It is therefore substantially larger than the space adopted in a shell model calculation [3].

We adopted a method exploiting the Gramm-Schmidt orthogonalization procedure to produced a basis of TDA phonons free of spurious admixtures induced by the center of mass motion and by the particle number violating Bogoliubov transformation. The computed cross section is shown in Figure 1. One may observe the strong impact of the two-phonon states on the cross section. Indeed, in going from TDA (left panel) to the space which includes also the two-phonon states (mid panel), the $E1$ strength gets dramatically quenched and fragmented in the GDR region. The three phonons have a more modest impact (right panel).

Another feature is the appearance of a small hump at low-energy once the two- and three-phonon states are included. The calculation allows the analysis of its fine structure. It yields, in fact, the same number of peaks observed in the experiments [11, 12, 13]. The strengths they carry, however, are one order of magnitude smaller than the measured ones.

Extending the comparative analysis further up in energy, we find that the strength collected by all the states up to ~ 15 MeV accounts for $\sim 10\%$ of the classical energy weighted sum rule in agreement with experiments [11, 16]. It is to be pointed out, however, that neither the experimental or the theoretical spectra exhibit a clear cut separation from the GDR peaks. Only a continuous sequence of peaks is obtained.

The analysis of the phonon composition may help to explain such a strong fragmentation. The states of this low-energy region are composed of one-phonon coexisting with two-phonon components. The latter couple octupole or dipole excitations to quadrupole or hexadecapole surface vibrational modes. Only the lowest 1^- state has a large one-phonon component. Also the state describing the third peak has a TDA phonon with an appreciable weight. This is composed of the valence neutron qp configuration $(0d_{5/2}, 0f_{7/2})_\nu$ in opposition of phase with the core excited neutron $(0d_{5/2}, 0p_{3/2})_\nu$ and proton $(1s_{1/2}0p_{1/2})_\nu$ configurations. It describes a genuine oscillation of the neutron skin against the core.

This mode, however, is excited with a relatively small strength. Indeed, the main role is played by the *qp* neutron configurations with large weight while the many proton states contribute with small amplitudes. Moreover, the mode is damped by the coupling and the coexistence with multiphonon excitations.

The one-phonon states contributing to the GDR are consistently composed of core excited neutron and proton components in opposition of phase. They describe genuine GDR excitations. On the other hand, they are strongly coupled to multiphonon excitations which induce a severe damping.

In summary, the two-phonon components play a crucial role in fragmenting and shaping the GDR and are determinant in pushing a residual strength down in the low-energy sector in agreement with experiments. Only one of the peaks may be associated to the PDR.

The detailed and exhaustive description of the $E1$ response was made possible by the availability of the explicit multiphonon structure displayed by the EMPM wavefunctions describing the single $E1$ levels. This represents an important advance with respect to the other approaches which extend the RPA.

REFERENCES

1. N. Paar, D. Vretenar, E. Khan, and G. Colò, Rep. Prog. Phys. **70**, 691 (2007).
2. A. Tamii *et al.*, Phys. Rev. Lett. **107**, 062502 (2011).
3. H. Sagawa and T. Suzuki, Phys. Rev. C **59**, 3116 (1999).
4. G. Colò and P. F. Bortignon, Nucl. Phys. A **696**, 427 (2001).
5. E. Litvinova, P. Ring, V. Tselyaev, Phys. Rev. Lett. **105**, 022502 (2010)
6. F. Andreozzi, F. Knapp, N. Lo Iudice, A. Porrino, and J. Kvasil, Phys. Rev. C **75**, 044312(2007).
7. F. Andreozzi, F. Knapp, N. Lo Iudice, A. Porrino, and J. Kvasil, Phys. Rev. C **78**, 054308(2008).
8. D. Bianco,F. Knapp, N. Lo Iudice, F. Andreozzi, and A. Porrino Phys. Rev. C **84**, 014313(2012).
9. D. Bianco,F. Knapp, N. Lo Iudice, F. Andreozzi, and A. Porrino Phys. Rev. C **86**,(2012).
10. I. Poltoratska *et al.*, Phys. Rev. C **85**, 041304(R) (2012).
11. A. Leistenschneider *et al.*, Phys. Rev. Lett. **86**, 5442 (2001)
12. E. Tryggestad *et al.*, Phys. Lett. B **541**, 52 (2002)
13. E. Tryggestad *et al.*, Phys. Rev. C **67**, 064309 (2003).
14. M. Hjorth-Jensen, T. T. Kuo, E. Osnes, Physics Reports **261**, 125 (1995).
15. R. Machleidt, Phys. Rev. C **63**, 024001 (2001).
16. T. Aumann, Nucl. Phys. A **805** , 198c (2008).

Spectroscopy of nuclei near and beyond the neutron drip line by direct reactions at new-generation RI beam facilities

T. Nakamura

Tokyo Institute of Technology, 2-12-1 O-Okayama, Meguro, Tokyo 152-8551, Japan

Abstract. The new-generation RI-beam facility, RIBF (RI Beam Factory) at RIKEN, where high intense intermediate/high energy RI beams have become available, offers expanded opportunities to study structures near the drip lines. The direct reactions, and among others breakup reactions at such incident energies, play crucial roles to explore the neutron-drip line region. Some of the earlier experimental results at RIBF using the inclusive Coulomb/nuclear breakup on neutron-rich isotopes near N=20 and N=28 are presented. We have recently launched a new spectrometer, SAMURAI, at RIBF, where kinematically complete measurements of breakup reactions of very neutron rich nuclei can be performed. We present briefly about the new experiments performed at SAMURAI.

Keywords: RI-beam facility, Coulomb and nuclear breakup, Halo nuclei
PACS: 25.60.-t,25.60.Gc

RI BEAM FACTORY

The RI Beam Factory (RIBF) at RIKEN Nishina Center has started its operation in 2007 as the first-commissioned next generation RI beam facility [1]. With the newly constructed three ring cyclotrons, fRC (fixed frequency Ring Cyclotron, K= 570 MeV), IRC (Intermediate-stage Ring Cyclotron, K= 980 MeV), and SRC (Superconducting Ring Cyclotron, K= 2500 MeV), the facility is now capable of accelerate a whole range of heavy ions up to ^{238}U at 345 MeV/nucleon with high intensities. In 2012, the typical intensity of ^{48}C at 345 MeV/nucleon is 100-200 pnA, and that of ^{238}U 10-15 pnA.

The in-flight RI beam separator BigRIPS has capability to produce RI beams with high intensities, in particular for nuclei far from the stability. The large acceptance (momentum 6%, angles 80(H)$\times$100(V) mrad^2 [2]) allows us to collect sufficient portion of projectile- or in-flight fission fragments. The second stage of the BigRIPS can tag the beam particle on event-by-event basis after being geometrically selected by the magnetic rigidity combined with the energy loss difference. With this new facility, about 50 new isotopes have already been observed [3, 4], and half-lives of some of the key neutron-rich isotopes near the path of the r-process has been newly determined [5].

BREAKUP REACTIONS AND EXOTIC NUCLEI

Coulomb and nuclear breakup at intermediate/high energies

One of the important experimental probes for nuclei far from the stability is breakup reaction at intermediate/high energies. When we approach the neutron drip line, where exotic structure such as halo appears, one important feature is the closeness of the valence neutron to the continuum in energies. The breakup reactions thus play important roles since the cross section is significantly large.

The breakup reaction shows very different characteristics, depending on the target [6, 7]. A heavy target such as Pb induces primarily Coulomb breakup, while a light target such as C induces nuclear breakup.

The Coulomb breakup is used to extract the $E1$ response of the nucleus since it is essentially the photo absorption process. The Coulomb breakup cross section is written as,

$$\frac{d\sigma(E1)}{dE_{\rm x}} = \frac{16\pi^3}{9\hbar c} N_{E1}(E_{\rm x}) \frac{dB(E1)}{dE_{\rm x}}, \tag{1}$$

where $N_{E1}(E_{\rm x})$ denotes the number of the virtual photons for the electric dipole transition with energy of $E_{\rm x}$ [8]. The simplicity that the cross section can be factorized allows us to extract the $E1$ strength distribution.

One of the important and unique features of halo nuclei is the strong enhancement of the $B(E1)$ spectrum just above the neutron decay threshold (Soft $E1$ excitation). This phenomenon is now well understood by the direct breakup mechanism, where the $E1$ response reflects the halo spatial properties [9, 10, 11, 12, 13, 6]. Hence, the Coulomb breakup becomes one of useful tools to probe the halo wave function.

Nuclear breakup of an unstable nucleus with a light target at intermediate/high energies also offers a useful spectroscopic tool. The momentum distribution of the core fragment after $1n$ removal can be used to extract the orbital angular momentum of the removed neutron. When a measurement is combined with that of the γ ray emitted from the core fragment, the core configuration of the projectile can also be extracted, including the spectroscopic factor C^2S. The combined analysis of Coulomb and nuclear breakup further enhances this capability due to different sensitivities to the spatial distribution of the wave function around the surface of exotic nuclei.

Inclusive breakup experiments at ZDS at RIBF

The breakup reaction, when measured in complete kinematics, can be used to extract the $B(E1)$ energy spectrum in Coulomb breakup. However, when we explore the nuclei, lying very far from the stability, because of its low beam intensity, the inclusive Coulomb breakup can be useful as a first experimental approach. As such motivations, the inclusive breakup cross sections ($1n$ and/or $2n$ removal cross sections) of ^{19}B, ^{19,20,22}C, ^{29,31}Ne, and ^{33,35,37}Mg at 220-240 MeV/nucleon have been measured at ZDS (Zero Degree Spectrometer) at RIBF, at RIKEN [14, 15]. The $1n$ removal cross sections for Ne, Mg, and Si isotopes are summarized in Fig. 1.

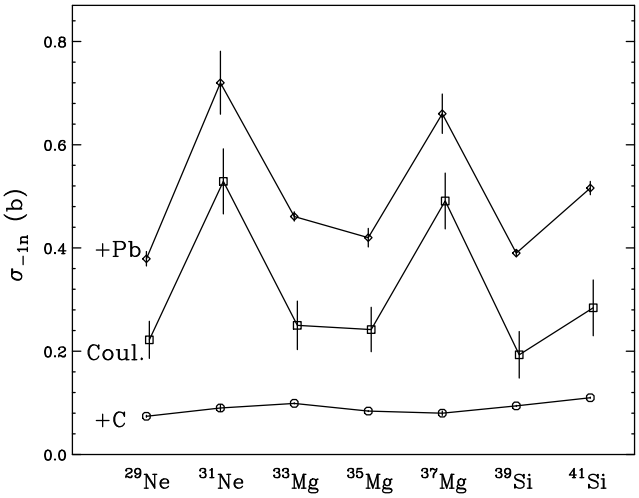

FIGURE 1. 1*n* removal cross sections of ^{29,31}Ne, ^{33,35,37}Mg, and ^{39,41}Si on C (circles) and Pb (diamonds) at 220-240 MeV/nucleon. The Coulomb breakup cross sections on Pb (squares) are estimated by subtracting the nuclear breakup contribution estimated from the ones with the carbon target. The data, except for ^{31}Ne [14], are preliminary.

As shown, the cross section for ^{31}Ne and ^{37}Mg are significantly larger ($\sim$ 0.5 b), expected for the halo nucleus. As detailed in Ref. [14], the nucleus ^{31}Ne has been identified as a new 1*n* halo nucleus, evidenced by this enhanced Coulomb breakup cross section. We are further investigating the structure of these nuclei by using the combinatorial analysis of nuclear and Coulomb breakup.

Breakup reaction experiments at SAMURAI facility

The kinematically complete measurement of the breakup reaction, where all the momenta of the outgoing particles in the forward direction are measured in coincidence, allows us to obtain the invariant mass of the excited state, which can be translated into the excitation energy event by event. For instance, in the Coulomb breakup one can map $B(E1)$ as a function of the excitation energy by using Eq. (1). $B(E1)$ distribution contains information of the ground state wave function, such as C^2S (spectroscopic factor), ℓ (orbital angular momentum), and $S_{\rm n}$ (separation energy) of the halo state. The kinematically complete measurement is also a suitable tool to study the *nn* correlation. Such a method is called invariant-mass spectroscopy.

The SAMURAI (**S**uperconducting **A**nalyser for **MU**lti-particles from **RA**dio **I**sotope Beams) has started its operation in 2012, in order to realize the invariant mass spectroscopy of RI beam with high efficiency at RIBF. The layout of SAMURAI facility is shown schematically in Fig. 2. SAMURAI comprises the superconducting magnet with a maximum magnetic field of 3.1 Tesla ($B_{max}L$=7.1 Tm), beam detectors, heavy ion detectors including two large multi-wire drift chambers (FDC1 and FDC2), and the neutron detector array NEBULA (**NE**utron-detection system for **B**reakup of **U**nstable nuclei with **L**arge **A**cceptance).

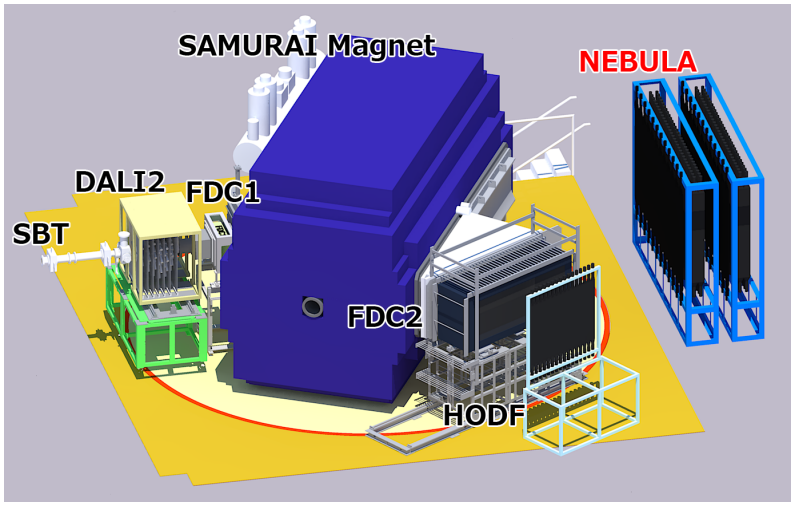

FIGURE 2. The setup used for the day-one campaign experiments at the SAMURAI facility at RIBF, RIKEN. The beam comes from the left to the target position which is surrounded by the DALI2 (NaI(Tl) γ-ray array). The outgoing fragment is bent by the SAMURAI superconducting magnet, traced by the drift chambers (FDC1,FDC2) before and after bending, and its charge and TOF is measured by the hodoscope(HODF). The neutron goes through the gap of the magnet and is measured in NEBULA, neutron detector array.

In May, 2012, we have successfully completed the day-one campaign experiment, which includes the kinematically complete measurement of Coulomb breakup of two neutron halo nuclei ^{19}B and ^{22}C. The beam intensity of ^{19}B was about 100 pps, and that of ^{22}C was about 15 pps, about 3-4 orders of magnitude larger than those obtained in the previous facility (RIPS). The intensities are significantly larger as such, compared to other RI beam facilities in the world as well.

SUMMARY

The importance and usefulness of the breakup reactions at intermediate/high incident energies in the new-generation RI beam facility has been demonstrated. Inclusive breakup measurements at the new-generation RI beam facility, RIBF at RIKEN, were presented, where evidence for the 1n halo structure in ^{31}Ne is shown. The new facility SAMURAI, which is constructed partially for the invariant mass spectroscopy of very neutron-rich nuclei, has commissioned in 2012. The first series of physics experiment, including the kinematical complete measurement of the Coulomb breakup of ^{19}B and ^{22}C at about 240 MeV/nucleon have been successfully performed. This demonstrates the powerfulness of the facility, so that we expect that such breakup reactions are applied for more exotic and heavier nuclei along the drip lines in the near future. We also note that Coulomb breakup is also useful for probing the pygmy dipole resonances (PDR), which is also sensitive to the neutron-skin thickness and the symmetry energy of the equation of state, one of the most sought-after subjects.

ACKNOWLEDGMENTS

The author would like to thank the collaborators of the ^{31}Ne experiment [14]. The author also would like to thank the SAMURAI day-one campaign collaboration. The present work was supported in part by a Grant-in-Aid for Scientific Research (B) (No. 22340053), and that on Innovative Areas (No. 24115005) from the Ministry of Education, Culture, Sports, Science and Technology (MEXT, Japan).

REFERENCES

1. Y. Yano, Nucl. Instrum. Methods Phys. Res. B **261**, 1009 (2007).
2. T. Kubo, Nucl. Instrum. Methods Phys. Res. B **204**, 97 (2003).
3. T. Ohnishi *et al.*, J. Phys. Soc. Jpn. **77**, 083201 (2008).
4. T. Ohnishi *et al.*, J. Phys. Soc. Jpn. **79**, 073201 (2010).
5. S. Nishimura *et al.*, Phys. Rev. Lett. **106**, 052502 (2011).
6. T. Nakamura and Y. Kondo, Clusters in Nuclei vol. 2 (Lecture Notes in Physics vol 848) ed C. Beck (Berlin:Springer), pp 67-119 (2012).
7. T. Aumann and T. Nakamura, Phys. Scr. **T152**, 014012 (2013).
8. C. Bertulani and G. Baur, Phys. Rep. **163**, 299 (1988).
9. T. Nakamura *et al.*, Phys. Lett. B **331**, 296 (1994)
10. R. Palit *et al.*, Phys. Rev. C **68**, 034318 (2003).
11. N. Fukuda *et al.*, Phys. Rev. C **70**, 054606 (2004).
12. T. Nakamura *et al.*, Phys. Rev. Lett. **83**, 1112 (1999).
13. T. Nakamura *et al.*, Phys. Rev. Lett. **96**, 252502 (2006).
14. T. Nakamura *et al.*, Phys. Rev. Lett. **103**, 262501 (2009).
15. N. Kobayashi *et al.*, Phys. Rev. C **86**, 054604 (2012).

Beta-decay In Light Dripline Nuclei

Karsten Riisager[a]

[a]*Dept. of Physics and Astronomy, Aarhus University, Ny Munkegade 120, DK-8000 Aarhus C*

A brief overview of beta-decay processes in light exotic nuclei is given. The two main subjects are how beta-decay processes change in the light nuclei and how beta-decays provide new structure information. Based on examples of recent results some identified open questions are posed as challenges for the next generation facilities such as EURISOL.

INTRODUCTION

Weak interactions play a role in nuclei mainly through beta-decays. They have historically played an important role in unravelling the intricate structure of the interaction and conversely beta-decay has served as a reliable probe of nuclear structure for decades [1]. This contribution focuses on the continuing role of beta-decays in light exotic nuclei, but it should be mentioned that nuclei still give access to detailed studies of the weak interaction (in light nuclei several interesting nuclei, one example is ^{6}He, are very useful for these studies; see [2] and references therein and [3] for the beta-beam development). The phenomenology of beta-decays changes away from stability and allow us to extract structure information that often is complementary to (and very competitive to) that obtained via nuclear reactions. The field has in recent years been reviewed in [4,5] and a further general review of spin-isospin excitations also appeared recently [6]. I refer to these references for the detailed formalism of beta-decay, including detailed definitions of beta-strength etc, and will in the following focus on the physics concepts. As should become clear from the examples given, beta-decay and reaction studies are complementary and will both be important for future RIB physics.

BETA-DECAY AWAY FROM STABILITY

Beta-decay takes place within an "isobaric mass parabola" and Q-values therefore increase towards the driplines so that significantly more nuclear structure can be accessed in the decays. At the same time nucleon separation energies decrease so beta-delayed particle emission will constitute an increasing proportion of the decays. The βn decays are only retarded by angular momentum barriers whereas charged particles also feel the Coulomb barrier. Light nuclei are special in the sense that there is still no severe retardation of charged particle emission in contrast to heavier nuclei where it is

a major limiting factor. There βα is essentially always suppressed and βp only achieves a significant branching ratio 1-2 nucleons away from the dripline (for odd-Z).

Beta-delayed multi-particle emission will also be energetically allowed close to the driplines, but is only a dominant decay mode for A=8,9 and for very neutron-rich nuclei. It is of course also of interest in other nuclei since it proceeds via highly excited states in the daughter nucleus and can give unique physics information: particle emission can populate many more states than the ones allowed by beta-decay spin-parity selection rules.

Studies of the mirror symmetry between corresponding β^+ and β^- transitions seem to be sensitive to nuclear structure rather than weak interaction effects. Significant progress have been obtained during the last decades, but challenges remain as shown by the A=9 multiplet where quite a large asymmetry in B_{GT} values remain unexplained [7].

The isobaric analogue state (IAS) transitions play a key role (for nuclei close to N=Z even a dominating role) for decays of proton-rich nuclei. There are still not many detailed studies of isospin symmetry breaking and in particular very little information on where the Fermi strength that does not go to the IAS, but to states with the same isospin, ends up. Ernst Roeckl pointed out to me that γ-decay is an important decay channel for the IAS so that the intensity seen in proton decays can be noticeably reduced compared to the sum rule value. This effect has to my knowledge not yet been investigated systematically.

STRUCTURE INFORMATION FROM BETA-DECAY

As mentioned above βp decays can for a sufficiently exotic initial nucleus populate as many states as typical nuclear reactions and it can therefore provide information e.g. on states relevant for astrophysical processes. One example is the $^{29}P(p,\gamma)^{30}S$ reaction [8] where the relevant states are populated in the β2p and βpγ branches from ^{31}Ar decays. This type of study should be feasible for many decays at the proton dripline.

Once beta-delayed particle emission becomes prominent problems arising from continuum structures can be investigated in a complementary way to nuclear reactions. One example is the broad levels occurring in very light nuclei where the very existence has sometimes been put into question such as in ^{8}Be or ^{12}C. States of several MeV width have been proposed here and could in both cases be fed in beta decays, by ^{8}B and ^{12}N, respectively [9]. States that like these are hard to extract in a convincing manner from a single data set need to be populated in different ways to be credible.

The beta decay of halo nuclei has been a fruitful source of challenges that have not all been met. The βd decays seem to be halo specific in that two-neutron halos decay in an almost decoupled manner into final state deuterons. The analogous βp decay of a one-neutron halo state will be much less likely due to the smaller phase space and has not yet been observed. The general beta strength distribution is at the moment known with some precision for the halo nuclei ^{6}He, ^{11}Li and ^{11}Be and roughly known for ^{14}Be, but it is still not possible to say whether the prediction of the Gamow-Teller

Giant Resonance becoming accessible in light very neutron-rich nuclei [10] is correct or not.

The comparison of data on light nuclei to ab initio calculations have emerged during the last decade as an important tool, several theoretical talks at this topical meeting focus on this line of research. It may be useful to remind that meaningful comparisons level by level can only take place at low excitation energy, at higher excitation energy we reach the chaotic regime. This can be relevant also in decays in light nuclei, a recent example is the decay of ^{23}Al where essentially random behaviour was observed at 8 MeV excitation energy [11]. At this point only average quantities carry meaningful and testable information, as is well known from studies in heavier nuclei. The obvious, and currently open, questions are where the transition from regular behaviour to chaos takes place and, somewhat more ``optimistically", whether we in beta decays may be able to see also the transition into the Ericsson fluctuation regime in which levels start to overlap.

FUTURE PROGRESS

Let me end with a few comments on where EURISOL (and other future higher intensity facilities) may contribute beyond what is currently possible. One should not forget the possible role of specialized installations such as the suggested ISOL@Myrrha that may play a complementary role.

Several types of experiments will with our present experimental techniques require long beamtimes and/or significantly increased intensities of the radioactive beams. This can be due to very small branching ratios of the interesting physics or due to inherent low detection efficiency, e.g. neutron detection with accurate time-of-flight (this applies even more if one attempts to do neutron coincidences) or gamma-detection with crystal spectrometers.

We will of course benefit also from instrumentation improvements. Among the many techniques that have been developed but not yet put into routine use I would like to mention polarized beams, as employed at Triumf for measuring the ^{11}Li decay [12], and storage in traps, again pioneered by our weak interaction colleagues, that could improve in particular detection of low-energy particles.

REFERENCES

1. A. Bohr and B.R. Mottelson, Nuclear Structure, Vol. 1 (Benjamin, 1969).
2. N. Severijns and O. Naviliat-Cuncic, Ann. Rev. Nucl. Part. Sci. 61 (2011) 23.
3. C. Volpe, Prog. Part. Nucl. Phys. 64 (2010) 325.
4. B. Blank and M.J.G. Borge, Prog. Part. Nucl. Phys. 60 (2008) 403.
5. M. Pfützner, M. Karny, L.V. Grigorenko and K. Riisager, Rev. Mod. Phys. 84 (2012) 567.
6. Y. Fujita, B. Rubio and W. Gelletly, Prog. Part. Nucl. Phys. 66 (2011) 549.
7. Y. Prezado et al., Phys. Lett. B576 (2003) 55.
8. K. Setoodehnia et al., arXiv:1210.1194.
9. S. Hyldegaard, PhD thesis, Aarhus University 2010.
10. H. Sagawa, I. Hamamoto and M. Ishihara, Phys. Lett. B303 (1993) 215.
11. O. Kirsebom et al., Eur. Phys. J. A47:130 (2011).
12. Y. Hirayama et al., Phys. Lett. B611 (2005) 239.

Halo Nuclei: Stepping Stones Across the Dripline

Haik Simon[a]

[a]*GSI Helmholtzzentrum für Schwerionenforschung GmbH, Planckstrasse , 64291 Darmstadt, Germany.*

INTRODUCTION

This paper capitalizes on the production of unbound nuclear systems in the continuum. The advent of intense secondary beams allows producing systems across the neutron and proton drip-lines where adding neutrons or protons, respectively, leads to unbound systems. The synthesis of extremely neutron-rich systems [1] can be achieved e.g. by adding neutrons or removing protons in transfer reactions at low beam energies, or, for the case shown here by selectively removing neutrons or protons from energetic secondary beams in inverse kinematics in order to cross the neutron drip-line, as shown in figure 1. Other production mechanisms at high beam energies include fragmentation reactions where several nuclei are removed from stable beams or pion absorption experiments.

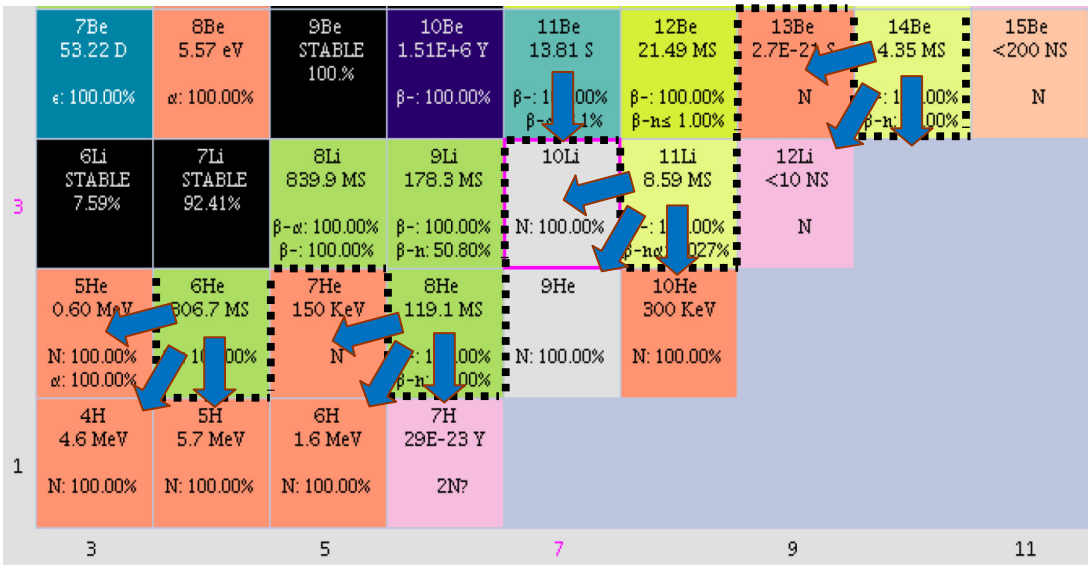

FIGURE 1. Example reactions used to produce neutron-rich unbound systems by selectively removing protons or neutrons from incident exotic nuclei at the neutron-dripline.

At the boundaries: Three body correlations

Looking at figure 1, one may recognize, that the neutron-rich bound nuclei at the outskirt of the nuclear landscape are surrounded by unbound systems, whilst adding or removing neutrons. This suggests, in turn, that the pairing correlation in the two neutrons accounts for a strong clustering in these systems, which often leads to a charged core plus to neutron cluster description. This picture has been suggested already in the early years of this field for the description of ^{11}Li [2] and can be verified by the observed momentum correlation patterns that are subject of this paper.

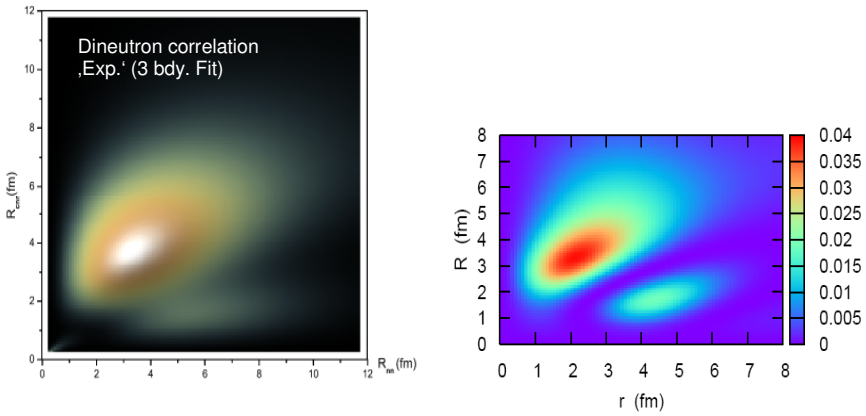

FIGURE 2. Direct comparison of spatial three body correlations depicted in density plots which show the separation of the charge core to the centre-of-mass of the two halo neutrons (R_{cnn}, R), versus the distance between the two neutrons (R_{nn},r) in ^{11}Li. The graph on the left-hand-side [3] is extracted from a phenomenological wave function resulting from a fit to a collection of data sets, and, in particular, the three body momentum correlations presented in this paper. The graph on the right-hand-side shows the result of a theoretical calculation by K. Hagino et al [4].

Figure 2 shows two density plots, where one is deduced by o fit to all experimental data [3], while the other is the result of a theoretical study [4] of the pairing interaction for the halo neutrons of ^{11}Li. Both descriptions are based on the assumption, that ^{11}Li can be described in a three body cluster picture. The opening angle between the two neutrons has been extracted from Coulomb breakup data by T. Nakamura et al. and is discussed elsewhere in these proceedings. One can compare the value here, which is $\theta_{nn}\approx62°$ with their value of $\theta_{nn}\approx48°$, and find it in reasonable agreement. However, this angle is a mean value and comprises two components: (i) a configuration where both neutrons are coupled to a neutron pair with total spin S=0, where the opening angle distribution peaks at about 30°, and (ii) a configuration with S=1, where the opening angle distribution peaks at about 100°. Here the former can be interpreted as a di-neutron pair which appears dominant in the ground-state wave-function.

In conclusion the ^{11}Li ground-state seems to be quite well understood and could be unambiguously reconstructed by the Coulomb excitation data which puts constraints on the n-n distance by yielding the distance between charged core and centre-of-mass of the two neutrons, and by the rich harvest from momentum correlation data [5] which allows to constraint possible assumptions in several dimensions. This is also supported by recent high precision data on masses [6,7] and nuclear moments [8,9].

Stepping across the drip-line

It is tempting [10] to presume a direct correspondence between ^{11}Li and ^{10}He if their nuclear structure is assumed to be governed by valence neutron interactions. Figure 3 shows the momentum correlations in ^{10}He [11].

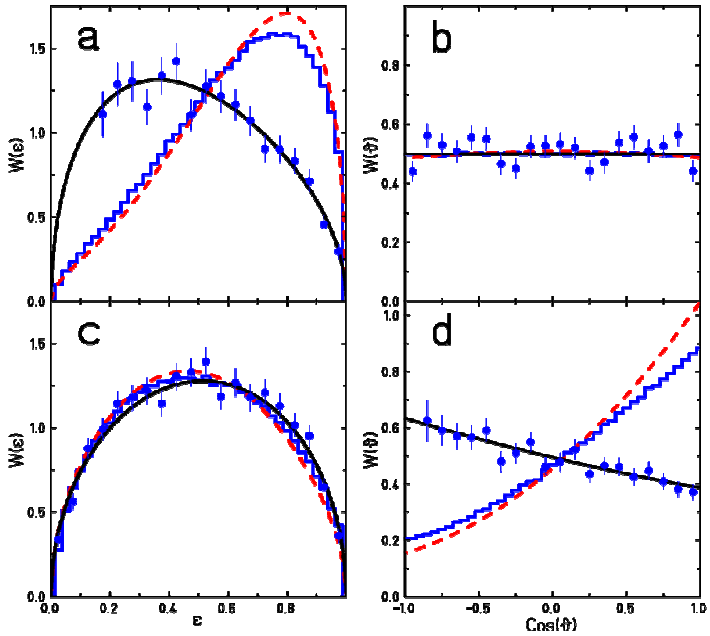

FIGURE 3. Momentum correlations for ^{10}He in Jacobi co-ordinates. The relative angle between momenta (ϑ) and the fractional energy in the two-body sub-systems (ε) is shown for two sets of co-ordinates (a,b) and (c,d) where the subsystem is either formed by two neutrons relative to the core or by ^{9}Li relative to the second neutron, respectively. The black lines are a fit to the data including the experimental response. The red lines show the corresponding correlations in the seed nucleus ^{11}Li, where the blue histograms include the effect of the experimental apparatus.

The observed correlations show clear deviations of the ^{11}Li ground-state from the relative motion in the continuum of ^{10}He. This points to the fact, which has also been observed in ^{10}Li while populating it in the proton removal from ^{11}Be and neutron removal from ^{11}Li [12] at high beam energies, namely, that the final state interaction governs completely the observed kinematical correlations.

The experiments presented in this paper have been carried out at GSI, Darmstadt. The beam velocity for all data shown in this paper is about 67% of the velocity of light. One therefore applies the sudden approximation and does not expect a considerable reconfiguration *during* the reaction process.

The spectra of ^{13}Li and ^{12}Li have been populated [13,14] from ^{14}Be as seed nucleus in one proton and 1p1n removal reactions and correlation studies yielded the scattering length for the ^{11}Li-n interaction (a_s=-13.7(1.6) fm) and a resonance in ^{13}Li at 1.47(35) MeV with a width of about 2 MeV. In the mean time additional experiments have been carried out at the NSCL, East Lansing, with ^{14}B as seed with stronger d-wave components in the ground state wave functions where also additional d-states [15] in ^{12}Li have been claimed. Recently a new run with ^{14}Be has been performed [16] with

similar, but not equal results. It would be therefore highly desirable to gain additional information on the ^{14}Be ground-state configuration, in order to be able to perform a similar comparison as previously shown for the ^{10}He case. The ^{13}Be properties have been studied in several breakup experiments [5,17,18], again with ^{14}Be and ^{14}B as seed nuclei. The resulting relative energy spectra show striking similarity, and would point to an interpretation similarly to the ^{10}Li case, namely, that the spectrum is entirely determined by the ^{12}Be-n final state interaction. The interpretation of the data has been studied also [19] based on theoretical considerations, by estimating the influence of the reaction mechanism on the data. Nevertheless, no conclusive picture could be obtained up to now. There is still controversy in the interpretation of the data. Partially this is due to the fact that ^{12}Be cannot be considered to be a 'good core' as it is easily polarizable. ^{14}Be exhibits rather a ^{10}Be+n+n+n+n structure. The interpretation of the data measured with gamma-coincidences [17] for the first time is unfortunately also not conclusive as there is a long lived state in ^{12}Be* which will decay outside the reaction zone. In all cases where ^{12}Be* is in the exit channel the relative energy spectra will show components shifted down by the missing gamma energy from the excited states. To decompose these states in terms of the initial angular momenta of the neutrons in the seed nucleus a different approach for analyzing these spectra has been followed. By studying the width of the recoil momentum distribution, which reflects the initial momentum distribution of the knocked-out neutron, in dependence on relative energy in ^{13}Be, it is possible to decompose [20] the involved angular momenta in the final state. The conclusions drawn in [17] are confirmed and new information on the ^{14}Be ground-state properties can be gathered.

This work is in parts the result of a collaborative effort of the R^{3}B collaboration. The author wants to thank all collaborators here. This work has been supported by the Helmholtz International Center for FAIR within the framework of the LOEWE program, by the Helmholtz Alliance Program contract number HA216/EMMI, by the GSI-TU Darmstadt Cooperation agreement, and by the BMBF, the German ministry for science and education (06DA70471, 06DA9040I, 06MT238).

REFERENCES

1. P.G. Hansen, *nature* **328,** 476 (1987).
2. P.G. Hansen, B. Jonson, *Europhys. Lett.* **4,** 409 (1985).
3. N.B. Shulgina, B. Jonson, and M.V.Zhukov, *Nucl. Phys.* **A825,** 175 (2009).
4. K. Hagino, et al., *Phys. Rev. Lett.* **99**, 022506 (2007).
5. H. Simon, et al., *Nucl. Phys.* **A 791,** 267 (2007).
6. M. Smith, et al., *Phys. Rev. Lett.* **101,** 202501 (2008).
7. C. Gaulard C, et al., *Nucl. Phys.* **A 826,** 1 (2009).
8. W. Nörtershäuser, T. Neff, R. Sanchez, I. Sick, *Phys. Rev.* **C 84,** 024307 (2011).
9. R. Neugart, et al., *Phys. Rev. Lett.* **101,** 132502 (2008).
10. Shigeyoshi Aoyama, *Phys. Rev. Lett*. **89,** 052501 (2002).
11. HJohansson, et al., *Nucl. Phys.* **A847,** 66 (2010).
12. B. Jonson, K. Riisager, *Phil. Trans. R. Soc Lond.* **A356**, 2063 (1998).
13. Y. Aksyutina, H. Johansson et al., *Phys. Lett.* **B666,** 430 (2008).
14. H.T. Johansson , Y. Aksyutina, et al., *Nucl. Phys.* **A847,** 66 (2010).
15. C.C. Hall C C, et al., *Phys. Rev.* **C81,** 021302 (2010).
16. Z. Kohyley, et al., *Phys. Rev.* **C87,** 011304 (2013).
17. Y. Kondo, et al., *Phys. Lett.* **B690**, 245 (2010).
18. Randisi G 2012 PhD thesis Univ. Caen, France; J..L. Lecouey, *Few Body Systems* **34,** 21 (2010).
19. G. Blanchon G, et al., *Nucl. Phys.* **A784,** 49 (2007).
20. Yu. Aksyutina, et al., *Phys. Lett.* **B718,** 1309 (2013).

Study Of Light Exotic Nuclei With CHIMERA Detector At LNS

L.Acosta[b], C.Agodi[b], F.Amorini[b], A.Anzalone[b], L.Auditore[d], I.Berceanu[g], M.Buscemi[b,c], G.Cardella[a], M.BChatterjiee[h], E.DeFilippo[a], L.Francalanza[b,c], R.Gianì[b,c], L.Grassi[b,c], E.La Guidara[a], G.Lanzalone[b,e], I.Lombardo[b,f], D.Loria[d], T.Minniti[d], A.Pagano[a], E.V.Pagano[b,c], M.Papa[a], S.Pirrone[a], G.Politi[a,c], A.Pop[g], F.Porto[b,c], F.Rizzo[b,c], E.Rosato[f], P.Russotto[a], S.Santoro[d], A.Trifirò[d], M. Trimarchi[d], G.Verde[a], M.Vigilante[f]

[a] *INFN - Sezione di Catania, Via S. Sofia, 95123 Catania, Italy*
[b] *INFN - Laboratori Nazionali del Sud, Via S. Sofia, Catania, Italy*
[c] *Dip. di Fisica e Astronomia, Università di Catania, Via S. Sofia, Catania, Italy*
[d] *INFN Gruppo collegato di Messina & Dip. di Fisica, Università di Messina, Italy*
[e] *Facoltà di Ingegneria e Architettura, Università Kore, Enna, Italy*
[f] *INFN Sezione di Napoli & Dipartimento di Fisica, Università Federico II, Napoli, Italy*
[g] *Institute for Physics and Nuclear Engineering, Bucharest, Romania*
[h] *Saha Institute for Nuclear Physics, Kolkata, India*

INTRODUCTION

Exotic beams, produced through the in-flight fragmentation method are available at LNS with a usable intensity after the successful upgrading of the fragmentation beam line [1]. Using the CHIMERA detector [2] implemented by a recent upgrade of Pulse Shape method in silicon detector [3], we started various experimental campaigns with different aims: a) study of transfer, pick-up, knock-out reactions induced by light neutron rich nuclei, on proton and deuteron targets in order to search for a dependence of such cross sections by the halo structures. b) Study of the isospin dependence of reaction dynamics [4,5] around 30 A·MeV using exotic beams in the region of mass 30 produced by ^{36}Ar fragmentation, and around ^{68}Ni produced by ^{70}Zn fragmentation. In this short report we will concentrate on the first item showing a new method that we developed in order to obtain angular distribution in binary reactions by using kinematical constraints.

Experimental Setup and Data Analysis

The fragmentation beam was produced by using an $^{18}O^{7+}$ primary beam delivered by the INFN-LNS Superconducting Cyclotron at 55 A·MeV. The beam line magnetic elements were set to maximize production of ^{11}Be ions (Bρ=2.78Tm). The beam was identified particle by particle by using a tagging system consisting of a Double Side Silicon Strip Detectors (DSSSD) and a large surface Micro-Channel Plate (MCP) detector [18]. The MCP detector was placed approximately 13 m before the tagging strip and was used as start of the time of flight (TOF) measurement of the beam

particles (the stop being delivered by the DSSSD). In fig 1 it is reported the quality of the identification obtained by plotting the TOF as a function of the energy loss (ΔE) measured in the DSSSD.

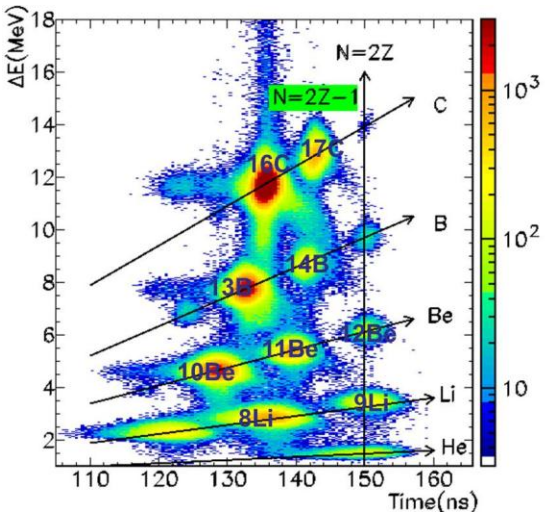

FIGURE 1. Identification scatter plot of the fragmentation beam. Arrows show the loci for the different charges and N/Z ratio.

In the figure 1 it is possible to distinguish the "cocktail" of fragmentation beams identified in the tagging strip. Thus the first step of the data analysis consists on the selection of the beam under study with the use of appropriate cuts. Events were further selected, searching for kinematical coincidences. Only events with charged particles multiplicity equal to two were analyzed, strongly reducing contamination due to carbon in the polyethylene target, and to reactions in the DSSSD. Other constraints were taken into account by using conservation laws. Firstly, due to momentum conservation the relative azimuthal angle Δϕ between the two fragments must be 180°. In fig. 2, we plot this angle as measured for the reactions, ^{8,9}Li+p→^{8,9}Li+p.

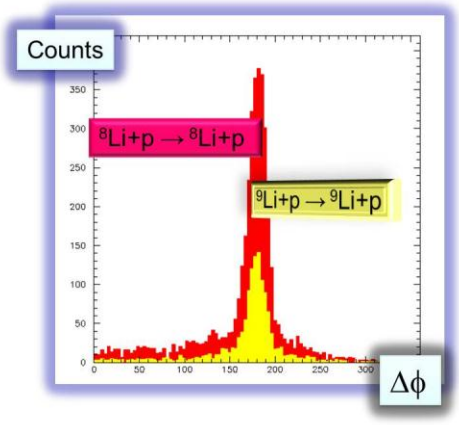

FIGURE 2. Relative azimuthal angle Δϕ measured for coincidence events in the reactions, ^{8,9}Li+p→^{8,9}Li+p

We can recognize the binary events concentrated in the peak around 180°.

The following selection, based on energy conservation law, requires that the sum of kinetic energies of the two detected particles is equal to the beam energy plus the Q-value. In fig.3 we plot the total energy detected in coincidences between deuterons and B ions in the reaction ^{13}B+p.

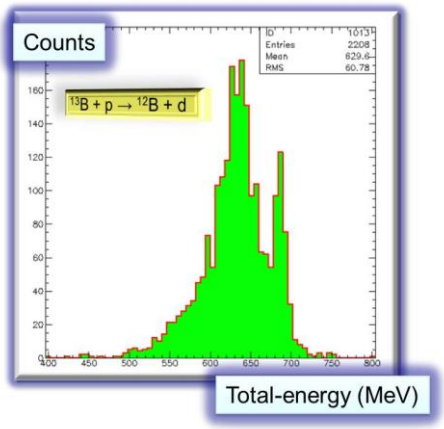

FIGURE 3. Total energy spectrum for the reaction ^{13}B+p→B+d

Notice in this plot a peak close to the value of 690 MeV, that roughly corresponds to the total available energy. The second peak correspond to 1n-decay channel of ^{12}B*. Due to the relatively poor CsI(Tl) energy resolution for heavy fragments, it is quite difficult to discriminate the decay path towards to the ground state of a specific nucleus. This cannot be in fact disentangled with respect to excited states at energy lower than particle decay. However, in the reactions ^{10}Be+p→^{9}Be+d and ^{10}Be+d → ^{9}Be+t, only ^{9}Be$_{gs}$ can be populated because the first excited level at 1.684 MeV is unbound, decaying to the n+2α channel. Because in this case the final channel is well defined, we can easily convert the deuteron/triton energy spectrum in the CM angular distribution. This can be done by using kinematic relations, taking into account beam intensity, target thickness, and detector efficiency.

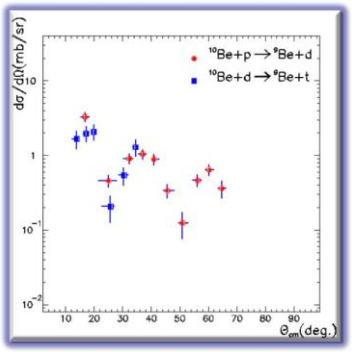

FIGURE 4. Angular distribution extracted for the reactions ^{10}Be+p→^{9}B$_{gs}$+d, ^{10}Be+d→^{9}B$_{gs}$+t.

In fig.4 the preliminary angular distribution for the *p,d* (full dots) and *d,t* reactions (squares) are reported. The cross sections and the angular distributions for the two reaction channels are quite similar. It seems that the difference in the final state can be neglected and that the cross section is determined mainly by the characteristics of the transferred neutron. The value of the size of the angular bins of each point was chosen by the need to get a reasonable statistical error. We emphasize that this method to extract the angular distribution allows to automatically correct for the position and direction spread of fragmentation radioactive beams.

This method can be used in the measurement of the energy of the heavy fragment, around Fermi energy, if nuclei with only unbound excited levels are investigated as in the case of ^{9}Be. The method can be however extended also to the case of bound and unbound excited levels especially if coincidence gamma ray measurements are performed allowing for discrimination of the different contributions of the decay process. In next experiments we will also profit of the new telescopes FARCOS [6] we are going to realize, to detect the heavy reaction partner with high mass identification, energy resolution and ϕ granularity. This will allow an improved identification of excited states and also to study the decay characteristics of neutron decay in unbound nuclei. This original method to measure the angular distribution could be applied in the future Eurisol experiments.

REFERENCES

1. see http://fribs.lns.infn.it/upgrade-results.html
2. A.Pagano et al, Nucl. Phys. A 734 (2004) 504
3. A.Pagano, Nuclear Physics News, 22:1(2012)25.
4. E.De Filippo et al Phys. Rev. C 71, 044602 (2005)
5. F. Amorini et al, Phys. Rev. Lett. 102 (2009) 112701
6. L. Acosta et al., EPJ Web of Conferences,31 ,0035 (2012).

THE RESONANCES OF ^{18}Ne

Enrico Maglione[a], Lídia S. Ferreira[b] and Ning Yu

[a] *Dipartimento di Fisica "G. Galilei", Via Marzolo 8, I-35131 Padova, Italy*
and Istituto Nazionale di Fisica Nucleare, Padova, Italy.
[b]*Centro de Física das Interacções Fundamentais, and Departmento de Física, Instituto Superior* Técnico, Universidade Técnica de Lisboa, Av Rovisco Pais, 1049 001, Lisboa, Portugal .
[c]*Central China Normal University, CCNU, Wuhan, CHINA.*

INTRODUCTION

The determination of resonances in ^{18}Ne is an important issue to obtain the reaction rates in processes relevant for the energy production and element generation in nuclear astrophysics events. Breakout paths from the hot CNO cycle involve sequences of alpha particle reactions that proceed through the ^{18}Ne resonances, which are above the a decay threshold.

The reaction ^{17}F(p,γ) ^{18}Ne is particularly important in late nucleosynthesis of massive stars in the pre-supernovae phase, where the rp-process leads to the production of nuclei up to Cadmium. Many reaction chains include this process that can go via direct or resonance capture of the proton. A few experiments have been devoted to determine the energy levels of ^{18}Ne, but still some uncertainty prevails, requiring further experimental studies , thus relevant in the contex of the EURISOL project.

Widths and spin assignments of some relevant levels for the astrophysical processes have been estimated from the properties of the mirror nucleus ^{18}O [1] and data from stable beam studies [2], or from indirect measurements [3-7], provided the resonance parameters for several states above 7 MeV of excitation energy.

The inverse of the reaction ^{17}F(p,γ)^{18}Ne, is just the emission of a proton from an excited state of ^{18}Ne. Therefore, proton emission can be a process to study these reactions and grasp the underlying nuclear structure involved in the process.

One and two proton emission from ^{18}Ne has been observed in an experiment performed at LNS by Raciti and collaborators[8]. They observed 2p decay not only from the 6.15 MeV 1^-, distinguishing di–proton (31%) and democratic (69%) mechanisms, but also from the known 7.06 MeV, 7.91 MeV, and 8.5 MeV levels. These states are above the threshold for sequential decay and could have spin and parity 1^- or 2+. However, there were other higher lying excited states around 8.5 MeV, 10.7 MeV, 12.5 MeV, and 13.7 MeV, for which there is a favorable energy window for sequential decay, going after the emission of the first proton to excited states of ^{17}F, instead of the ground state, and decaying finally to the ground state of ^{16}O after the second emission. In fact, the authors of Ref. 8 found that almost 30% of the decay goes to the

sequential channel. This is quite surprising, since simple barrier penetration considerations would favour decay with the largest amount of energy being carried out by the proton. Thus, one expects that the emission of the first proton would lead to the ground state of 17F that is bound, and consequently the second proton would not be emitted. Another surprising fact is that these states are quite narrow.

The authors of Ref. 9 also confirmed correlated two proton emission only from the excited 6.15 MeV state in 18Ne, in good agreement with previous results.

From the discussion above, we can see that if on one side the assignment of spin levels in 18Ne is quite relevant for the determination of astrophysical reaction rates, on the other side, the interpretation of proton decay data can provide unambiguous support to the identification of the nuclear energy levels.

Proton emission from the ground and excited states of exotic nuclei has been measured extensively in the last two decades [10], and a good theoretical interpretation of the decay process was achieved [11]. Using realistic mean field models, it was possible to predict the nuclear shape parameters and quantum numbers of the decaying states [12]. Fully self–consistent calculations, using more fundamental interactions based on relativistic density functionals derived from meson exchange and point coupling models, were also able to account for the experimental data of proton radioactivity from spherical nuclei [13]

A correct interpretation of the data has to be supported by a solid nuclear structure description of the parent and daughter nuclei. It is thus the purpose of this work to discuss a microscopic shell-model calculations for sequential two-proton decay from excited states in 18Ne, calculate the decay observables, and identify the levels which are the best candidates for decay.

THE SPECTRUM OF ^{18}Ne.

According to scattering theory, the half-life for decay from an initial state *i* to a final state *f* by one particle emission is given by, $T_{1/2} = \hbar \ln 2 / \Gamma^{if}_{j}$, where the decay width can be found from the relation[14],

$$\Gamma_j^{if} = S_j^{if} \frac{\hbar^2 k \alpha_j^2}{m}$$

with *m* and *k* standing for the mass and wave number of the proton. The spectroscopic factor S_{ij}, corresponds to the probability that taking away a particle with angular momentum j from an initial state *i*, will lead to a final state *f*. The quantity α_j is the asymptotic normalization of the proton single particle wave function in a state of spin *j*. It can be obtained from the solution of the Schrödinger equation with outgoing wave boundary conditions, with a realistic mean field potential[15].

The total width for decay is a sum of partial widths, for all possible channels with quantum numbers allowed by parity and momentum conservation, and for all final states, and is given by,

$$\Gamma^{i}_{Tot} = \sum_{jf} \Gamma^{if}_{j}$$

and the branching ratios *Br*, are simply the ratio between the partial decay width to the total width.

Besides the knowledge of the proton resonance, the spectroscopic factor is the most important quantity which is needed to obtain the decay width, and is determined from the matrix element of an annihilation operator between the initial and final states. In order to be able to calculate it, a shell-model calculation has to be performed to get the nuclear wave functions for a specific interaction.

We have chosen the interaction determined in Ref. 15. This interaction was developed with the intent to describe intruder $1\hbar\omega$ negative parity states which appear at low excitation energies of sd shell nuclei, besides the normal $0\hbar\omega$ positive parity states. A p–sd–pf model space was used with a 4He core allowing one nucleon jump between the major shells, and with parameters fitted to the experimental excitation energies. The interaction gives results in good agreement with experimental data for all sd nuclei.

TABLE 1. Calculated excited states in ^{18}Ne with a total width smaller than 200 keV and a branching ratio for decay to unbound states larger than 0.7. The spin and parity, and energy of the decaying level are given in the first two columns, while the branching ratio and width are shown in the third and fourth ones.

J^{π}	E(MeV)	Br	Γ^{i}_{Tot} (keV)
5^-	10.239	0.87	162
4^-	10.349	0.84	19
7^-	10.695	1.00	4
0^-	10.776	1.00	200
2^-	10.806	0.77	104
4^-	12.187	0.73	140
6^-	14.734	0.77	168

Performing a standard shell model calculation with this interaction, we have determined the energy spectra and wave functions of ^{18}Ne and ^{17}F, and the corresponding spectroscopic factors. Solving the Schrödinger equation with the mean field potential given in Ref. 16, the wave function of the proton resonance were found, and making use of Eq.1, the decay widths for proton emission were determined. Amongst more than a thousand states we have calculated for ^{18}Ne, we have selected only the ones which have a total width smaller than 200 keV, since only states with narrow widths were observed experimentally. In order to identify the events where the emission of a second proton is energetically possible, we have calculated the branching ratio for decay to unbound proton states in ^{17}F. The latter, is obtained considering the ratio for a width given by Eq. 2, where the summation is

restricted to unbound states, and the total width. Selecting the states whose branching ratio is larger than 0.7, we found that only a few negative parity states fulfill this condition, and they lie at quite high energies.
The results are reported in Table 1, and confirm the experimental findings of Ref. 8. Most probably, states with very high angular momentum have not been observed experimentally, since in the work of Ref. 8, the excitation mechanism used to populate the states was Coulomb excitation.

CONCLUSIONS

In our analysis we found evidence for states of negative parity at quite high energies, which are very narrow, and prefer to decay by one proton emission to the excited states of the daughter ^{17}F, rather than to the ground state, as observed in the experimental studies of Raciti and collaborators [8]. Since at these energies proton decay is faster than γ decay, the nucleus prefers to emit sequentially the second proton to reach ^{16}O, instead of a photon that would lead to bound states of ^{17}F. With this calculation, we have shown that through the interpretation of proton decay data one accesses nuclear structure information relevant to nuclear astrophysics.

ACKNOWLEDGMENTS

This work was supported by the Fundação para a Ciência e a Tecnologia (Portugal), within Project CERN/FP/123606/2011.

REFERENCES

1. M. Wiescher et al., *Astrophys. J.* **316,** 162 (1987).
2. K. I. Hahn et al., *Phys. Rev.* **C 54,** 1999 (1996).
3. B. Harss et al., *Phys. Rev.* **C 65**, 035803 (2002).
4. J. J. He et al., *Phys. Rev.* **C 80,** 042801(R) (2009).
5. K. A. Chipps et al., *Phys. Rev. Lett.* **102,** 152502 (2009).
6, D.W. Bardayan et al., *Phys. Rev.* **C 62,** 055804 (2000).
7. S. Almaraz-Calderon et al., *Phys. Rev.* **C 86,** 025801 (2012).
8. G. Raciti et al, Phys. Rev. Lett. **100**, 192503 (2008).
9. C. J. Lin et al., AIP Conference Proceedings 1409, American Institute of Physics, Melville, NY, 2011, pp. 98.
10. A. A. Sonzogni, *Nucl. Data Sheets* **95**, 1 (2002).
11. E. Maglione, L. S. Ferreira and R. J. Liotta, *Phys. Rev.* **C 59.** R589 (1999).
12. P. Arumugam, L.S. Ferreira and E. Maglione, *Phys. Lett.* **B 680.** 443-447 (2009).
13. L. S. Ferreira, E. Maglione and P. Ring, *Phys. Lett.* **B 701,** 508-511 (2011).
14. E. Maglione, L. S. Ferreira and R. J. Liotta, *Phys. Rev. Lett.* **81**, 539-541 (1998).
15. M. Bouhelal et al., *Nuc. Phys.* **A 864,** 113 (2011).
16. H. Esbensen and C. N. Davids, *Phys. Rev.* **C 63,** 014315 (2000).

Breakup Reactions measurements of Halo Nuclei around QFS conditions [1]

D. Galaviz[a], E. Cravo[a], R. Crespo[a,b], A. Deltuva[a], A. Henriques[a], J. Machado[a], P. Teubig[a], and P. Velho[a], for the R^{3}B Collaboration

[a]*Centro de Fisica Nuclear da Universidade de Lisboa, Av. Prof. Gama Pinto 2, 1649-003 Lisbon, Portugal*
[b]*Departamento de Física, Instituto Superior Técnico, Taguspark, Av. Prof. Cavaco Silva, Taguspark, 2780-990, Porto Salvo, Oeiras, Portugal*

INTRODUCTION

Knockout reactions constitute a very sensitive tool to investigate the single-particle or cluster structure of nuclei. Considering the particular case of one-neutron knockout studies, the measurement of the momentum distributions [1 - 4] of the remaining core has been and is used as a tool to determine the orbital angular momentum of the struck particle.

We aim to analyse the breakup of one-neutron halo nuclei, ^{15}C and ^{11}Be at Quasi-Free Scattering (QFS) kinematical conditions performed at the experimental setup of the R^{3}B (Reactions with Relativistic Radioactive Beams) collaboration at the GSI laboratory in Darmstadt, Germany. The theoretical interpretation of the results will be done by applying the Faddeev/Alt-Grassberger-Sandhas (AGS) fewbody reaction framework [7-9].

Recent calculations [5,6] suggested that at high incident energies at QFS conditions and fully exclusive observables at some suitable and some suitable configurations the ground state spectroscopic could be extracted with accuracy.

As a first step, the analysis of the core momentum distributions for the reactions p(^{15}C,^{14}C)n p and p(^{11}Be,^{10}Be)n p will be made.

THE HALO NUCLEI ^{15}C AND ^{11}BE

Both ^{15}C and ^{11}Be are well-established one-neutron halo nuclei that have been studied over the past years using various experimental techniques. In the following we present a summary on the current knowledge on the structure of these two halo nuclei.

[1] Work supported by the Portuguese FCT under the grant PTDC/FIS/103902/2008

The ^{15}C is a one-neutron halo nucleus with a neutron separation energy of S_n = 1.218 MeV. This nucleus has been experimentally investigated by means of transfer reactions [10-12], nuclear breakup [13-15] and Coulomb Dissociation [16,17] studies. Table 1 summarizes the spectroscopic factors for the dominant $|^{14}C(0^+) \otimes 2s_{1/2}>$ configuration extracted from the analysis of differebt experiments. Essential one expects no contributions from exited states of the core ^{14}C. This makes ^{15}C a very suitable case to apply the Faddeev/AGS formalism to the interpretation of the breakup reaction on a proton target.

TABLE 1. Ground state spectroscopic factors of ^{15}C for the configuration $|^{14}C(0^+) \otimes 2s_{1/2}>$. The table summarizes the results obtained from experiments using different reaction techniques.

Experimental Probe	**Reference**	**Spectroscopic factor $\|^{14}C(0^+) \otimes 2s_{1/2}>$**
$^{13}C(^{18}O,^{16}O)^{15}C$	F. Cappuzzello *et al.* [10]	~ 1.0
$^{14}C(d,p)^{15}C$	J. R. Goss *et al.* [11]	0.88
	G. Murillo *et al.* [12]	1.03
	F. Flavigny *et al.* [13]	0.89
	J. R. Terry *et al.* [14]	0.88 ± 0.04
$^{9}Be(^{15}C,^{14}C)X$	J. Tostevin *et al.* [15]	0.74 ± 0.09
		0.84 ± 0.10
		0.90 ± 0.10
	T. Nakamura *et al.* [16]	0.91 ± 0.06
		0.72 ± 0.05
$^{208}Pb(^{15}C,^{14}C)X$	U. D. Pramanik *et al.* [17]	0.92 ± 0.07
		0.73 ± 0.05

The nucleus ^{11}Be is probably the most well-established one-neutron halo nucleus, with a neutron separation energy of S_n = 0.503 MeV. In this case, as shown in Table 2, in addition to the dominant $|^{10}Be(0^+) \otimes 2s_{1/2}>$ contribution to the ground state, there is also a contribution where the core is in his first excited state.

The predictive power of the fewbody Faddeev/AGS multiple scattering formalism in understanding the experimental data from the resonant and non-resonant breakup of ^{11}Be on a proton target [18] has been shown in [19]. Our goal is to apply the same few body formalism to the measurement of the neutron breakup reaction of ^{11}Be on a proton target at QFS conditions. In this approach the Faddeev/AGS assumes the core to be inert. The role of core excitation in the breakup observables would not be addressed presently. However its role would need to be addressed in the future.

TABLE 2. Ground state spectroscopic factors of ^{11}Be for the configuration $|^{10}\text{Be}(0^+) \otimes 2s_{1/2}>$. The table summarizes the results obtained from experiments using different reaction techniques.

Experimental Probe	Reference	Spectroscopic factor $\|^{10}\text{Be}(0^+) \otimes 2s_{1/2}>$
^{10}Be(d,p)^{11}Be	D. Auton [20]	0.73 ± 0.06
	B. Zwieglinski *et al.* [21]	0.77
	K. T. Schmitt *et al.* [22]	0.71 ± 0.05
p(^{11}Be,^{10}Be)d	S. Fortier *et al.* [23]	0.66
		0.79
^{9}Be(^{11}Be,^{10}Be)X	J. Tostevin *et al.* [15]	0.95 ± 0.15
		0.90 ± 0.14
	T. Aumann *et al.* [24]	0.74
^{48}Ti(^{11}Be,^{10}Be)X	V. Lima *et al.* [25]	0.46 ± 0.15
^{nat}Pb(^{11}Be,^{10}Be)X	R. Palit *et al.* [26]	0.61 ± 0.05
	N. Fukuda *et al.* [27]	0.72 ± 0.04

EXPERIMENTAL CAMPAIGN AT THE LAND/R^{3}B SETUP

During the summer 2010, the GSI experiment S393, "Neutron-rich Nuclei and Beyond the Dripline in the Range Z=4 to Z=10 Studied in Kinematically Complete Measurements of Direct Reactions at Relativistic Energies" was carried out by the R^{3}B collaboration at the LAND/R^{3}B experimental setup. A schematic view of the experimental setup is shown in Figure 1.

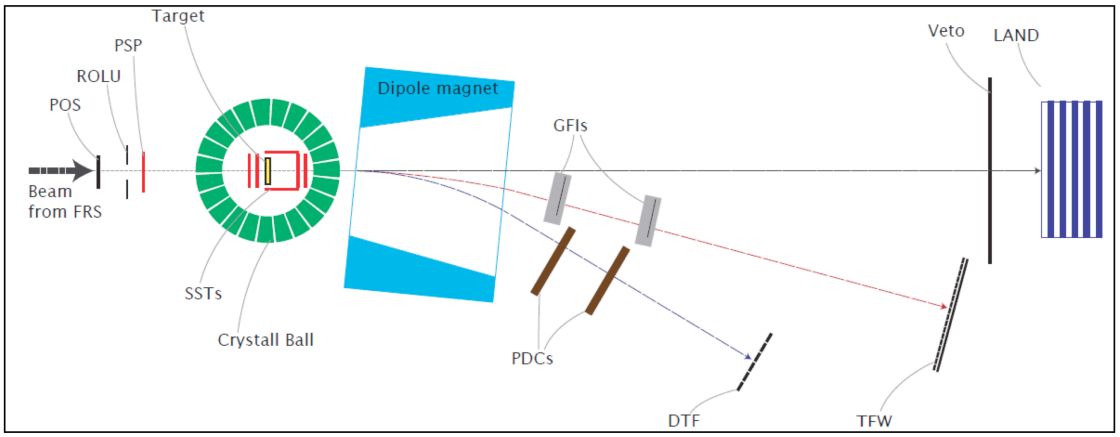

FIGURE 1. Schematic view of the LAND/R3B experimental setup used during the experimental campaign S393. The description of the detector acronyms is provided in the text. Highlighted is shown the path of the particles involved in neutron-knockout reactions on a proton target studied in this experiment at Quasi-Free Scattering conditions.

In this experiment, a primary particle beam of ^{40}Ar was accelerated up to 600 MeV/u at the SIS synchrotron of the GSI laboratory. The ions were transported to the fragmentation target of the FRS (FRagment Separator), where they interacted with a Beryllium target of 4 g/cm^2 thickness. The light exotic and stable nuclei produced were selected by the FRS and guided towards the LAND/R^{3}B experimental setup.

Isotopes from elements between Lithium and Neon with $1.5 \leq A/Z \leq 3$ were studied by means of Coulomb Dissociation, nuclear breakup and nucleon knockout on hydrogen at QFS conditions.

Various kinds of target materials (^{208}Pb, ^{12}C, CH_2) were used during the experiment, being the polypropylene target of particular interest for the study of neutron knockout reactions on the halo nuclei ^{15}C and ^{11}Be.

The R^3B experimental setup allows the characterization of all particles involved in the reaction process, making it possible the measurement of semi-inclusive neutron knockout cross-sections.

STATUS OF THE ANALYSIS

The analysis of the data is ongoing. The calibration of all detection systems involved in the analysis of (p,pn) reactions in inverse kinematics is in its final stage. Preliminary estimates of the angular resolution achieved in the measurement of the recoil heavy isotopes allow for a minimum momentum resolution of 26 MeV/c (^{15}C) and 19 MeV/c (^{11}Be), which should be sufficient to characterize the expected halolike narrow core momentum distributions.

REFERENCES

1. D. Bazin *et al.*, *Phys. Rev. Letters* **74**, 3569 (1995).
2. T. Nakamura *et al.*, *Phys. Rev. Lett.* **83**, 1112 (1999).
3. R. Palit *et al.*, *Phys. Rev. C* **68**, 034318 (2003).
4. Y. Kondo *et al.*, *Phys. Rev. C* **79**, 014602 (2009).
5. R. Crespo *et al.*, *Eur. Phys. J. A* **42**, 609 (2009).
6. R. Crespo *et al.*, *Phys. Rev. C* **79**, 014609 (2009).
7. L. D. Faddeev, *Zh. Eksp.Theor. Fiz.* **39**, 1459 (1960)
8. E. O. Alt, P. Grassberger and W. Sandhas, *Nucl. Phys. B* **2**, 167 (1967).
9. W. Glöcke, *The Quantum Mechanical Few-Body Problem,* Berlin/Heidleberg: Springer-Verlag, 1893.
10. F. Cappuzzello *et al.*, *Phys. Lett. B* **711**, 347 (2012).
11. J. R. Goss *et al.*, *Phys. Rev. C* **12**, 1730 (1975).
12. G. Murillo *et al.*, *Nucl. Phys. A* **579**, 125 (1994).
13. F. Flavigny *et al.*, *Phys. Rev. Lett.* **108**, 252501 (2012).
14. J. R. Terry *et al.*, *Phys. Rev. C* **69**, 054306 (2004).
15. J. Tostevin *et al.*, *Phys. Rev. C* **66**, 024607 (2002).
16. T. Nakamura *et al.*, *Phys. Rev. C* **79**, 035805 (2009).
17. U. D. Pramanik *et al.*, *Phys. Lett. B* **551**, 63 (2003).
18. A. Shrivastava *et al.*, *Phys. Lett. B* **596**, 54 (2004).
19. E. Cravo *et al.*, *Phys. Rev. C* **79**, 064610 (2009).
20. D. Auton, *Nucl. Phys. A* **157**, 305 (1970).
21. B. Zwieglinski *et al., Nucl. Phys. A* **315**, 124 (1979).
22. K. T. Schmitt *et al.*, *Phys. Rev. Lett.* **108**, 192701 (2012).
23. S. Fortier *et al.*, *Phys. Lett. B* **461**, 22 (1999).
24. T. Aumann *et al.*, *Phys. Rev. Lett.* **84**, 35 (2000).
25. V. Lima *et al.*, *Nucl. Phys. A* **795**, 1 (2007).
26. R. Palit *et al.*, *Phys. Rev. C* **68**, 034318 (2003).
27. N. Fukuda *et al.*, *Phys. Rev. C* **70**, 054606 (2004).

Summary

Björn Jonson[a]

[a] *Fundamental Physics, Chalmers University of Technology, S-412 96 Göteborg, Sweden*

Let me at to start with thank the organizers for their work organizing this meeting and for setting up such a stimulating programme.

Nuclear physics research has during the past three decades become more and more directed towards the understanding of the intricate properties of nuclei in the drip-line regions. A key ingredient in this endeavour is the continuous, painstaking and often ingenuous development of techniques to identify, isolate and manipulate exotic nuclear species. The availability of vast amounts of exotic nuclei, studied both *in situ* and as energetic radioactive beams, has given a multitude of experimental information building the base for a deeper understanding their properties. To allow this, novel detector techniques and new, powerful analysis methods have been key ingredients. In the same time period theory has experienced an unprecedented development hand in hand with the experimental progress. The state-of-the art of the technical progress, the experimental information and the most recent theoretical developments in this field of nuclear physics was recently highlighted in a Nobel Symposium entitled "Physics with Radioactive Beams" [1].

There has over these three decades in particular been a focus on the lightest elements. In fact, all bound isotopes up to the element oxygen have been identified and have been subject for a multitude of different experimental and theoretical investigations. It is therefore very timely to organize this meeting about the present status and future possibilities in the physics of light exotic nuclei.

As we all know the production of exotic nuclei has had a very rapid development, from the time of the first experiments at ISOLDE at CERN. Today one may say that the field is experiencing a new paradigm in its development. Funds for several advanced general-purpose facilities worldwide are being built or are planned. The two basic methods for production of exotic nuclei are (i) the In-Flight technique and (ii) the ISOL method. For an extensive review see Ref. [2].

Meetings like this one has an important aspect in that they collect experts, both in experimental techniques and in up-to-date theory, to discuss in an informal manner questions like deviations between theory and present-day experiments, new experiments needed to guide theory, new calculations needed to design appropriate experiments. Such discussions may in the long term be of major importance for the design of the future facility, as schematically illustrated in Figure 1.

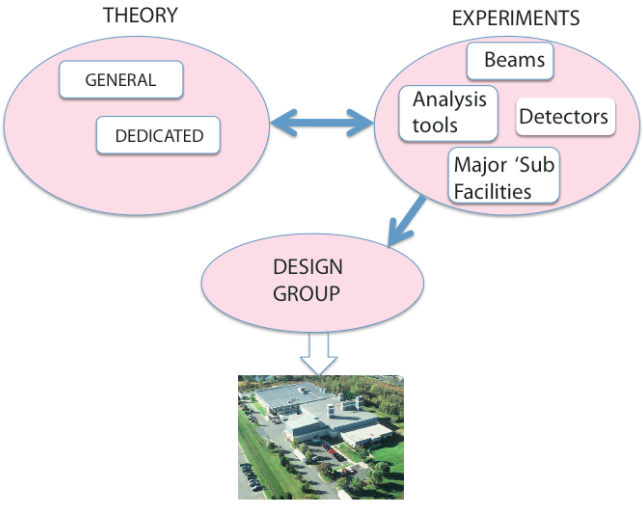

FIGURE 1. An illustration about how the interaction between state-of-the art theory and experiments may form the basis for the design of the future radioactive-beam facilities.

We have today a general consensus that the future of our field of physics in Europe should be based on two major facilities

- FAIR at the GSI Helmholtzcentrum für Schwerionenforschung GmbH in Darmstadt, Germany, and
- EURISOL, where the location is not yet decided but where SIPRAL 2, HIE ISOLDE and SPES are interesting first step facilities.

These proceedings contain detailed papers from the different talks given at the meeting and I shall not in my written version repeat what I said in my talk. I note, however, the progress from many different groups, which shows that we may enter the new period of experimental possibilities with a lot of confidence. Experiments with reactions using halo nuclei, clustering aspects, beta decay and unbound nuclei are examples. Nuclear astrophysics with ISOL beams is maybe one of the key points in the next decade and we heard an excellent description about the progress in this part of our field. Theory, with the role of 3N-forces, the shell model in the next decade and *ab initio* calculations directly relevant for the future EURIOL physics, is today a stronger player than ever before in our filed. We have seen how the link between experiment and theory for exotic nuclei has grown stronger over the years to the benefit to all of us. There is also a new link that has been born out of the increased complexity of both experiments and theory – the need for computer power. In fact, here we may today say that our field is standing on three legs: experiments, theory and e-Science. This is an important aspect of our field with clear links to the society.

FIGURE 2. EURISOL as an umbrella organisation in the initial steps towards a dedicated facility.

As a final remark I would say that I am very optimistic about our field in general and about EURISOL in particular. But, we face today an economic situation in Europe that goes far beyond what we had envisaged some years ago. I think therefore that it would be very unwise to start to try to raise funds for EURISOL as a new, dedicated facility. Therefore my recommendation for the next years to come would be that we make EURISOL an umbrella-type organization, where SPIRAL 2, HIE ISOLDE and SPES together work for the best use of the resources available. We should try to avoid the same type of equipment at all facilities so that the broadest possible programme may be conducted. In this way we, together with FAIR, could keep our leading role in the field of physics.

REFERENCES

1. Proceedings of the Nobel Symposium NS 152, Phys. Scr. **152** (2013).
2. Y. Blumenfeld, T. Nilsson , P. Van Duppen, *ibid* 014023